SCALABLE DECENTRALIZED NAVIGATION AND CONTROL ALGORITHMS FOR LARGE SCALE SPACECRAFT FORMATIONS

A Dissertation

Presented to the Faculty of the Graduate School

of Cornell University

in Partial Fulfillment of the Requirements for the Degree of

Doctor of Philosophy

by

Terence H. McLoughlin

January 2009

SCALABLE DECENTRALIZED NAVIGATION AND CONTROL ALGORITHMS FOR LARGE SCALE SPACECRAFT FORMATIONS

Terence H. McLoughlin, Ph.D.

Cornell University 2009

Future NASA missions requiring spacecraft formation flying require an extremely high level of autonomy and robustness when compared to single spacecraft systems. This is especially true for formations with a large number of spacecraft, which naturally have a higher likelihood of collision, and those that are to be flown in deep space, which are located too far from the Earth to allow for direct ground-based control. Further, it is likely that the individual spacecraft will have a limited amount of resources for sensing and communication. This dissertation is devoted to the development of decentralized navigation and control algorithms for such systems. The algorithms developed efficiently utilize the limited sensing and communication resources at each spacecraft in order to maintain an accurate estimate of the formation state. Formation keeping is achieved through the calculation of a reference point which damps noise in the formation state estimates, of which the reference point is a function. In the absence of an intra-spacecraft communication subsystem, optimal sensor switching algorithms are developed which yield accurate formation state estimates. With communication, individual spacecraft state estimates are iteratively fused to form formation-optimal state estimates. Numerical simulations demonstrate the efficacy of these methods when compared, in terms of fuel usage and formation positioning error, to an ideal system where each spacecraft has comparatively high sensing and communication capability.

BIOGRAPHICAL SKETCH

I was born in Staten Island, NY, the youngest of three boys, to John and Linda McLoughlin. I graduated from Monsignor Farrell High School. I received a B.S. in Electrical and Computer Engineering from the State University of New York at Buffalo where my studies were focused on signal and image processing.

To my Father and Mother

ACKNOWLEDGEMENTS

Words can not do justice to those in whose debt I am for helping make this dissertation possible. They have been there for me during everything that has gone wrong, including a collapsed apartment, destroyed furniture, a totaled car, broken limbs, a black eye or two, and the Red Sox winning the World Series; and everything that has gone right, including having the opportunity to work with brilliant people on a daily basis, getting over the many hurdles involved in the development of this dissertation, and the good times I've had in the process, which are far too numerous to list.

Mark Campbell took me into his group when we both first joined Cornell and I am grateful for his guidance and confidence. I'd also like to thank my committee members, past and present, for their valuable input: Professors Raffaelo D'Andrea, Hod Lipson, Mason Peck, and Mark Psiaki.

I am grateful to my Mother, Linda, my Father, John, and two brothers, John and Brian, whose love and support has never wavered.

To my fellow students, including Jarurat Ousingsawat, Brett Streetman, Mike Sherback, Armann Gylfason, Bernardo Cordovez, Edgar Cuji, Justin Atchison, Mike Tolley, Jay Schuren, Michele Carpenter, and Maureen Lynch: I wish you nothing but the greatest success in your lives.

Finally, as I sit here in the early morning, putting the finishing touches on this dissertation, I am most grateful to my girlfriend, Jamie Drahos, who has been there for me, day in and day out.

TABLE OF CONTENTS

LIST OF TABLES

LIST OF FIGURES

CHAPTER 1

INTRODUCTION

NASA is currently studying several large scale spacecraft formation missions, many to be flown at the Earth-Sun libration points. The location affords scientists a much clearer view of the universe, while providing a convenient gravitational pull enabling the formation to be Earth following. The Micro-Arcsecond X-ray Imaging Mission (MAXIM) [31] is an X-ray interferometer composed of up to 33 spacecraft and will be able to image the event horizon of a black hole. The Terrestrial Planet Finder (TPF) [4] mission shall enable scientists to find and study extra-solar planets similar to our own. While several designs are currently under review, a TPF design by Lockheed Martin is composed of four, possibly six, free flying spacecraft which will function as an infrared interferometer. The Stellar Imager (SI) [12] mission postulates that stellar activity is key to understanding life in the universe. Specifically, SI is a large, ultraviolet optical sparse aperture telescope/Fizeau Interferometer designed to study distant stars. The SI formation is designed to be flown at the Earth-Sun libration point, as is TPF. The design of SI requires a large array of satellites in an irregular placement in order to accomplish its goals.

The combination of interferometric sensing and high-N (N is the number of spacecraft in the formation) formations make these and similar missions especially challenging. Interferometry missions are especially challenging due to the high tolerance requirements. Such missions are currently slated to employ a multiple resolution control architecture: conventional thrusters and RF range and bearing sensors are to be used for coarse spacecraft control, and laser sensors and adaptive optics will provide fine optical path control [12, 31]. The Autonomous Formation

Flying sensor (AFF) has been identified as a key component for the coarse control component [2, 19]. The AFF provides range and bearing measurements between spacecraft based on GPS technology. Large formations of spacecraft present interesting challenges to the scientific community including: low fuel usage control for given precision requirements, fleet estimation given limited sensor and communication resources, and accurate reference point tracking to reduce fuel in the presence of the other challenges. Developing scalable algorithm tools is critical to the success of these missions.

Formation-based missions require an extremely high level of autonomy and robustness when compared to single spacecraft missions. This is especially true for dense, high-N formations, which naturally have a higher likelihood of collision, and those that are to be flown beyond earth-orbit, which are located too far from the Earth to allow for direct ground-based control. Further, it is likely that the individual spacecraft will have a limited amount of resources for sensing and communication. Some current formation navigation and control techniques that address these issues follow a leader-follower scheme [29]. These approaches are well known to be suboptimal and provide each spacecraft with only a limited picture of the full formation state. This lack of knowledge significantly degrades ability of the spacecraft to detect and avoid collisions.

Chapter 2 describes the development of a decentralized formation centroid estimation architecture that, when coupled with a local controller, parameterizes the degree to which a spacecraft is a leader or a follower, eliminating the rigid classification of spacecraft as strictly leaders or followers. Measurements are provided by a range/bearing sensor similar to the AAF sensor. A formation centroid calculation is introduced that automatically compensates for noise in the estimation and

sensing subsystems. The centroid calculation is shown to significantly improve the sensitivity, and therefore the reaction time, of the local controller to a collision scenario.

In the case where there are few or one AFF sensors on each spacecraft, a sensor scheduling algorithm is developed that maximizes the information collected across the formation. Chapters 2 and 3 describe solutions to the infinite horizon sensor scheduling problem. The scheduling problem is posed as an infinite horizon optimization of either the time-averaged formation information or covariance matrices, or the time-averaged formation centroid information or covariance matrices. An approximation allows the scheduling problem to be formulated as a mixed-integer quadratic program. This problem is initially solved using a standard quadratic programming solver for the unconstrained solution. The integer constraint is then satisfied by rounding this solution. Optimality of the rounding operation is improved by finding an integer-preserving linear transformation and rounding in the integer transformed space. The transformation is found as one that attempts to diagonalize the Hessian of the cost function. The resulting integrated sensing/control architecture is compared via Monte Carlo simulation to an ideal system where each spacecraft has full sensing capability of the entire fleet. Results show that performance degradation in terms of RMS position error and fuel usage is very small compared to the ideal, full knowledge solution, and that the system outperforms the traditional leader-follower architecture.

In Chapter 4 a communication subsystem is introduced that allows for the transmission of data between pairs of spacecraft. A distributed estimation system is developed that requires only the transmission of local state estimates from one spacecraft to the next in a circular manner about the formation. The state fusion

algorithm performed at each spacecraft is formulated as a least squares problem using the transmitted state estimate, the locally stored state estimate, and locally calculated covariance and cross-covariance matrices. Time delays in the communication subsystem are accounted for by storing previous estimates and associated covariance matrices at each spacecraft. Maneuvers in the form of thrust commands that are unknown to the spacecraft in the formation are accounted for by modeling such system inputs as Gaussian process noise. Results show that the resulting state estimates, while suboptimal (compared to an extended Kalman filter operating on the measurements), are statistically consistent and are always conservative with respect to the optimal extended Kalman filter. Monte Carlo simulations of the proposed estimator with a formation keeping controller in an eight spacecraft formation show that the formation exhibits good performance even in the presence of large single-hop time delays (20-30 s) in the communication subsystem.

CHAPTER 2

INFORMATION WEIGHTED REFERENCE POINT AND CONSTRAINED SENSOR SCHEDULING

2.1 Introduction

Typical single spacecraft systems are allowed to drift with respect to an external frame, as it is not crucial (and would be fuel expensive) to reposition the satellite with respect to a model-based reference track. Multiple satellite missions can relax the positioning of the formation in an external reference frame over small time horizons, but each individual spacecraft must control its relative position with respect to the fleet (using minumum fuel) for mission performance and safety [31, 4, 12]. In addition, it is unlikely that the spacecraft will have the ability to sense position in an external reference frame at a sufficiently high bandwidth to allow for control with respect to the external frame. Moreover, sensitivity of these factors grows with the number of spacecraft in the system. While formations of two or three spacecraft can be designed with full relative sensing and communication to the fleet, affording an accurate estimate the relative states of all spacecraft in the fleet, formations of sixteen or more spacecraft will certainly be constrained in the number of relative spacecraft measurements, as well as the number of communication links and available communication bandwidth. This, in turn, will have an effect on the system performance (relative position error and fuel usage) of each spacecraft in the formation.

The objective of the work in this Chapter is to develop a coordination architecture for future formations of spacecraft that is scalable in terms of integrated sensing and estimation, and control. More specifically, under the constraints of a

single range/bearing sensor, a relative control and estimation approach is developed that allows the formation as a whole to drift, thereby saving fuel, yet also attains very good relative positioning performance. Simulation results compared to the centralized solution show minimal degradation in terms of RMS positioning error and fuel usage. In addition, results compare favorably to current leader-follower concepts. Information filtering theory [24] is used to develop a sensor scheduling scheme for the AFF sensor. Maximizing information, or maximizing knowledge of the formation at each spacecraft in the cluster, is used to develop switching logic for relative sensing subsystem. The resulting GNC architecture can be considered to be *cyclic*, using the nomenclature introduced in the survey in Ref. [29].

In related work, the virtual center formation reference point algorithm was introduced in Ref. [30]. The algorithm is centralized based on the transmission of relative state estimates maintained across the fleet. The weights used are based on fuel reserve states, attempting to balance fuel usage across the fleet. The work in this Chapter includes a decentralized calculation of the virtual center, requiring very little communication. Also, the weights are based on the error covariance of the the state estimates, leading to a system that compensates for increased noise in the estimation and sensing subsystems, which can result from spacecraft occlusions and hardware failures. The decentralized LQG architecture introduced in Ref. [10] produces optimal performance for nonlinear plants and actuators using a communication architecture where all spacecraft communicate with one another. However, the resulting control law is suitable only for actuators that can produce continuous unbounded inputs to the plant. The control used in this Chapter is a time-optimal controller for accurate formation keeping using binary on/off thrusters[9].

The sensor scheduling problem was first introduced in Ref. [22]. The paper contained several variations of the problem and algorithms for solving for optimal sequences over short time horizons. The algorithm developed in Ref. [27] also produces an optimal schedule for short time horizons. A real time implementation a sliding window is used, where only the first measurement of the optimal schedule is taken and the process is repeated at each time step. Optimality, however, is not guaranteed over long time horizons. Reference [18] finds an infinite horizon measurement scheme by choosing measurements at random; the probability of choosing each sensor is determined by solving a set of Riccati equations. The scheduling algorithm described in the sequel produces an optimal periodic infinite horizon measurement schedule that can be determined *a priori*. That the optimal infinite horizon measurement schedule is periodic was first proposed in Ref. [15]. The optimal schedule in Ref. [15] is determined by generating sequences at random.

This Chapter is outlined as follows: Section 2.2 details the general formation keeping problem in terms of the system dynamics, available measurements and associated estimator, controller, and also includes assumptions and notation used throughout. Section 2.3 describes the information weighted virtual center estimation algorithm and describes the leader follower parameterization scheme. Section 2.4 introduces the sensor scheduling problem and a solution and simple example are presented in Section 2.5. Full simulation results are presented in Section 2.6 followed by conclusions in Section 2.7.

2.2 Problem Statement

The formation control problem addressed in this Chapter is motivated by SI-type missions and is formulated as follows: given a fleet of N spacecraft, each equipped with a single range/bearing sensor (RBS), find a sequence of measurements that adaptively maximizes, in some sense, knowledge of the fleet. Maximizing knowledge of the fleet directly benefits state error tracking, robustness and collision avoidance, and, in Section 2.6, is shown to indirectly benefit performance in terms of lowering fuel usage. Several assumptions are made: 1) the range/bearing generates bearing measurements expressed in the inertial reference frame, 2) the RBS is omni-directional, i.e. it can provide range and bearing measurements with a full spherical field of view at any range, 3) acquisition of signal at the RBS is instantaneous and measurements within the nominal range/bearing performance specifications of the AFF sensor (2cm, 1arcsec) as described in Ref. [2] are provided instantaneously, 4) thrust maneuvers at each spacecraft are transmitted over a communication subsystem to all other spacecraft, 5) second order free-space dynamics govern the system. Assumption 1 is reasonable as future missions will necessarily be equipped with high resolution inertial attitude sensors for the optics subsystem. Attitude uncertainties can be incorporated into the RBS noise terms. Assumption 4 is reasonable as binary thrust commands can be transmitted over data links with very low bandwidth. Assumption 5 has been found to be accurate for deep space missions on a 0.5-1 day horizon[28, 23]. The remaining assumptions shall be addressed at the end of the Chapter.

2.2.1 Spacecraft Dynamics

Each spacecraft is governed by second order dynamics, thus for N spacecraft, the discrete-time dynamics of the i-th spacecraft, $\forall\ i \in \{1, ..., N\}$, are as follows,

$$x_i(k+1) = Ax_i(k) + B_u u_i(k) + B_w w_i(k), \tag{2.1}$$

$$x_i(k) = \begin{bmatrix} x_i^{(1)}(k) \\ \dot{x}_i^{(1)}(k) \\ x_i^{(2)}(k) \\ \dot{x}_i^{(2)}(k) \end{bmatrix},\ u_i(k) = \begin{bmatrix} u_i^{(1)}(k) \\ u_i^{(2)}(k) \end{bmatrix},\ w_i(k) = \begin{bmatrix} w_i^{(1)}(k) \\ w_i^{(2)}(k) \end{bmatrix}, \tag{2.2}$$

$$A = \begin{bmatrix} 1 & \Delta T & 0 & 0 \\ 0 & 1 & 0 & 0 \\ 0 & 0 & 1 & \Delta T \\ 0 & 0 & 0 & 1 \end{bmatrix},\ B_u = B_w = \frac{1}{m} \begin{bmatrix} \Delta T^2/2 & 0 \\ \Delta T & 0 \\ 0 & \Delta T^2/2 \\ 0 & \Delta T \end{bmatrix}, \tag{2.3}$$

where x_i is the state of spacecraft i in an inertial frame, u_i is the control input, w_i is zero mean white process noise with covariance Q, m is the mass of each spacecraft (assumed to be identical for each spacecraft in the fleet) and ΔT is the sampling time. Two dimensional systems are presented here for simplicity but the approach is fully generalized to three dimensions. Without loss of generality, the process noise w_i and w_j are considered to be uncorrelated, i.e. $E\left[w_i(k)w_j(k)^T\right] = 0$.

Given the linear dynamics and the lack of an inertial position sensor, the i-th spacecraft maintains estimates of $N-1$ relative states. The relative dynamics are found by subtracting Eq. 2.1 from itself and replacing i with j,

$$x_{ji}(k+1) = Ax_{ji}(k) + B_u u_{ji}(k) + B_w w_{ji}(k), \tag{2.4}$$

$$\{x, u, w\}_{ji}(k) \triangleq \{x, u, w\}_j(k) - \{x, u, w\}_i(k)\ \forall\ j \neq i. \tag{2.5}$$

Note that this requires the mass of each spacecraft to be identical. This is for

simplicity; the following treatment can be easily modified when this is not the case. The key is that the state transition matrices are identical across the fleet eliminating the need for inertial states, and thus, inertial state measurements.

Equations 2.4 and 2.5 can be rewritten to yield a full set of dynamics *relative* to spacecraft i:

$$\mathbf{x}_i(k+1) = \mathbf{A}\mathbf{x}_i(k) + \mathbf{B_u}\mathbf{u}_i(k) + \mathbf{B_w}\mathbf{w}_i(k) \tag{2.6}$$

$$\{\mathbf{x},\mathbf{u},\mathbf{w}\}_i(k) \triangleq \begin{bmatrix} \vdots \\ \{x,u,w\}_{ji}(k) \\ \vdots \end{bmatrix}_{j\in\{1,\ldots,N\}\setminus i}, \tag{2.7}$$

$$\{\mathbf{A},\mathbf{B_u},\mathbf{B_w}\} \triangleq \begin{bmatrix} \{A,B_u,B_w\} & & \\ & \ddots & \\ & & \{A,B_u,B_w\} \end{bmatrix}. \tag{2.8}$$

Equation 2.7 is read as an augmented vector consisting of the $N-1$ relative vectors defined in Eq. 2.5 such that $\mathbf{x}_i \in \mathbb{R}^{4(N-1)}$ and $\{\mathbf{u}_i, \mathbf{w}_i\} \in \mathbb{R}^{2(N-1)}$. Similarly, Eq. 2.8 is block diagonal such that $\mathbf{A} \in \mathbb{R}^{4(N-1)\times 4(N-1)}$ and $\{\mathbf{B_u}, \mathbf{B_w}\} \in \mathbb{R}^{4(N-1)\times 2(N-1)}$. It follows from the assumptions that $\mathbf{w}_i$ is zero mean and its covariance is $E\left[\mathbf{w}_i(j)\mathbf{w}_i(k)^T\right] = \mathbf{Q}\delta_{jk}$ where,

$$\mathbf{Q} = \begin{bmatrix} 2Q & Q & \cdots & Q \\ Q & 2Q & & \vdots \\ \vdots & & \ddots & Q \\ Q & \cdots & Q & 2Q \end{bmatrix}. \tag{2.9}$$

The relative state vectors are shown conceptually in Figure 4.1.

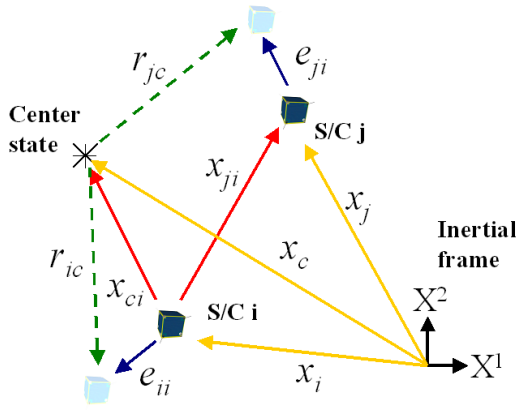

Figure 2.1: Virtual center state x_{ci} relative to spacecraft i, denoted by *. Also shown are reference states $r_{\cdot c}$, error states $e_{\cdot i}$ and relative state x_{ji}.

2.2.2 Virtual Center

For formation control, a reference state for each vehicle in the formation must be defined. Following Ref. [30], a *virtual center state*, x_c, is defined relative to the desired formation geometry in the inertial reference frame; a local frame centered at x_c is then defined such that the difference between the inertial frame and the virtual center frame is only a translation. A local reference frame at each spacecraft i is similarly defined and the location of the virtual center in the i-th local frame is denoted by $x_{ci} = x_c - x_i$, similar in notation to Eq. 2.5. Over relatively short time horizons, the formation is allowed to drift in the inertial frame. Therefore, it is sufficient to specify the reference states in the virtual center frame, denoted by $r_{ic} \in \mathbb{R}^4 \ \forall \ i \in \{1, ..., N\}$. The set of N reference states are arranged in a single column vector as follows:

$$\mathbf{r}(k) \triangleq \begin{bmatrix} r_{1c}(k) \\ \vdots \\ r_{Nc}(k) \end{bmatrix} \in \mathbb{R}^{4N}. \tag{2.10}$$

It is convenient to rearrange this vector for each spacecraft such that, for spacecraft i, its reference state appears first followed by the $N-1$ reference states of the remote spacecraft. Therefore,

$$\mathbf{r}_i(k) \triangleq \begin{bmatrix} r_{ic}(k) \\ \mathbf{r}_{ri}(k) \end{bmatrix}, \in \mathbb{R}^{4N} \; \mathbf{r}_{ri}(k) \triangleq \begin{bmatrix} \vdots \\ r_{jc}(k) \\ \vdots \end{bmatrix}_{j \in \{1,\ldots,N\}\backslash i} \in \mathbb{R}^{4(N-1)}. \tag{2.11}$$

These reference states are assumed to be known to each spacecraft in the system. The relative state, reference state and error state vectors in the given system are shown in Figure 2.1 for a small formation.

2.2.3 RBS Measurements

The measurements provided by the RBS are relative range and bearing to a remote spacecraft, each corrupted with white Gaussian noise. Thus, at each time step k, a measurement is made to one or more remote spacecraft,

$$\mathbf{z}_i(k) \triangleq \begin{bmatrix} \vdots \\ z_{ji}(k) \\ \vdots \end{bmatrix}_{j \in M_i(k)} = \mathbf{h}\left(\mathbf{x}_i(k), k\right) + \mathbf{v}_i(k) \tag{2.12}$$

$$z_{ji}(k) = h(x_{ji}(k)) + v_{ji}(k), \tag{2.13}$$

$$h(x_{ji}(k)) = \begin{bmatrix} R_{ji}(k) \\ \phi_{ji}(k) \end{bmatrix} = \begin{bmatrix} \sqrt{(x_{ji}^{(1)}(k))^2 + (x_{ji}^{(2)}(k))^2} \\ \tan^{-1} \frac{x_{ji}^{(2)}(k)}{x_{ji}^{(1)}(k)} \end{bmatrix}. \tag{2.14}$$

where v_{ji} is zero mean, white Gaussian noise with covariance R and $M_i(k) \subseteq \{1,\ldots,N\}\backslash i$ is the index set of measurements which may vary with time as selected by switching logic external to the sensor. Note that typically M_i contains only one element when each spacecraft is equipped with a single RBS. Because the spacecraft is also equipped with an inertial attitude sensor, the relative range/bearing

measurements are assumed to be made in the inertial frame without loss of generality; the statistical errors present in the attitude sensor are assumed to be built into the RBS noise covariance R. The sensor is assumed to be able to provide measurements at all ranges.

2.2.4 Extended Information Filter

At each spacecraft i, estimates of the relative states $\mathbf{x}_i$, denoted by $\hat{\mathbf{x}}_i$, are maintained via an extended information filter (EIF)[24]. The EIF is a convenient choice because it can be used to fuse measurements from multiple sensors and because the information matrix is used as a weight in the virtual center calculation described in Section 2.3. The filter is statistically equivalent to the extended Kalman filter and maintains an information state, $\hat{\mathbf{y}}_i(k \mid l) \triangleq \mathbf{Y}_i(k \mid l)\hat{\mathbf{x}}_i(k \mid l)$, and an information matrix,

$$\mathbf{Y}_i(k|l) \triangleq \left(E\left[\left(\mathbf{x}_i(k) - \hat{\mathbf{x}}_i(k \mid l)\right)\left(\mathbf{x}_i(k) - \hat{\mathbf{x}}_i(k \mid l)\right)^T \mid Z^l\right]\right)^{-1} \tag{2.15}$$

where $\hat{\mathbf{x}}_i(k|l)$ is the estimate of $\mathbf{x}_i(k)$ given the measurements up to and including time step l, denoted by Z^l. The EIF prediction and update steps are,

$$\hat{\mathbf{y}}_i(k|k-1) = \mathbf{Y}_i(k|k-1)\left[\mathbf{A}\hat{\mathbf{x}}_i(k-1|k-1) + \mathbf{B_u}\mathbf{u}_i(k)\right], \tag{2.16}$$

$$\mathbf{Y}_i(k|k-1) = (\mathbf{A}\mathbf{Y}_i^{-1}(k|k)\mathbf{A}^T + \mathbf{Q})^{-1}, \tag{2.17}$$

$$\begin{aligned}\mathbf{y}_i(k|k) &= \mathbf{y}_i(k|k-1) + \mathbf{C}_i(k)^T\mathbf{R}^{-1}(k)\mathbf{C}_i(k)\hat{\mathbf{x}}_i(k|k-1) \\ &\quad \mathbf{C}_i(k)^T\mathbf{R}^{-1}(k)\left[\mathbf{z}_i(k) - \mathbf{h}\left(\hat{\mathbf{x}}_i(k|k-1), k\right)\right],\end{aligned} \tag{2.18}$$

$$\mathbf{Y}_i(k|k) = \mathbf{Y}_i(k|k-1) + \mathbf{C}_i(k)^T\mathbf{R}^{-1}(k)\mathbf{C}_i(k), \tag{2.19}$$

where,

$$\mathbf{C}_i(k) = \begin{bmatrix} \vdots \\ C_{ji}(k) \\ \vdots \end{bmatrix}_{j \in M_i(k)} = \left. \frac{\partial \mathbf{h}}{\partial \mathbf{x}_i} \right|_{\hat{\mathbf{x}}_i(k|k-1)} . \tag{2.20}$$

A useful approximation to the time varying $C_{ji}(k)$ consists of evaluating the Jacobian at the formation reference states. That is,

$$\bar{C}_{ji} = \left. \frac{\partial h}{\partial x_{ji}} \right|_{r_{jc} - r_{ic}} . \tag{2.21}$$

Throughout the Chapter, an information matrix with a single argument, e.g. $\mathbf{Y}(k)$ will be used as shorthand for the updated information matrix, $\mathbf{Y}(k|k)$.

2.2.5 Time Optimal Controller

An optimal controller (minimum time) based on thrust limited ($u_i^{(\{1,2\})} \in \{-U_{max}, 0, U_{max}\}$) propulsion is used in the same vein as that developed in Ref. [9]. Because the satellite can be represented with second order free space dynamics in each axis (decoupled), a feed forward, formation keeping controller based on minimum time optimal control is developed. The controller is activated if the satellite drifts away from its reference position by more than an error ellipse, which is written as

$$\left[e_{ii}(k) \right]^T \left[\text{diag}\{ e_{max}^{(1)}, \dot{e}_{max}^{(1)}, e_{max}^{(2)}, \dot{e}_{max}^{(2)} \} \right] \left[e_{ii}(k) \right] > 1 \tag{2.22}$$

where $e_{max}^{(\cdot)}, \dot{e}_{max}^{(\cdot)}$ are tuning parameters and $e_{ii}(k) = x_{ci}(k) + r_{ic}(k)$. If this occurs, a minimum time controller is calculated in each axis. For second order dynamics, the minimum time controller is a bang-bang controller with a single switch. Thus,

the control is given by

$$u^{(\cdot)}(k) = \begin{cases} -\text{sgn}(e^{(\cdot)} + \dot{e}^{(i)}|\dot{e}^{(\cdot)}|/2)U_{max}, & 0 < k - k_o < T^{(\cdot)}_{mt1,i}/T \\ \text{sgn}(e^{(\cdot)} + \dot{e}^{(\cdot)}|\dot{e}^{(\cdot)}|/2)U_{max}, & T^{(\cdot)}_{mt1,i}/T < k - k_o < T^{(\cdot)}_{mtF,i}/T \end{cases} \tag{2.23}$$

where k_o is the time at the start of the maneuver. The switch time and final control time are written as

$$T^{(\cdot)}_{mt1,i} = \frac{-\dot{e}^{(\cdot)}_{ii}(k) \pm \sqrt{1/2(\dot{e}^{(\cdot)}_{ii}(k))^2 - e^{(\cdot)}_{ii}(k)\bar{U}_{max}}}{\bar{U}_{max}} \tag{2.24}$$

$$T^{(\cdot)}_{mtF,i} = \frac{-\dot{e}^{(\cdot)}_{ii}(k) \pm \sqrt{2(\dot{e}^{(\cdot)}_{ii}(k))^2 - 4e^{(\cdot)}_{ii}(k)\bar{U}_{max}}}{\bar{U}_{max}} \tag{2.25}$$

where $\bar{U}_{max} = U_{max}/m$. It is noted that other control methodologies, such as bounds on relative velocity, minimum fuel, etc. could be used, but this controller is sufficient to evaluate the proposed architecture.

2.3 Distributed Information Weighted Virtual Center

In Ref. [30], it is proposed that the virtual center state is calculated at each time step by minimizing a weighted squared error in the relative formation states under the assumption that minimizing the error minimizes the control effort required to

null the error. Relative to spacecraft i, the virtual center is written as,

$$x_{ci}^{*} = \arg\min_{x_{ci}} \mathbf{e}_i^T W_i \mathbf{e}_i, \tag{2.26}$$

$$\mathbf{e}_i = \begin{bmatrix} e_{ii} \\ \begin{bmatrix} \vdots \\ e_{ji} \\ \vdots \end{bmatrix}_{j\in\{1,\ldots,N\}\setminus i} \end{bmatrix} \in \mathbb{R}^{4N}, \tag{2.27}$$

$$e_{ii} = x_{ci} + r_{ic} \in \mathbb{R}^4, \tag{2.28}$$

$$e_{ji} = x_{ci} - (x_{ji} - r_{jc}) \in \mathbb{R}^4, \tag{2.29}$$

where W_i is an arbitrary symmetric weighting matrix. The errors e_{ji} are referred to as the remote error states and e_{ii} the local error state. In Ref. [30], the center state is maintained at a single spacecraft, e.g. spacecraft $i = 1$, and W_1 is related to the fuel reserve states of each spacecraft in the fleet. The error state of a spacecraft that has low fuel is given a higher weight than that of a spacecraft with higher fuel, reducing the error and thus the control effort of the low fuel spacecraft. This has the advantage of balancing fuel across the fleet, however this approach is centralized and communication intensive because spacecraft 1 must transmit the resulting center state to the fleet at each time step. Another disadvantage is that it relies on $N - 1$ accurate relative state estimates $\hat{\mathbf{x}}_1$ at spacecraft 1. Estimates of each relative state can be maintained at spacecraft 2 through N and transmitted to spacecraft 1 to reduce the computational load, however this would require additional communication bandwidth.

2.3.1 Distributed Virtual Center

A decentralized implementation of the virtual center algorithm is proposed here where each spacecraft in the fleet calculates a local estimate of the virtual center $\hat{x}_{ci} = E[x_{ci}] \ \forall \ i \in \{1, ...N\}$ based on relative state estimates using measurements generated by local sensors. If each spacecraft maintains $N-1$ noise-free relative states and uses identical weights ($W_i = I$), then the resulting center states are equivalent, i.e. $\hat{x}_{ci} + x_i = \hat{x}_{cj} + x_j \ \forall \ i, j \in \{1, ...N\}$, equivalent to the centralized implementation in Ref. [30]. This implementation, while decentralized, is infeasible as it requires $N-1$ noise-free range/bearing sensors.

Rewriting the center state in Eq. 2.26 at spacecraft i in terms of the $N-1$ relative state estimates, $\hat{\mathbf{x}}_i$, yields,

$$\hat{x}_{ci} = \arg\min_{x_{ci}} \left(\Phi x_{ci} - (\Gamma\hat{\mathbf{x}}_i - \mathbf{r}_i)\right)^T W_i \left(\Phi x_{ci} - (\Gamma\hat{\mathbf{x}}_i - \mathbf{r}_i)\right), \tag{2.30}$$

where

$$\Phi = \begin{bmatrix} I_4 \\ \vdots \\ I_4 \end{bmatrix}, \ \Gamma = \begin{bmatrix} 0_{4\times 4(N-1)} \\ I_{4(N-1)} \end{bmatrix}. \tag{2.31}$$

The well known solution to this linear least squares problem is:

$$\hat{x}_{ci} = \left(\Phi^T W_i \Phi\right)^{-1} \Phi^T W_i (\Gamma\hat{\mathbf{x}}_i - \mathbf{r}_i), \tag{2.32}$$

$$= (\sum_{j=1}^{N}\sum_{k=1}^{N}[W_i]_{jk})^{-1}\Phi^T W_i(\Gamma\hat{\mathbf{x}}_i - \mathbf{r}_i), \tag{2.33}$$

where $[\cdot]_{jk}$ denotes the jk-th 4-by-4 sub-block of $\cdot$. The covariance of the center

state is:

$$\begin{aligned}
\mathbf{P}_{ci} &= E\left[\left(x_{ci}-\hat{x}_{ci}\right)\left(x_{ci}-\hat{x}_{ci}\right)^{T}\right], && (2.34)\\
&= \left(\Phi^{T}W_{i}\Phi\right)^{-1}\Phi^{T}W_{i}\Gamma\mathbf{P}_{i}\Gamma^{T}W_{i}^{T}\Phi\left(\Phi^{T}W_{i}\Phi\right)^{-1}, && (2.35)\\
&= \left(\sum_{j=1}^{N}\sum_{k=1}^{N}[W_{i}]_{jk}\right)^{-1}\left(\sum_{j=1}^{N}\sum_{k=1}^{N}[W_{i}\Gamma\mathbf{P}_{i}\Gamma^{T}W_{i}^{T}]_{jk}\right)\cdot \\
&\quad \left(\sum_{j=1}^{N}\sum_{k=1}^{N}[W_{i}]_{jk}\right)^{-1}, && (2.36)
\end{aligned}$$

where $\mathbf{P}_i = \mathbf{Y}_i^{-1}$ is the covariance of the relative state estimates. Care must be taken when choosing the weights W_i because the covariance of the center state estimate can become large or infinite if the covariance of any of the relative states of the spacecraft are large or infinite, corresponding to poorly observed or unobserved remote spacecraft, which is an inherent trait of the system given the large number of spacecraft.

2.3.2 Information Weighted Virtual Center

The algorithm described in Section 2.3.1 can run locally at the spacecraft with any number of $n \leq N-1$ relative state estimates to solve for the virtual center. Thus, if any spacecraft are poorly observed, the corresponding entries in W_i can be set to zero in order to avoid numerical problems and to accurately calculate the virtual center. In the limiting case, where $n = 0$ at spacecraft i, the virtual center estimate reduces to $\hat{x}_{ci} = -r_{ic}$. In this case, the spacecraft does not perform any correcting maneuvers because the error state is $e_{ii} = \hat{x}_{ci} + r_{ic} = 0$. This idea can be generalized by incorporating the information content of the relative state estimates $\hat{\mathbf{x}}_i$, contained in $\mathbf{Y}_i$, in the weighting matrix W_i. In other words, states with high information (low uncertainty) are weighted more in the calculation. Because $\mathbf{Y}_i$

serves as a weight on only the remote error states $e_{ji}\ \forall\ j \in [1, N] \setminus i$, a weight on the local error state e_{ii}, denoted by G_i is introduced such that

$$W_i = \begin{bmatrix} G_i & \\ & \mathbf{Y}_i \end{bmatrix}. \tag{2.37}$$

This form of the weighting matrix has the benefit of preventing any poorly observed spacecraft from hindering the virtual center estimate. Substituting the above into Eqs. 2.33 and 2.36, and inverting Eq. 2.36 to yield the center state information matrix yields,

$$\hat{x}_{ci} = \left(G_i + \sum_{j=1}^{N-1} \sum_{k=1}^{N-1} [\mathbf{Y}_i]_{jk} \right)^{-1} \left(\Phi^T \mathbf{Y}_i \left(\hat{\mathbf{x}}_i - \mathbf{r}_{ri} \right) - G_i r_{ic} \right), \tag{2.38}$$

$$\mathbf{Y}_{ci} = \mathbf{P}_{ci}^{-1} = \left(G_i + \sum_{j=1}^{N-1} \sum_{k=1}^{N-1} [\mathbf{Y}_i]_{jk} \right) \left(\sum_{j=1}^{N-1} \sum_{k=1}^{N-1} [\mathbf{Y}_i]_{jk} \right)^{-1} \cdot \left(G_i + \sum_{j=1}^{N-1} \sum_{k=1}^{N-1} [\mathbf{Y}_i]_{jk} \right). \tag{2.39}$$

In this formulation, unobserved (poorly observed) spacecraft correspond to zero (near zero) information on the unobserved states, resulting in a zero (near zero) weight on those states in the virtual center calculation. In such a case, the order of the filter, and the order of the associated center state calculation, may be reduced to eliminate the states corresponding to the unobserved or poorly observed spacecraft. Such reductions, however can lead to an unstable formation. For instance, in a two spacecraft system, spacecraft 1 need not maintain a good estimate of the state of spacecraft 2 as long as spacecraft 2 is monitoring spacecraft 1; this is the typical leader follower scheme. However, if spacecraft 2 has a poor estimate of spacecraft 2, the spacecraft will drift apart. More detailed discussion of the connectivity requirements is given in the next section.

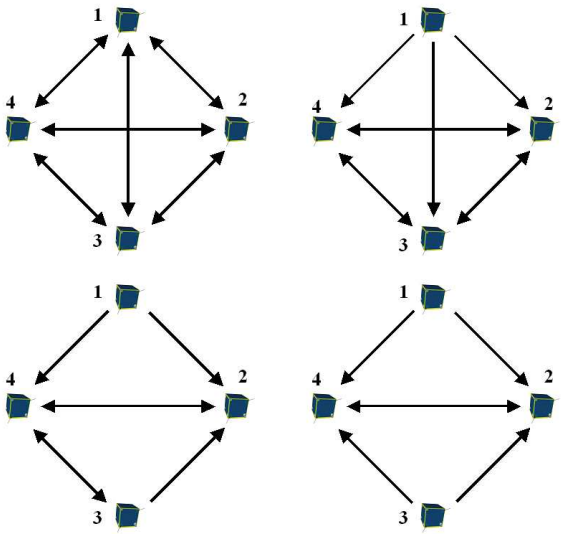

Figure 2.2: Control dependency graphs (CDG) for a four spacecraft system. The formation in the lower right is unstable as it consists of two independent leaders: spacecraft 1 and 3.

2.3.3 Interpretation of Information Weighting: Control Dependency Graph

Using the information matrix as a weight also has a direct effect on the control dependency graph (CDG). The CDG is a directed graph that illustrates the dependency of each local controller on the state of each spacecraft in the formation [29]. Typically, the dependencies are considered binary with respect to the local control laws: either there is or there is not a dependency. However, the virtual center calculation allows for a continuum of dependency that is based on the entries in the weighting matrices W_i. Considering spacecraft i, if the weight on the relative state of a particular spacecraft j tends to zero, then state x_{ji} does not factor into the calculation. If the same weight goes to infinity, then the virtual center approaches $x_{ji} - r_{jc}$ reducing spacecraft i to a simple follower of spacecraft j.

Consider the CDGs in Figure 2.2, where an arrow from spacecraft i to j denotes a dependency of the control on spacecraft j on the state of spacecraft i. The formation in the upper left results from $\mathbf{Y}_{ij} \neq 0$ and $G_i < \infty \; \forall \; i, j$. Spacecraft 1 is made a leader when $\mathbf{Y}_1 = 0$ (equivalently, $G_1 \to \infty$), resulting in the CDG in the upper right. Spacecraft 3 becomes a follower of spacecraft 4 when $\mathbf{Y}_{31} = \mathbf{Y}_{32} = 0, \; \mathbf{Y}_{34} \neq 0$, resulting in the CDG in the lower left. The formation in the lower right is unstable as both spacecraft 1 and 3 are leaders. In this case, the system as a whole is unstable, and therefore spacecraft 1 and 3 will begin to drift and the formation will stretch or contract depending on the relative motion of spacecraft 1 and 3. Spacecraft 2 and 4 will attempt, unsuccessfully, to maintain their desired relative states to both spacecraft 1 and 3. Such a fault is detectable at spacecraft 2 and 4 by evaluating the center state cost in Eq. 2.26. As the formation stretches or contracts, the center state cost will grow; if it reaches some threshold, a fault can be considered to have occurred and appropriate measures may be taken. These measures would consist of finding the source of the fault, of which the possibilities are numerous. The fault may be due to an error in the controller, or a bad actuator. It may also be due to errors in the inertial attitude determination subsystem. In cases such as these, if the fault cannot be corrected, the spacecraft should be removed from the formation and parked at a safe distance. If this is not possible, it may be necessary to move the formation to a safe distance while the problem is being addressed. If the problem lies within the sensing and estimation subsystem as described above, however, an algorithm can be developed that would traverse the CDG to find broken or weak links due to low information. If such links are found, the faulty spacecraft can attempt to reestablish the broken link by reinitializing the sensor/estimator, possibly with estimates that are communicated to it from other spacecraft, or the spacecraft can

be isolated from the formation while diagnostics can be performed.

These observations lead to a necessary, but not sufficient, condition for formation stability: that there exists at least one spacecraft from which there extends a path along the CDG to every other spacecraft in the formation. Stability in this case is defined as the formation being able to drive the relative error to zero in the local reference frame.

2.3.4 Hybrid Leader Follower Using G_i

The free weights G_i in Eq. 2.37 can also be used to control the degree to which each spacecraft "leads" or "follows" the fleet, thus allowing the designer to select a hybrid mix of leader-follower for each spacecraft. For example, in a two spacecraft system, and $G_1 = \infty$ and $G_2 = 0$, a leader follower scheme results where spacecraft 1 is the leader (drifts with no control) and 2 is the follower. It is proposed to define G_i in the general problem for N spacecraft as the following:

$$G_i = \frac{g_i}{N-1} \sum_{j=1}^{N-1} \sum_{k=1}^{N-1} [\mathbf{Y}_i]_{jk} + c \cdot I. \tag{2.40}$$

This term is an average of the weights on the $N-1$ remote error states (or equivalently, an average of the information of the remote relative states) weighted by g_i, and an additive weight $c \cdot I$. The constant $c \cdot I$ is necessary to keep the inverse in Eq. 2.38 from becoming singular; as such, c can be made relatively small. Substituting Eq. 2.40 into Eqs. 2.38 and 2.39, the resulting center state estimate and

information matrix at spacecraft i are

$$\begin{aligned}
\hat{x}_{ci} &= \left[c \cdot I + \left(1 + \frac{g_i}{N-1}\right) \sum_{j=1}^{N-1} \sum_{k=1}^{N-1} [\mathbf{Y}_i]_{jk}\right]^{-1} \times \\
&\quad \left[\Phi^T \mathbf{Y}_i \left(\hat{\mathbf{x}}_i - \mathbf{r}_{ri}\right) - \left(c \cdot I + \frac{g_i}{N-1} \sum_{j=1}^{N-1} \sum_{k=1}^{N-1} [\mathbf{Y}_i]_{jk}\right) r_{ic}\right] \qquad (2.41) \\
\mathbf{Y}_{ci} &= \left(1 + \frac{g_i}{N-1}\right)^2 \left(\sum_{j=1}^{N-1} \sum_{k=1}^{N-1} [\mathbf{Y}_i]_{jk}\right) + 2c(1 + \frac{g_i}{N-1})I + \\
&\quad c^2 \left(\sum_{j=1}^{N-1} \sum_{k=1}^{N-1} [\mathbf{Y}_i]_{jk}\right)^{-1} \qquad (2.42)
\end{aligned}$$

Note that as $\mathbf{Y}_i$ approaches zero, perhaps as a result of a failure of the RBS on spacecraft i and a lack of measurements provided to the EIF, $\mathbf{Y}_{ci}$ approaches ∞. Thus the center state estimate, $\hat{x}_{ci}$ approaches a constant $-r_{ic}$, as it should, and no control is spent.

The designer can now adjust g_i to fit mission specific needs. In missions such as SI, which consist of a single large hub spacecraft and $N-1$ smaller reflector spacecraft, it may be desirable to place a g_i on the hub spacecraft that is different from the reflector spacecraft, depending on the mission phase. If the formation is in the observation phase, it may be necessary to make the hub spacecraft an effective leader. This may also be the case if the system is designed such that the hub is responsible for stabilizing the orbit of the formation about L_2. The hub is made a leader by setting $q_{hub} = \infty$ during such orbit corrections. Given the position of the hub in the inertial frame, trajectories in the inertial frame for the follower spacecraft can easily be translated via the reference states $\mathbf{r}(k)$. Conversely, the weight on the hub spacecraft may be lowered during housekeeping activities.

The scalar g_i can also be used to incorporate the local fuel reserve state by allowing g_i to approach ∞ for low fuel, and some small value or zero for high fuel. As an example, the constant g_i could be chosen based on the function $g_i(F_i) =$

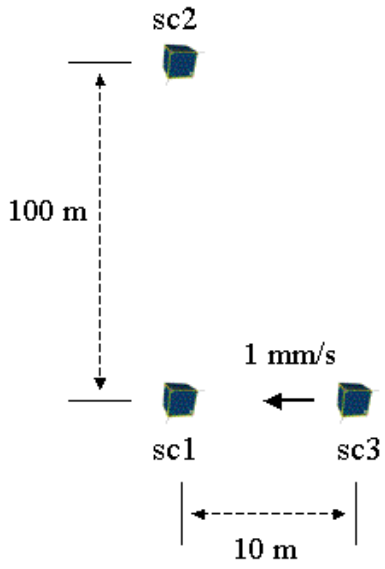

Figure 2.3: Collision scenario for evaluating the information weighted virtual center algorithm. Spacecraft 1 and 2 are stationary while spacecraft 3 approaches spacecraft 1 at a rate of 1 mm/s.

$a/F_i + b$ where $F_i \in [0, 1]$ is the normalized fuel reserve state, and a and b are tuning parameters that can be chosen, for example, by choosing g_i values when the spacecraft's fuel reserves are full, and half-full. Denoting these values respectively as q_i^{full} and q_i^{half} such that $g_i^{full} < g_i^{half}$ yields,

$$g_i(F_i) = \frac{g_i^{half} - g_i^{full}}{F_i} + 2g_i^{full} - g_i^{half}. \tag{2.43}$$

2.3.5 Collision Avoidance

An additional benefit of the information weighted virtual center is that the coupling of two spacecraft grows with decreasing range between the spacecraft. This is due to the increase in information in the nonlinear measurement with decreasing range. As a result is the increased information, the weight in the corresponding

virtual center increases, leading to increased sensitivity. Consider the formation in Figure 2.3. If each spacecraft is stationary and spacecraft 1 gets RBS measurements to spacecraft 2 and 3 at each time step, $\mathbf{Y}_1$ is considered to be block diagonal such that

$$\mathbf{Y}_1 = \begin{bmatrix} [\mathbf{Y}_1]_{22} & [\mathbf{Y}_1]_{23} \\ [\mathbf{Y}_1]_{23}^T & [\mathbf{Y}_1]_{33} \end{bmatrix} \tag{2.44}$$

where the subscripts denote the information in the estimate of the state spacecraft 2 or 3 relative to spacecraft 1. It can be shown that in steady state $[\mathbf{Y}_1]_{33} > [\mathbf{Y}_1]_{22}$ due to the relative proximity of spacecraft 3 to spacecraft 1. In this case, when solving for the virtual center $\hat{x}_{c1}$ as in Eq. 2.38, the effect of the error $e_{31} = x_{c1} - (\hat{x}_{31} - r_{3c})$ will be greater than the effect of the error $x_{c1} - (\hat{x}_{21} - r_{2c})$ and so the resulting x_{c1} will be more dependent on $\hat{x}_{31}$. This can be seen by the inspection of the term $\left(\Phi^T \mathbf{Y}_i \left(\hat{\mathbf{x}}_i - \mathbf{r}_{ri}\right) - G_i r_{ic}\right)$ in Eq. 2.38. Figure 2.4 shows that the collision is detected earlier in the information weighted center calculation as compared to the case where the unweighted virtual center is used.

2.4 Sensor Scheduling

Spacecraft in formation-based missions such as SI will most likely be equipped with only a single RBS, and therefore, only a single range/bearing measurement is provided at each time step. Thus, an algorithm is introduced which switches the measurements of the RBS among the spacecraft based on maximizing a function of the information matrix. Maximizing both the center state information and formation information is considered. The general sensor scheduling problem, first described in Ref. [22] has been addressed in many settings. Many approaches[18, 27, 22] attempt to find a schedule over a short time horizon and use heuristic algorithms

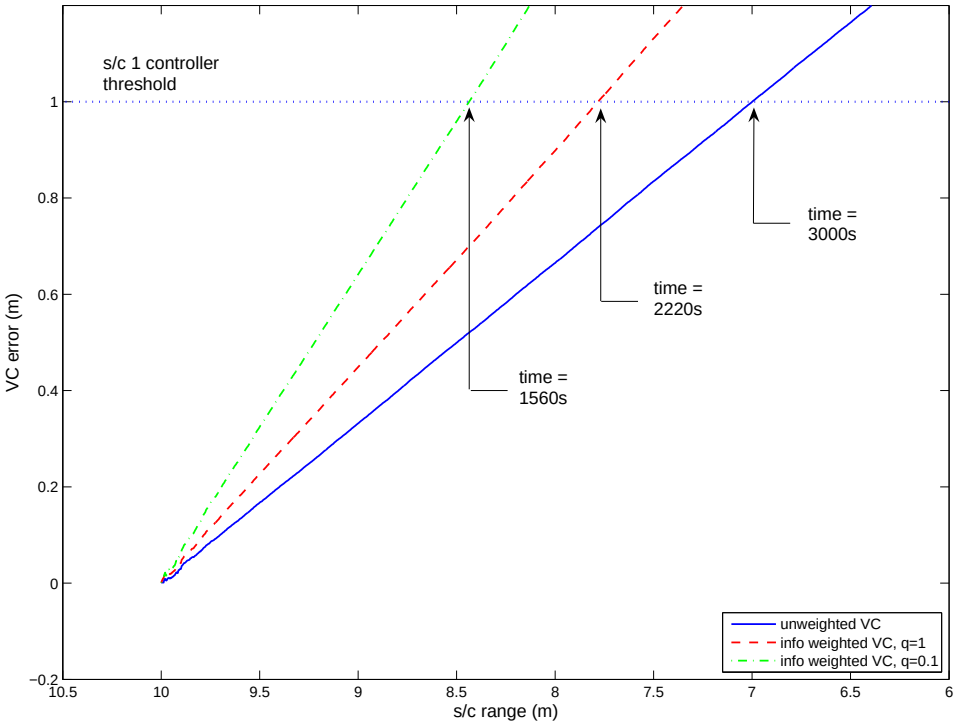

Figure 2.4: Higher information for the closer spacecraft leads to increased sensitivity to a collision.

to solve for optimal and near-optimal sequences. However, because most future spacecraft missions consider long time horizons with respect to the sampling rate, it is proposed here to pose the problem as finding a schedule that minimizes a function of the covariance (or information) in an infinite time horizon. If the optimal measurement schedule can be represented by a simple measurement control law or stored in a lookup table, less computation will be required to determine the measurement at each time step.

2.4.1 Infinite Time Sensor Scheduling Problem

Considering a single spacecraft (omitting the i subscripts) and a single measurement, the finite time horizon sensor scheduling problem is cast as minimizing a cost function,

$$J_{K_F} \triangleq \frac{1}{K_F} \text{ trace} \sum_{k=1}^{K_F} f(\mathbf{Y}(k)), \tag{2.45}$$

where $\mathbf{Y}(k)$ is the updated information matrix as a function of sensor selection decision variables. It evolves according to Eqs. 2.17 and 2.19 which can be simplified to an information form of the Riccati equation

$$\begin{aligned}\mathbf{Y}(k+1) = \mathbf{A}^{-T}\mathbf{Y}(k)\mathbf{A}^{-1} + \mathbf{C}(k)^T R(k)^{-1}\mathbf{C}(k) - \\ \mathbf{A}^{-T}\mathbf{Y}(k)\mathbf{A}^{-1}\mathbf{B_w}\left(\mathbf{B_w}^T\mathbf{A}^{-T}\mathbf{Y}(k)\mathbf{A}^{-1}\mathbf{B_w} + \mathbf{Q}^{-1}\right)^{-1}\mathbf{B_w}^T\mathbf{A}^{-T}\mathbf{Y}(k)\mathbf{A}^{-1}.\end{aligned} \tag{2.46}$$

The measurement matrices, $\mathbf{C}(k)$, are selected from the finite measurement set, $\mathbf{C}(k) \in \{\bar{C}_{ji} \mid j \in N_i\}$, with corresponding measurement noise covariances $R(k) \in \{R_{ji} \mid j \in N_i\}$ where N_i is an index set of available measurements, via the measurement control law $\boldsymbol{\mu}_{K_F} = \{\mu(1), ..., \mu(K_F)\}$ such that $\mu(k) \in N_i$ and $\mathbf{C}(k) = \bar{C}_{\mu(k)i}$. For the fleet estimation problem outlined in Section 2.2, the index set is the set of remote spacecraft measurements, $N_i = \{1, ..., N\} \setminus i$. Without loss of generality, the sensor noise covariance is assumed to be identical for all measurements and will be denoted by $\mathbf{R}$, i.e. $R_{ji} = R_{ki} = \mathbf{R}\ \forall\ j, k \in N_i$. Since what follows is dependent on a fixed number of (approximately) constant measurement matrices, the resulting scheduling algorithm is therefore appropriate only for fixed formations with constant reference states $\mathbf{r}$.

Several cost functions are considered, consisting of, respectively, maximizing the center state information (CI) and formation information (FI), and minimizing

the center state covariance (CC) and formation covariance (FC):

$$J_{K_F}^{CI} \triangleq -\frac{1}{K_F} \text{trace} \sum_{k=1}^{K_F} \Phi^T \mathbf{Y}(k) \Phi \tag{2.47}$$

$$J_{K_F}^{FI} \triangleq -\frac{1}{K_F} \text{trace} \sum_{k=1}^{K_F} \mathbf{Y}(k) \tag{2.48}$$

$$J_{K_F}^{CC} \triangleq \frac{1}{K_F} \text{trace} \sum_{k=1}^{K_F} \left(\Phi^T \mathbf{Y}(k) \Phi \right)^{-1} \tag{2.49}$$

$$J_{K_F}^{FC} \triangleq \frac{1}{K_F} \text{trace} \sum_{k=1}^{K_F} \mathbf{Y}(k)^{-1}. \tag{2.50}$$

The summation is important to give an average over the full period K. Note that the information costs $J_{K_F}^{CI}$ and $J_{K_F}^{FI}$ are defined in the negative to allow minimization.

The infinite time problem consists of minimizing $J_\infty^{(\cdot)} = \lim_{K_F \to \infty} J_{K_F}^{(\cdot)}$ with corresponding measurements $\boldsymbol{\mu}_\infty$. An analytical solution to this general problem has not yet been found. In a recent paper by Gupta and Murray [18], the sensor schedule is modeled as a random process such that at each time step, a measurement j is selected from the measurement set N_i with probability λ_j^r, with the constraint

$$\sum_{j \in N_i} \lambda_j^r = 1. \tag{2.51}$$

The algorithm in Ref. [18] solves for the set of probabilities that minimize an upper bound on the expected value of the covariance, which is determined by a set of Riccati-like equations. Although the algorithm produces the optimal λ_j^r, it converges only for stable systems and can be shown to be sub-optimal for the formation keeping problem. Consider the scheduling of a single RBS for a three spacecraft system, where spacecraft 1 and 2 are equidistant to spacecraft 3, which is estimating the virtual center based on measurements and estimates to spacecraft 1 and 2. Figure 2.5 shows the center state information for several random

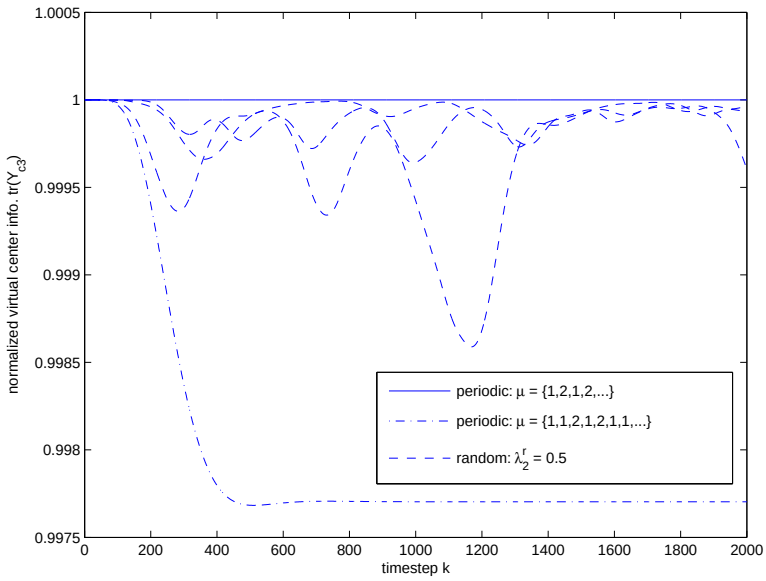

Figure 2.5: Comparison of periodic and random measurement sequences.

and periodic sequences. The figure shows that the instantaneous information of the random sequence is always less than that of the periodic sequence with measurement sequence $\boldsymbol{\mu} = \{1, 2, 1, 2, \ldots\}$.

2.4.2 Periodic Sensor Scheduling Problem

It is proposed that the optimal infinite horizon measurement sequence for any linear time invariant system is periodic. This was originally suggested in Ref. [15] and an algorithm to find the optimal periodic measurements based on generating sequences at random was developed. Here, the periodic formulation is posed as finding the periodic measurement sequence that minimizes $J_\infty^{(\cdot)}$. Thus for a given periodic measurement sequence,

$$\boldsymbol{\mu}_\infty = \{\bar{\boldsymbol{\mu}}_K, \bar{\boldsymbol{\mu}}_K, ...\},\ \bar{\boldsymbol{\mu}}_K = \{\bar{\mu}(0), \bar{\mu}(1), ..., \bar{\mu}(K-1)\}, \tag{2.52}$$

where K is the (dimensionless) period of the sequence, the resulting cost is

$$J_{\infty}^{(\cdot)} = \frac{1}{K} \text{ trace} \sum_{k=0}^{K-1} f(\mathbf{Y}^p(k_o + k)), \tag{2.53}$$

where $\mathbf{Y}^p(k)$ is a steady state periodic information matrix which is found by solving a periodic Riccati equation [7], k_o is an arbitrary constant and f corresponds to the variants in Eqs. 2.47-2.50.

The information resulting from a periodic measurement sequence can be determined by a modified algebraic Riccati equation. Using the periodic identity $C(k) = C(\tau K + k)\ \forall\ \tau, k \in \{0, 1, ...\}$, the periodic system is represented by the time-invariant dynamics,

$$\begin{aligned}
\tilde{\mathbf{x}}(\tau+1) &= \tilde{\mathbf{A}}\tilde{\mathbf{x}}(\tau) + \tilde{\mathbf{B}}_{\mathbf{w}}\tilde{\mathbf{w}}(\tau), && (2.54)\\
\tilde{\mathbf{z}}(\tau) &= \tilde{\mathbf{C}}_{\tau K}\tilde{\mathbf{x}}(\tau) + \tilde{\mathbf{D}}_{\tau K}\tilde{\mathbf{w}}(\tau-1) + \tilde{\mathbf{v}}(\tau), && (2.55)\\
\tilde{\mathbf{x}}(\tau) &\triangleq \mathbf{x}(\tau K), && (2.56)\\
\tilde{\mathbf{w}}(\tau) &\triangleq \begin{bmatrix} \mathbf{w}(\tau K)^T & \cdots & \mathbf{w}(\tau K + K - 1)^T \end{bmatrix}^T, && (2.57)\\
\tilde{\mathbf{z}}(\tau) &\triangleq \begin{bmatrix} \mathbf{z}(\tau K - (K-1))^T & \cdots & \mathbf{z}(\tau K)^T \end{bmatrix}^T, && (2.58)\\
\tilde{\mathbf{v}}(\tau) &\triangleq \begin{bmatrix} \mathbf{v}(\tau K - (K-1))^T & \cdots & \mathbf{v}(\tau K)^T \end{bmatrix}^T, && (2.59)\\
\tilde{\mathbf{A}} &\triangleq \mathbf{A}^K, && (2.60)\\
\tilde{\mathbf{B}}_{\mathbf{w}} &\triangleq \begin{bmatrix} \mathbf{A}^{K-1}\mathbf{B}_{\mathbf{w}} & \mathbf{A}^{K-2}\mathbf{B}_{\mathbf{w}} & \cdots & \mathbf{B}_{\mathbf{w}} \end{bmatrix}, && (2.61)\\
\tilde{\mathbf{C}}_k &\triangleq \begin{bmatrix} \mathbf{C}(k-(K-1))\mathbf{A}^{-(K-1)} \\ \mathbf{C}(k-(K-2))\mathbf{A}^{-(K-2)} \\ \vdots \\ \mathbf{C}(k) \end{bmatrix}, && (2.62)\\
\left[\tilde{\mathbf{D}}_k\right]_{ij} &\triangleq \begin{cases} -\mathbf{C}(k-(K-i))\mathbf{A}^{i-j}\mathbf{B}_{\mathbf{w}} & \text{if } i < j \\ 0 & \text{otherwise} \end{cases} && (2.63)
\end{aligned}$$

The matrices in Eqs. 2.54 and 2.55 are time invariant with respect to τ when the system dynamics are time invariant and the measurements are periodic with period K. Thus an EIF can be run on the system represented by Eqs. 2.54 and 2.55 and will yield an identical estimate and information matrix as when running the EIF on the system represented by Eqs. 2.6 and 2.12. The information matrix prediction step is,

$$\tilde{\mathbf{Y}}(\tau+1|\tau) = \left(\tilde{\mathbf{A}}\tilde{\mathbf{Y}}(\tau|\tau)^{-1}\tilde{\mathbf{A}}^T + \tilde{\mathbf{B}}_{\mathbf{w}}\tilde{\mathbf{Q}}\tilde{\mathbf{B}}_{\mathbf{w}}^T\right)^{-1} \tag{2.64}$$

where $\tilde{\mathbf{Q}} \triangleq \text{diag}(\mathbf{Q}, \ldots, \mathbf{Q})$. This equation is the standard EIF prediction equation analogous to Eq. 2.17. However, the $\tilde{\mathbf{D}}_{\tau K}\tilde{\mathbf{w}}(\tau-1)$ term in Eq. 2.55 leads to a non-standard update step

$$\begin{aligned}\tilde{\mathbf{Y}}(\tau+1|\tau+1) = \tilde{\mathbf{Y}}(\tau+1|\tau) + \left(\tilde{\mathbf{C}}_{\tau K}^T + \tilde{\mathbf{Y}}(\tau+1|k)\tilde{\mathbf{S}}_{\tau K}\right)\cdot \\ \left(\tilde{\mathbf{R}} + \tilde{\mathbf{D}}_{\tau K}\tilde{\mathbf{Q}}\tilde{\mathbf{D}}_{\tau K}^T + \tilde{\mathbf{S}}_{\tau K}^T\tilde{\mathbf{Y}}(\tau+1|\tau)\tilde{\mathbf{S}}_{\tau K}\right)^{-1}\left(\tilde{\mathbf{C}}_{\tau K}^T + \tilde{\mathbf{Y}}(\tau+1|\tau)\tilde{\mathbf{S}}_{\tau K}\right)^T\end{aligned} \tag{2.65}$$

where $\tilde{\mathbf{S}}_{\tau K} \triangleq \tilde{\mathbf{B}}_{\mathbf{w}}\tilde{\mathbf{Q}}\tilde{\mathbf{D}}_{\tau K}^T$ and $\tilde{\mathbf{R}} \triangleq \text{diag}(\mathbf{R}, \ldots, \mathbf{R})$. The information matrix $\tilde{\mathbf{Y}}(\tau|\tau)$ is the information matrix corresponding to the state estimate $\mathbf{x}(\tau K)$, i.e. $\tilde{\mathbf{Y}}(\tau|\tau) = \mathbf{Y}(\tau K)$.

2.5 Numerical Solution

The cost associated with a given sequence $\bar{\boldsymbol{\mu}}_K$ can be determined by combining Eqs. 2.64 and 2.65 and setting $\tilde{\mathbf{Y}}(\tau+1|\tau+1) = \tilde{\mathbf{Y}}(\tau|\tau) = \mathbf{Y}^p(\tau K)$, solving for $\mathbf{Y}^p(\tau K)$ and propagating the result forward $K-1$ times via Eq. 2.46 to solve for $\mathbf{Y}^p(\tau K+i), i \in \{1, \ldots, K-1\}$. Finding the optimal $\bar{\boldsymbol{\mu}}_K$ using an exhaustive search would require repeating this process $|N_i|^K$ times, where typically $|N_i| = N-1$ if all spacecraft are observed. This could be computationally expensive for large N or K.

A relaxation of the scheduling problem can be shown to be convex in a set of variables which correspond to the number of measurements made to each spacecraft, normalized by the period K. These variables are denoted by λ_j where $\lambda_j = |\{k \mid \bar{\boldsymbol{\mu}}_K(k) = j\}|/K \ \forall \ j \in N_i$ and each λ_j represents a quantity similar to the λ_j^r defined in Ref. [18] where each λ_j can be interpreted as a duty cycle value. For example, if measurements are being made to two spacecraft, denoted by 1 and 2, and if $\lambda_1 = 0.1$ and $\lambda_2 = 0.9$ then 10% of the duty is spent measuring range and bearing to spacecraft 1 and 90% is spent on spacecraft 2. The set of λ_j shall be denoted by Λ such that $\Lambda \triangleq \{\lambda_j \mid j \in N_i\}$. Clearly, $\sum_{j \in N_i} \lambda_j = 1$ and $\lambda_j K$ is constrained to be an integer such that $\lambda_j \in \{0, 1/K, 2/K, \ldots, 1\}$. If the integer constraint is relaxed such that $\lambda_j \in [0, 1]$, then the optimal set of duty cycles can be found by solving a linear matrix inequality (LMI) problem. Note that there are many sequences $\bar{\boldsymbol{\mu}}_K$ which satisfy a given Λ.

Based on the convexity of the relaxed version of the scheduling problem, a two-level algorithm is developed to solve for the optimal measurement schedule for a given K: (1) a (non-exhaustive) steepest descent search over the set of all possible Λ and (2) for each Λ a (non-exhaustive) search over all possible $\bar{\boldsymbol{\mu}}_K$. The remainder of this section consists of a description of this algorithm and the results of the algorithm as applied to a simple system consisting of three spacecraft. Denoted by 1,2 and 3, spacecraft 3 is equipped with a single RBS. The spacecraft are nominally located at the vertices of an equilateral triangle in the x-y plane such that spacecraft 3 is at the origin, spacecraft 1 is located 50 m from spacecraft 3 at a bearing of $-\pi/6$ rad from the y-axis, and spacecraft 2 is located 50 m from spacecraft 3 at a bearing of $+\pi/6$ rad from the y-axis. This example is used to explore the trends and solutions associated with the sensor scheduling problem. It should be noted that the trends described in this section have been observed for

larger and more complex systems.

Section 2.5.1 outlines the steepest descent search algorithm for the optimal Λ on the relaxed version of the problem, Section 2.5.2 presents a modification of the steepest descent search algorithm to find the true cost using three different methods of finding a suitable measurement sequence $\bar{\boldsymbol{\mu}}_K$, and Section 2.5.3 is a modified version of the algorithm that allows for a constraint on the minimum switching time of the RBS.

2.5.1 Duty Cycle Search (DCS)

For a fixed Λ, the LMI solution to the relaxed version of the problem can be rewritten as the solution to the Riccati equation

$$\begin{aligned}\hat{\mathbf{Y}} &= \tilde{\mathbf{A}}^{-T}\hat{\mathbf{Y}}\tilde{\mathbf{A}}^{-1} + K\hat{\mathbf{I}} - \\ &\quad \tilde{\mathbf{A}}^{-T}\hat{\mathbf{Y}}\tilde{\mathbf{A}}^{-1}\tilde{\mathbf{B}}_{\mathbf{w}}\left(\tilde{\mathbf{B}}_{\mathbf{w}}^{T}\tilde{\mathbf{A}}^{-T}\hat{\mathbf{Y}}\tilde{\mathbf{A}}^{-1}\tilde{\mathbf{B}}_{\mathbf{w}} + K\tilde{\mathbf{Q}}^{-1}\right)^{-1}\tilde{\mathbf{B}}_{\mathbf{w}}^{T}\tilde{\mathbf{A}}^{-T}\hat{\mathbf{Y}}\tilde{\mathbf{A}}^{-1} \quad (2.66)\end{aligned}$$

where

$$\hat{\mathbf{Y}} = \sum_{i=0}^{K-1}\mathbf{Y}^{p}(\tau K + i) \quad (2.67)$$

$$\hat{\mathbf{I}} = \sum_{j\in N_i}\lambda_j\bar{\mathbf{I}}_j \quad (2.68)$$

$$\bar{\mathbf{I}}_j = \sum_{i=0}^{K-1}(\mathbf{A}^{-i})^{T}C_j^{T}R^{-1}C_j\mathbf{A}^{-i} \quad (2.69)$$

with cost

$$\hat{J}_{\infty}^{(\cdot)} = \frac{1}{K}\,\mathrm{trace}f(\hat{\mathbf{Y}}), \quad (2.70)$$

Given the convexity of the relaxed problem in Λ, a steepest descent search algorithm is developed, shown in Algorithm 1. The convexity over the unconstrained

Λ guarantees convergence for small step size $\Delta\lambda$, however, the algorithm may converge slowly. For faster convergence, the step size may be set to $1/K$, which has the added benefit of satisfying the integer constraint on Λ.

Algorithm 1: Steepest Descent Search Algorithm for Optimal Duty Cycles

procedure GRADMINCOST(Λ_0)
  $\Lambda^* \leftarrow \Lambda_0,\ J^* \leftarrow \infty,\ m \leftarrow 1$
  while done = FALSE **do**
    $\Lambda^m \leftarrow \Lambda^*$, done $\leftarrow$ TRUE
    for $j, k \in N_i, j \neq k$ **do**
      $\Lambda^{m+1} \leftarrow \Lambda^m$
      $\lambda_j^{m+1} \leftarrow \lambda_j^{m+1} + \Delta\lambda$
      $\lambda_k^{m+1} \leftarrow \lambda_k^{m+1} - \Delta\lambda$
      $J^{m+1} \leftarrow \hat{J}_\infty^{(\cdot)}(\Lambda^{m+1})$
      if $J^{m+1} < J^*$ **then**
        $\Lambda^* \leftarrow \Lambda^{m+1}, J^* \leftarrow J^{m+1}$, done $\leftarrow$ FALSE
      end if
    end for
    $m \leftarrow m + 1$
  end while
end procedure

function $J = \hat{J}_\infty^{(\cdot)}(\Lambda)$
  Solve Eq. 2.66 for $\hat{\mathbf{Y}}$
  $J \leftarrow$ trace $f(\hat{\mathbf{Y}})/K$
end function

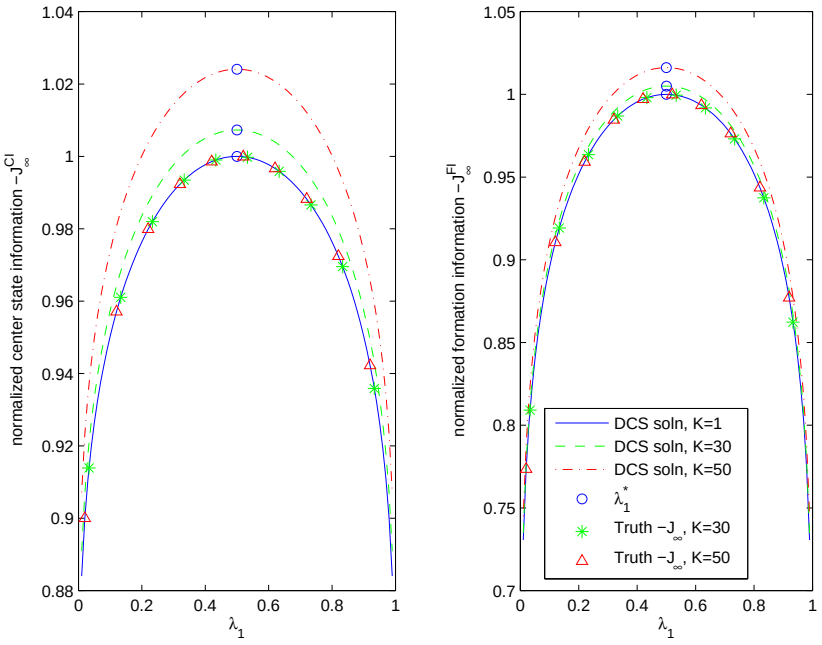

Figure 2.6: DCS results for $K = 1, 30, 50$. Shown is the optimal λ_1^* found for each case using DCS, the relaxed cost $\hat{J}_\infty^{(\cdot)}$ for all Λ and and the truth cost $J_\infty^{(\cdot)}$ found by the solution to the Riccati equation described in Section 2.5.2.

Figure 2.6 shows the results of the algorithm for the duty cycles Λ on the three spacecraft system using the information-based cost functions J_∞^{CI} and J_∞^{FI}. Because of the constraint $\lambda_1 + \lambda_2 = 1$, the cost as a function of only λ_1 is shown. The increase in information with K for the DCS case is due to the lack of the cross-covariance terms in the LMI-based cost. The results suggest that, although K is always necessarily greater than 1, it is sufficient to solve the LMI for $K = 1$ because the solution for Λ are identical for each K and yield cost that is closest to the truth solution. This is advantageous because the dimension of $\tilde{\mathbf{Q}}$ in Eq. 2.66 grows with increasing K. The resulting Λ can be rounded up or down to meet the integer constraint and can then be used as an initial guess for the SS algorithm.

2.5.2 Sequence Search

The convexity of the relaxed version of the problem as described in the previous section suggests that a steepest descent search algorithm may be used for the full problem as well. The Sequence Search (SS) algorithm is therefore identical to the DCS algorithm in Algorithm 1 with the exception of the cost function evaluation in line 9. For the SS algorithm, this function consists of choosing a sequence $\bar{\boldsymbol{\mu}}_K$ which satisfies the duty cycles Λ and evaluating the cost $J_\infty^{(\cdot)}$ by solving Eqs. 2.64 and 2.65 for the steady state periodic information matrix $\mathbf{Y}^p(\tau K)$, propagating the result via Eq. 2.46 to find $\mathbf{Y}^p(\tau K + i)$ for $i \in \{1, \ldots, K-1\}$ and Eq. 2.53 to find the cost. Clearly, for the SS algorithm it is necessary to set $\Delta\lambda = 1/K$. This modification is shown in Algorithm 2.

Algorithm 2: Sequence Search Cost Function for the Steepest Descent Search Algorithm

1: **function** $J = J_\infty^{(\cdot)}(\Lambda)$
2: Generate $\bar{\boldsymbol{\mu}}_K$
3: Solve Eqs. 2.64 and 2.65 for $\mathbf{Y}^p(\tau K)$
4: Find $\mathbf{Y}^p(\tau K + i)$ for $i \in \{1, \ldots, K-1\}$ via Eq. 2.46
5: $J \leftarrow \left[\text{trace} \sum_{k=0}^{K-1} f(\mathbf{Y}^p(\tau K + k))\right] / K$
6: **end function**

The SS algorithm requires a specific measurement sequence for a given Λ. There are, however, many sequences that yield the same Λ. In the three spacecraft example, let $K = 6$ and consider the measurement sequence on spacecraft 3 such that $\Lambda = \{\lambda_1, \lambda_2\} = \{0.5, 0.5\}$. Three sequences that match these parameters are: $\{1, 2, 1, 2, 1, 2\}$, $\{1, 1, 1, 2, 2, 2\}$ and $\{1, 1, 2, 2, 1, 2\}$. There are others, but these three are of interest because they are considered, in some sense, to be the fastest,

Table 2.1: Inter-sampling times Δk_j and sequence variances $\sigma^2,\ \sigma^2_{tot}$ for several measurement sequences.

$\bar{\boldsymbol{\mu}}$	$\Delta k_1 = \Delta k_2$	$\sigma^2(\Delta k_1) = \sigma^2(\Delta k_2)$	$\sigma^2_{tot}(\bar{\boldsymbol{\mu}})$
$\{1,2,1,2,1,2\}$	$\{2,2,2\}$	0	0
$\{1,1,2,2,1,2\}$	$\{1,2,3\}$	0.67	1.33
$\{1,1,1,2,2,2\}$	$\{1,1,4\}$	2	4

the slowest and intermediate, respectively. In order to quantify the switching speed, a variance in the sampling times to each spacecraft is defined. For a given sequence $\bar{\boldsymbol{\mu}}_K$, the set of times between each sample to spacecraft j is

$$\Delta k_j = \{n - m \ :\ \mu(m) = \mu(n) = j,\ \mu(p) \neq j\ \forall\ m < p < n\} \tag{2.71}$$

The mean of these inter-sample times is clearly $1/\lambda_j$ and $|\Delta k_j| = K\lambda_j$. For a given Λ, the variance of the entire sequence is the sum of the variances of the individual inter-sampling times to each spacecraft:

$$\sigma^2_{tot}(\bar{\boldsymbol{\mu}}) = \sum_{j\in N_i} \sigma^2(\Delta k_j) = \sum_{j\in N_i} \left[\frac{1}{K\lambda_j} \sum_{n=1}^{K\lambda_j} \left(\Delta k_j(n) - \frac{1}{\lambda_j} \right)^2 \right], \tag{2.72}$$

where $\Delta k_j(n)$ is the n-th element in Δk_j. This quantity is easily computed for periodic sequences. Table 2.1 shows Δk_j and σ^2_{tot} for the three sequences.

Figure 2.7 illustrates the change in cost with σ^2_{tot} for sequences with varying K. Three types of sequences are considered:

- Slow switching: all measurements are grouped together, e.g. $\bar{\boldsymbol{\mu}} = \{1,1,\ldots,2,2,\ldots,3,3,\ldots\}$,
- Fast switching: the sequence which minimizes σ^2_{tot} for each K, and
- Random switching: randomly generated sequences which satisfy the duty cycles Λ.

While the plot shows that the mean covariance J_{∞}^{FC} is not monotonically decreasing with decreasing σ_{tot}^2, the minimum cost for this case occurs when $\sigma_{tot}^2 = 0$. This property has been seen in all other examples the authors have explored, including many higher order problems (i.e. larger N and K). This understanding is clearer still when considering the slow switching case (σ_{tot}^2 large). In this case, as K increases only a single spacecraft is observed for an increasingly long period of time. In the limit, as K approaches infinity only a single spacecraft is observed and the information on all other spacecraft will go to zero, resulting in a high cost. Conversely, for fast switching, as K increases the cost can be made at least as small as the cost found for smaller K. Consider the optimal sequence for some fixed K, denoted by $\bar{\boldsymbol{\mu}}_K^*$. For a period length of $2K$, $3K$, etc., the sequences $\{\bar{\boldsymbol{\mu}}_K^*, \bar{\boldsymbol{\mu}}_K^*\}$, $\{\bar{\boldsymbol{\mu}}_K^*, \bar{\boldsymbol{\mu}}_K^*, \bar{\boldsymbol{\mu}}_K^*\}$, etc., will yield the same cost (as well as the same σ_{tot}^2). This places an upper bound on the cost for large K which will be lower than the cost associated with the slow switching case. Finally, for random switching, as K approaches infinity, the switching sequence approaches the random sequence found by the algorithm presented in Ref. [18].

This suggests that for systems with larger K or N, the optimal sequence may be found by minimizing σ_{tot}^2. An exhaustive search for the sequence with the minimum sampling variance would be computationally prohibitive for large K and N, however a fast switching sequence with minimum or near-minimum sampling variance can be found in a manner similar to the integer steepest descent search algorithm described above. Starting with an initial sequence $\bar{\boldsymbol{\mu}}_K^0$ the algorithm proceeds by swapping measurements for each pair of time instances $k_1, k_2 \in \{0, \cdots, K-1\}$ and evaluates the variance in Eq. 2.72. The sequence is updated by swapping the pair of measurements that yields the greatest decrease in variance, and the algorithm repeats until a minimum is achieved.

Algorithm 3: Sequence Search Algorithm for Fast Measurement Sequences

function $\bar{\mu}^*(\bar{\mu}_0)$
    $\bar{\mu}^* \leftarrow \bar{\mu}_0,\ J^* \leftarrow \infty,\ m \leftarrow 1$
    while done = FALSE **do**
        $\bar{\mu}^m \leftarrow \bar{\mu}^*$, done $\leftarrow$ TRUE
        for $j, k \in \{1, \ldots, K\}, j \neq k$ **do**
            $\bar{\mu}^{m+1} \leftarrow \bar{\mu}^m$
            $\bar{\mu}^{m+1}(j) \leftarrow \bar{\mu}^m(k)$
            $\bar{\mu}^{m+1}(k) \leftarrow \bar{\mu}^m(j)$
            $J^{m+1} \leftarrow$ result of Eq. 2.72
            if $J^{m+1} < J^*$ **then**
                $\bar{\mu}^* \leftarrow \bar{\mu}^{m+1}, J^* \leftarrow J^{m+1}$, done $\leftarrow$ FALSE
            end if
        end for
        $m \leftarrow m + 1$
    end while
end function

2.5.3 Constrained Sequence Search

The scheduling algorithm is extended to allow for a constraint on the minimum switching time of the RBS. The SS steepest descent search algorithm is modified to produce the optimal measurement schedule based on two parameters: K, the integer number of time steps in the periodic sequence, and K_{min}, the minimum switching time of the sensor, also in time steps. The algorithm proceeds in the

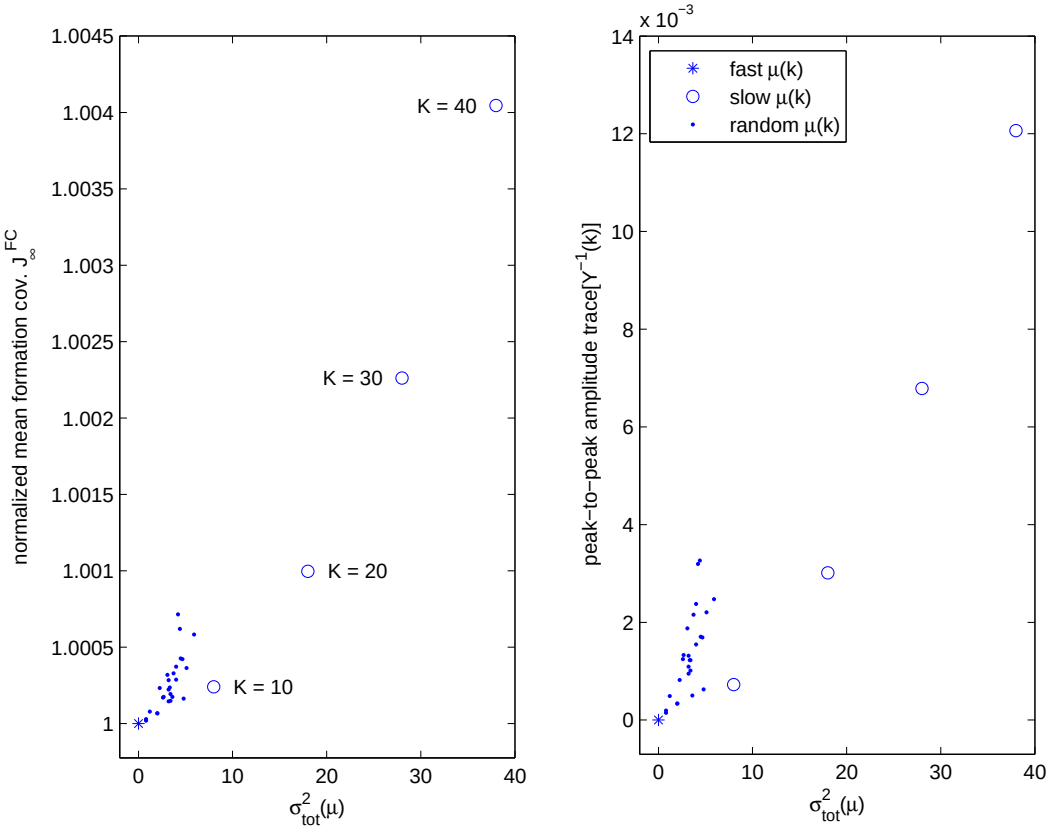

Figure 2.7: Shown is the resulting formation mean covariance J^{FC} and peak-to-peak relative amplitude of trace $(\mathbf{Y}^{-1}(k))$ for the three spacecraft system for various K where $\Lambda = \{1/2, 1/2\}$. The peak-to-peak relative amplitude is $(\max_k [\text{trace}\,(\mathbf{Y}^{-1}(k))] - \min_k [\text{trace}\,(\mathbf{Y}^{-1}(k))])\,/\,J^{FC}$.

same manner as SS and DSC, with the added constraint that $\lambda_i \geq K_{min}/K$. The implementation of the sequence generating algorithm is easily modified to account for the minimum switching time. As with the slow switching case, a decrease in performance is expected for increasing K_{min}. Figure 2.8 shows the center state information with increasing K_{min}, demonstrating this effect.

Figure 2.9 shows the effect of varying K and K_{min} on a modified version of the three spacecraft example. In this example, spacecraft 2 is nominally located 100 m from spacecraft 3 and remains at a bearing of $+\pi/6$ rad. Larger K_{min} requires

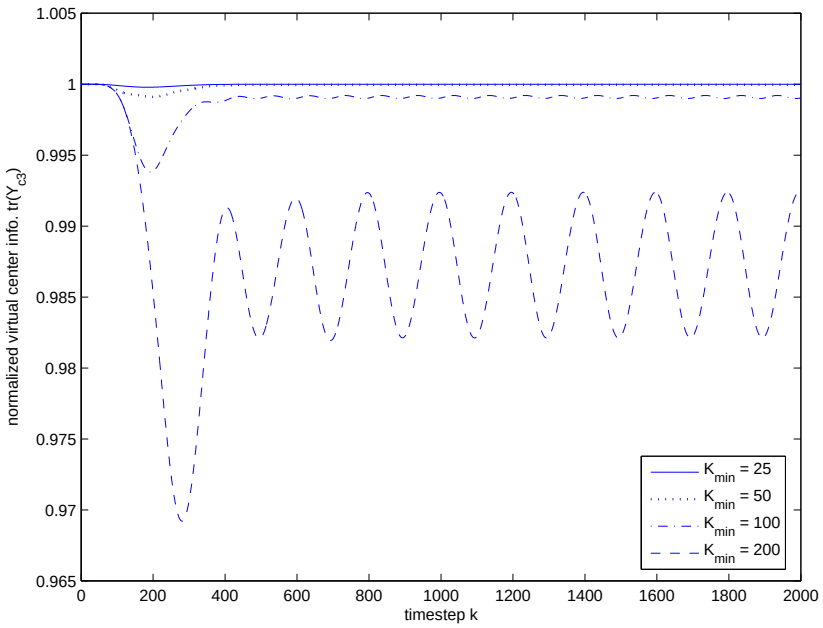

Figure 2.8: Mean information decreases with increasing K_{min} and peak-to-peak amplitude increases for $K = 1000$.

larger K in order to achieve higher mean information. Note that λ_1^* is always within $1/K$ of the optimal λ_1 as determined by the faster DCS algorithm. Figure 2.10 shows the optimal measurement sequences for each K_{min} when $K = 64$.

2.6 Simulation Results

An eight spacecraft 2D simulation of a formation similar in context to the SI mission is simulated in order to evaluate the estimation and fuel(control) performance. The eight spacecraft are randomly placed, as shown in Figure 2.11. Each spacecraft is simulated using free body dynamics with differing constant disturbance biases at each spacecraft in the range of 20-25 μN and a small random white noise component with a standard deviation of 1μN in X^1 and X^2. Each spacecraft is

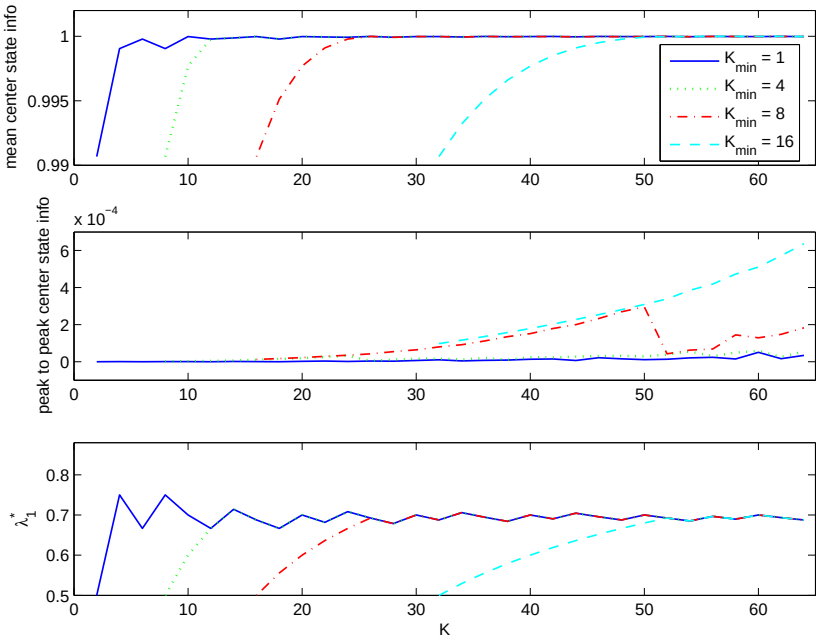

Figure 2.9: Effects of small K and K_{min} using the SS algorithm with fast switching on the modified three spacecraft example.

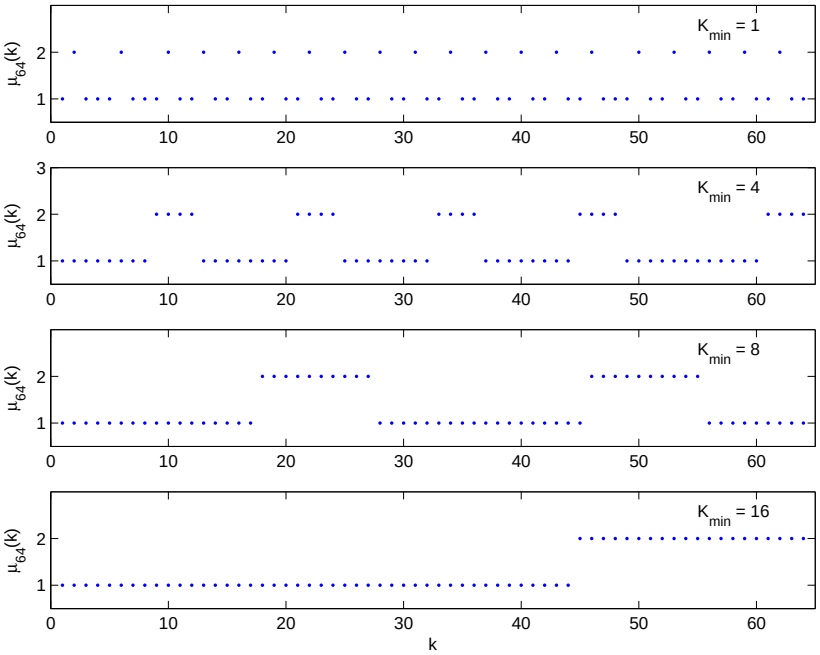

Figure 2.10: Optimal measurement sequences for $K = 64$ and $K_{min} = \{1,4,8,16\}$

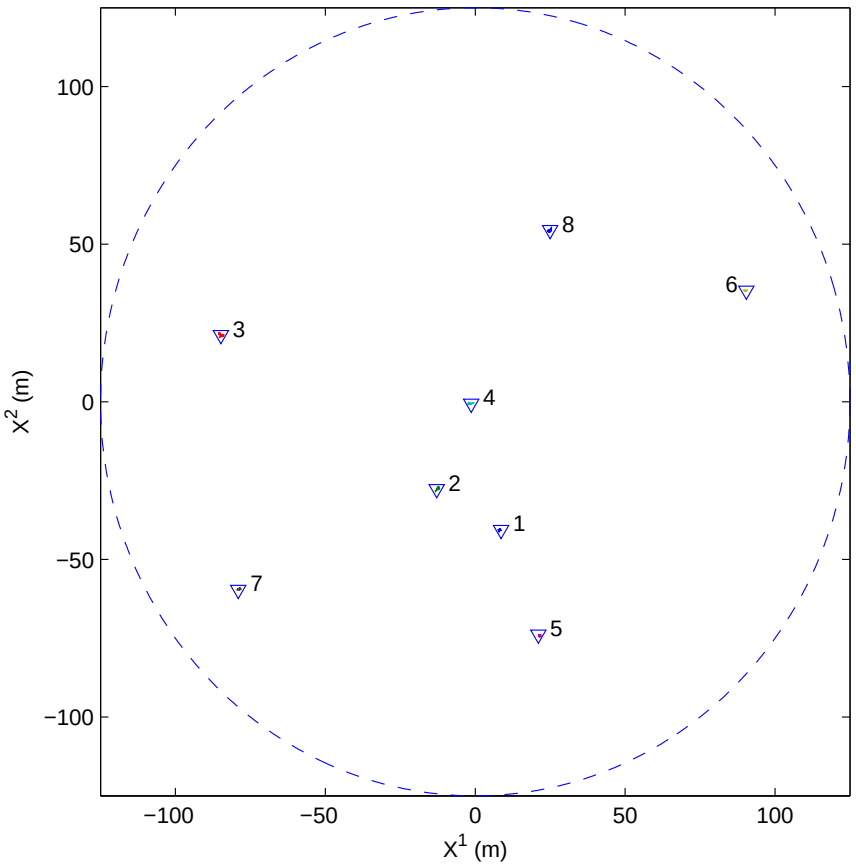

Figure 2.11: Eight spacecraft 250m baseline formation.

equipped with $1m$N thrusters in X^1 and X^2, and each RBS provides measurements with sensor noise standard deviation of (2cm, 1arcsec) in range and bearing at a rate of 0.25 Hz. The controller error ellipse is defined such that $e^{(1)}_{max} = e^{(2)}_{max} = 1$m and $\dot{e}^{(1)}_{max} = \dot{e}^{(2)}_{max} = 0$; Figure 2.12 shows the effect of the control law acting on a sample spacecraft.

Table 2.2 shows the results of the SS algorithm for each spacecraft i on the system shown in Figure 2.12 using the cost J^{CI}_{∞}. The resulting duty cycles are $\Lambda_i = \{\lambda_{ij} \mid j \in N_i\}, N_i = \{1, ..., N\} \setminus i$. The nominal ranges $\bar{R}_{ij} \triangleq \sqrt{(r^{(1)}_{ic} - r^{(1)}_{jc})^2 + (r^{(2)}_{ic} - r^{(2)}_{jc})^2}$ between each pair of spacecraft are also shown for comparison. The algorithm produces identical results for various initial guesses

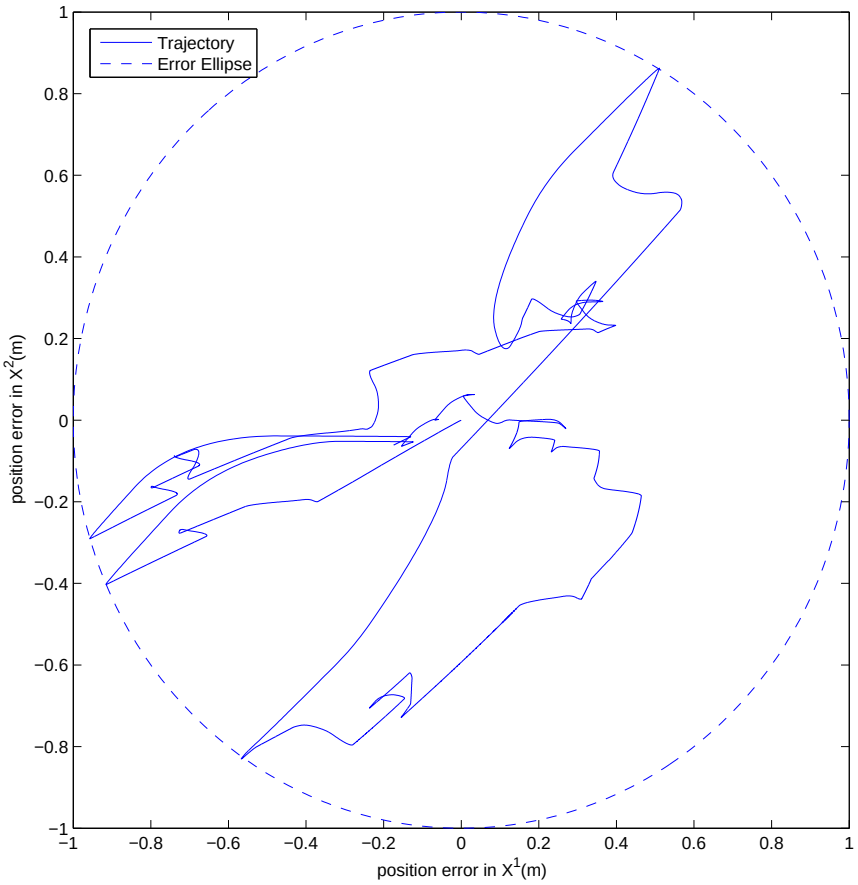

Figure 2.12: Spacecraft 8 position error and controller error ellipse.

including those generated by the LMI solution. The results show that there is a strong correlation between ranges and the λ_{ij}. Also, the formation and center state information vary little over the period K, and it is never advantageous to not observe a spacecraft, i.e. λ_{ij} is never zero. Figure 2.13 shows the measurement sequence and steady-state information for spacecraft 3. For the fast switching sequence shown, the information is relatively constant over the period K.

Figure 2.14 illustrates the effect of using the different cost functions $J_\infty^{(\cdot)}$ to optimize the measurement schedule at spacecraft 1. The horizontal axis represents each of the four cost functions for each of the seven spacecraft being sensed in order of decreasing range; spacecraft 2 is closest and spacecraft 3 is farthest away. Each

Table 2.2: Nominal Range $\bar{R}_{ij}$ and Corresponding λ_{ij} for $K = 28$

	$\bar{R}_{ij}$ (m)								$\lambda_{ij}K$							
i,j	1	2	3	4	5	6	7	8	1	2	3	4	5	6	7	8
1	-	25	112	41	35	112	90	97	-	12	1	5	7	1	1	1
2	25	-	87	29	57	121	74	90	12	-	1	10	2	1	1	1
3	112	87	-	86	142	176	81	115	3	6	-	6	2	1	7	3
4	41	29	86	-	77	99	98	61	7	13	1	-	2	1	1	3
5	35	57	142	77	-	129	101	128	14	6	1	3	-	1	2	1
6	112	121	176	99	129	-	194	68	4	3	2	5	3	-	1	10
7	90	74	81	98	101	194	-	154	4	7	6	4	4	1	-	2
8	97	90	115	61	128	68	154	-	3	4	2	9	2	7	1	-

cost function results in a measurement schedule that takes more measurements to spacecraft that are closer except J_∞^{FC}, which prefers spacecraft that are further away. Of the three that prefer closer spacecraft, J^{CC} has the largest variation of the duty cycle λ_j, i.e. highest lambda for spacecraft 2 and smallest for spacecraft 3; and J_∞^{FI} has the smallest variation. Figure 2.14 (bottom) represents the resulting information on each individual spacecraft normalized by the maximum (i.e. each group of seven is normalized by its max). The information resulting from the cost function J_∞^{FC} shows the least variation while the information resulting from J_∞^{CC} shows the most variation in information. This suggests that minimizing J^{FC} attempts to balance information throughout the formation.

In a final study, the distributed virtual center and sensor scheduling concepts are brought together in one comparison. All eight spacecraft are simulated, and

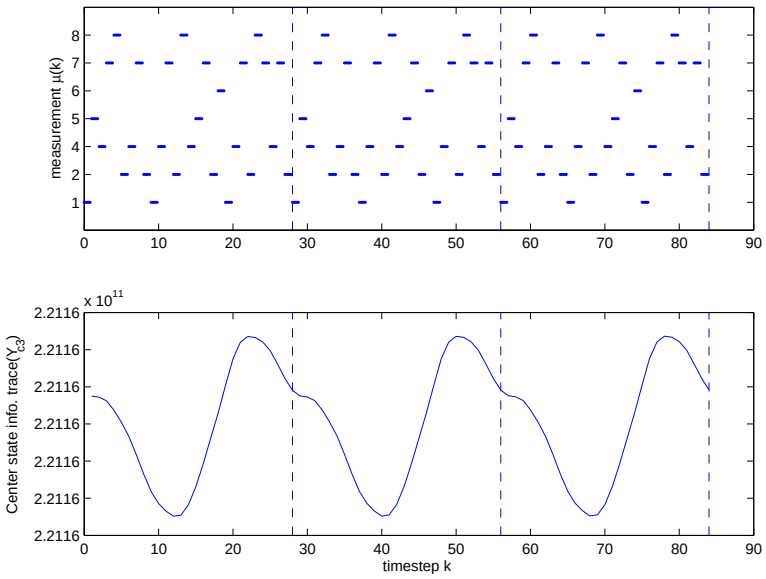

Figure 2.13: Top: Optimal measurement sequence at spacecraft 3; each horizontal tick represents a single measurement. Note that the sampling sequences to each sensor are nearly uniform. Bottom: The peak-to-peak amplitude of the resulting periodic information is several orders of magnitude less than the mean (due to fast switching, i.e. low $\sigma^2_{tot}(\bar{\boldsymbol{\mu}})$).

several cases are tested:

$n > 1$ Unweighted Each spacecraft is equipped with n range/bearing sensors that run concurrently and provide measurements to n spacecraft. Each sensor provides range/ bearing measurements to a single remote spacecraft throughout the simulation. In order to balance the network and ensure coupling, each spacecraft is sensed by exactly n spacecraft. The weights $W_i = I$ in the virtual center calculations. The sensor architecture is static, i.e. the RBSs do not switch between multiple remote spacecraft.

$n > 1$ Weighted Identical to the **$n > 1$ Unweighted** case except $W_i = \text{diag}(G_i, \mathbf{Y}_i)$ when calculating the virtual center and $g_i = 5$.

Switched Unweighted (SU) Each spacecraft is equipped with a single RBS and

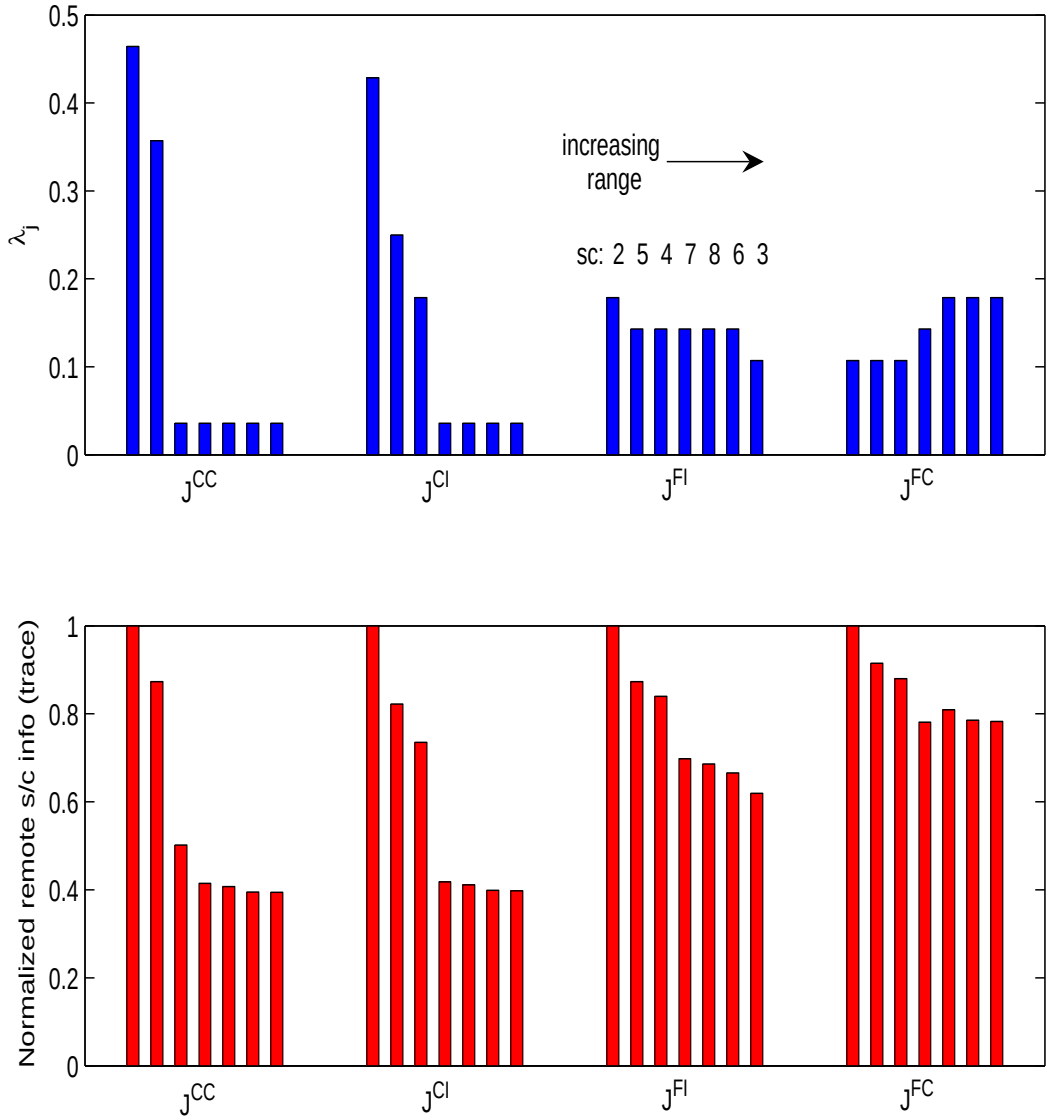

Figure 2.14: Optimal Λ and resulting information at spacecraft 1. The optimal Λ when using J^{FC} resulting in higher λ_j for spacecraft that are farther away while the other cost functions favor close spacecraft.

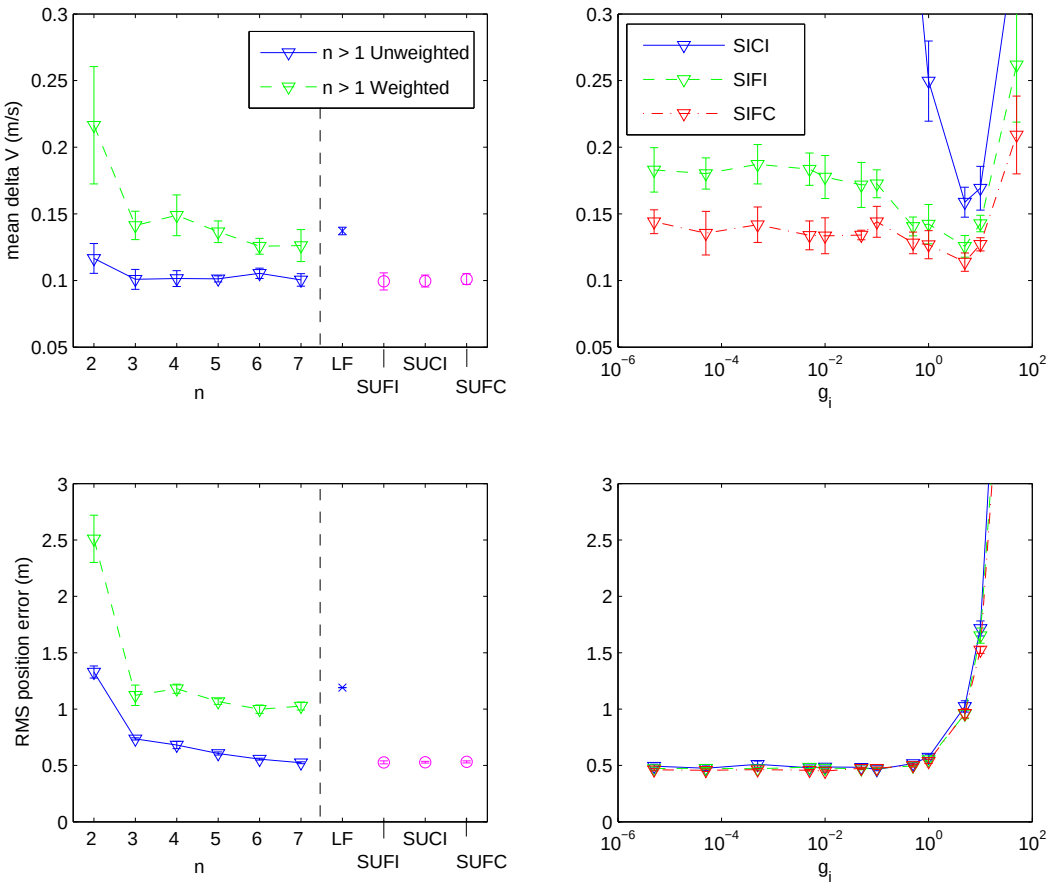

Figure 2.15: Simulation of distributed unweighted ($W_i = I$) and information weighted ($W_i = \text{diag}(G_i, \mathbf{Y}_i)$) virtual center for spacecraft equipped with $n \in \{2, ..., 7\}$ range/bearing sensors. Traditional leader follower (1 leader, 7 followers) and switched RBS ($n = 1$) are also compared.

the infinite horizon scheduling algorithm described in Section 2.4 is used. The weighting matrix $W_i = I$ when calculating the virtual center. Three different switching sequences are used: those determined by minimizing J_∞^{CI}, J_∞^{FI} and J_∞^{FC} are denoted by SUCI, SUFI, and SUFC respectively.

Switched Weighted (SI) Same as **SU** except the weighting matrix is $W_i = \mathbf{Y}_i$ when calculating the virtual center.

Leader Follower (LF) Unweighted virtual center where each spacecraft main-

tains an estimate to spacecraft 1 only. Spacecraft 1 performs no correction maneuvers.

For each case, multiple forty-eight hour simulations are performed. Figure 2.15 shows the mean fuel usage and RMS position error for each case with 1-σ error bars. Note that the $n > 1$ cases are unrealistic because they require more than one RBS, but are presented here for comparison purposes only. The results show that the switched network exhibits positioning performance superior in almost every case to the LF network, and superior even to the $n > 1$ solutions. Results suggest that the switched network with a single sensor is equivalent in performance to a nearly centralized (n=7) static sensor schedule solution. Also, there is a trade off between the robustness of the information weighted virtual center versus the performance of the unweighted weighted virtual center. The information weighted virtual center should therefore be used if failures in the estimation and sensing subsystems have a higher probability in order to allow for an accurate and stable estimate of the virtual center. Finally, it is noted that tuning g_i results in greatly improved performance for all information weighted cases.

2.7 Conclusions

The information weighted virtual center algorithm combined with the sensor switching algorithm has been presented. The algorithm is highly decentralized, requiring only the low bandwidth transmission of maneuvers, scalable and naturally mitigates errors in the estimation/sensor subsystem. These errors may be due to unobservability of spacecraft due to the limited field of view of the RBS and occlusions, loss of lock at the RBS, and changes in the measurement and process

noise covariances. The assumption that the RBS sensor provides omni-directional measurements can be relaxed by having the spacecraft select measurements based on a reduced set of available measurements. The periodic scheduling algorithm has been shown to be convex under mild assumptions and the LMI-based approximate solution can be used in the more accurate steepest descent search algorithm. Limitations in sensor switching frequency are incorporated by adding the appropriate constraints in the steepest descent search scheduling algorithm. Simulation results show the decentralized information weighted virtual center calculation coupled with optimal sensor scheduling to yield performance (estimation, fuel usage and positioning) that is superior to leader-follower using a single RBS sensor and comparable to a fully connected architecture where each spacecraft is equipped with $N-1$ range/bearing sensors.

CHAPTER 3

SENSOR SCHEDULING ANALYSIS AND NEAR-OPTIMAL SOLUTIONS

3.1 Introduction

The work in Chapter 2 focused on a problem similar to the one presented herein and an integer-constrained steepest descent search algorithm was developed. Although the algorithm performs well, it has been shown[25] that such algorithms are inherently flawed and may converge to suboptimal solutions. In this chapter, assuming the sensor schedule to be periodic, a linear matrix inequality (LMI) problem is formed. The LMI formulation is driven by assuming the process noise intensity to be small. The relaxed version of the problem is shown to be independent of the the schedule itself, but is convex in the measurement *rates* of each sensor. The LMI problem, however, is subject to an integer constraint on the measurement rates. Relaxing this constraint leads to a standard LMI problem which can be solved using off the shelf optimization software such as the MATLAB LMI toolbox. The integer constraint is then imposed via a set of algorithms which are based on judicious rounding of the elements of the unconstrained solution. These methods are inspired by algorithms which are based on solving integer constrained least squares problems, which are common in Global Positioning System (GPS) estimation problems[32, 25].

This Chapter is outlined as follows: the infinite horizon periodic sensor scheduling problem is formulated in Section 3.2. An approximation of the cost function and integer constrained solution is described in Section 3.3. Several examples which explore the accuracy of the approximation and associated solution are also

described. The Chapter concludes with Section 3.4.

3.2 Problem Statement

The dynamics of the system under consideration are,

$$x(k+1) = Ax(k) + Bw(k) \tag{3.1}$$

$$z(k) = C_{\mu(k)}x(k) + v_{\mu(k)}(k) \tag{3.2}$$

where $w(k)$ is zero-mean, Gaussian white noise, $\mu(k) \in M$ is a predetermined measurement schedule, $M = \{1, \ldots, N\}$ is a set of indices of measurements consisting of the measurement matrices $\{C_j \mid j \in M\}$ and associated measurement noises $\{v_j \mid j \in M\}$, each being white, Gaussian sources with covariance R_j. The measurement schedule $\boldsymbol{\mu}_\infty = \{\mu(1), \mu(2), \ldots\}$ minimizes the infinite horizon information based cost function,

$$J \triangleq \lim_{K_F \to \infty} -\frac{1}{K_F} \operatorname{trace} \sum_{k=1}^{K_F} Y(k \mid k). \tag{3.3}$$

where $Y(k \mid k)$ is the information matrix. The information matrix is defined as the inverse of the state estimate error covariance matrix,

$$Y(k \mid l) \triangleq \left(E\left[\left(x(k) - \hat{x}(k \mid l)\right) \left(x(k) - \hat{x}(k \mid l)\right)^T \mid Z^l \right] \right)^{-1} \tag{3.4}$$

where $\hat{x}(k \mid l)$ is the estimate of $x(k)$ given the measurements up to and including time step l, denoted by

$$Z^l \triangleq \{z(0), \cdots, z(l)\}. \tag{3.5}$$

The state estimate and information matrix are determined by an information filter (IF), which is statistically equivalent to the Kalman filter[24]. Instead of recursively updating an estimate $\hat{x}(k)$ and error covariance $P(k)$, an information state $\hat{y}(k)$

and information matrix $Y(k)$ are updated. The IF is used in order to formulate the convex optimization problem. The IF prediction equations are,

$$\hat{y}(k \mid k-1) = Y(k \mid k-1)\left[AY^{-1}(k-1 \mid k-1)\hat{y}(k-1 \mid k-1) + B_u u(k)\right], \quad (3.6)$$

$$Y(k \mid k-1) = (AY^{-1}(k \mid k)A^T + BQB^T)^{-1}, \quad (3.7)$$

and the update steps are,

$$\hat{y}(k \mid k) = \hat{y}(k \mid k-1) + z_I(k) \quad (3.8)$$

$$Y(k \mid k) = Y(k \mid k-1) + I(k), \quad (3.9)$$

where $z_I(k)$ and $I(k)$ are, respectively, the measurement information vector and matrix, defined as,

$$z_I(k) \triangleq {C_{\mu(k)}}^T R^{-1}_{\mu(k)} z(k), \quad (3.10)$$

$$I(k) \triangleq C^T_{\mu(k)} R^{-1}_{\mu(k)} C_{\mu(k)}. \quad (3.11)$$

Throughout this chapter, an information matrix with a single argument, e.g. $Y(k)$ will be used as shorthand for the updated information matrix, $Y(k \mid k)$.

To the authors knowledge, an analytical solution to this general problem has not yet been found. In a recent paper by Gupta and Murray[18], the sensor schedule is modeled as a random process such that at each time step, a measurement j is selected from the measurement set M with probability λ^r_j, with the constraint

$$\sum_{j \in M} \lambda^r_j = 1. \quad (3.12)$$

Ref. [18] introduces an algorithm which solves for the set of probabilities by minimizing an upper bound on the expected value of the covariance as determined by a set of Riccati-like equations. Although the algorithm produces the optimal sensor scheduling probability λ^r_j, it converges only for stable systems. This makes the

approach unsuitable for use in deep space mission examples, which are governed by second order dynamics.

It is proposed that the optimal infinite horizon measurement sequence for any linear time invariant system is periodic. This was originally suggested in Ref. [15] and an algorithm to find the optimal periodic measurements based on generating sequences at random was developed. In Chapter 2 it was shown that a periodic schedule yields a lower cost than a random schedule. The periodic formulation is posed as finding the periodic measurement sequence which minimizes J in Eq. 3.3. Thus for a given periodic measurement sequence,

$$\boldsymbol{\mu}_\infty = \{\boldsymbol{\mu}_K, \boldsymbol{\mu}_K, ...\},\ \boldsymbol{\mu}_K = \{\mu_K(1), ..., \mu_K(K)\}, \tag{3.13}$$

where K is the period of the sequence. The infinite horizon cost is independent of the initial information matrix $Y(0)$, leading to a reformulation of the cost as[5]

$$J = -\frac{1}{K}\ \text{trace} \sum_{k=0}^{K-1} Y^{\text{u}}(k + k_0), \tag{3.14}$$

where k_0 is an arbitrary integer constant and $Y^{\text{u}}(k) = Y(k \mid k)$ is the updated information matrix $Y(k \mid k)$ in steady state, which can be found by solving a periodic Riccati equation[7]. Similarly, $Y^{\text{p}}(k) = Y(k+1 \mid k)$ denotes the predicted information matrix $Y(k + 1 \mid k)$ in steady state.

3.3 LMI-based Solutions to Periodic Scheduling Problems

Given a periodic measurement sequence $\boldsymbol{\mu}_K$, the time varying system in Eqs. 3.1 and 3.2 can be written in LTI form as,

$$\begin{aligned}
\mathbf{x}_i(\tau+1) &= \mathbf{A}\mathbf{x}_i(\tau) + \mathbf{B}\mathbf{w}_i(\tau), && (3.15)\\
\mathbf{z}_i(\tau) &= \mathbf{C}_i\mathbf{x}_i(\tau) + \mathbf{D}_i\mathbf{w}_i(\tau-1) + \mathbf{v}_i(\tau), \quad i \in \{0,\ldots,K-1\} && (3.16)\\
\mathbf{x}_i(\tau) &\triangleq x\left(\tau K + i\right), && (3.17)\\
\mathbf{w}_i(\tau) &\triangleq \left[\begin{array}{ccc} w\left(\tau K+i\right)^T & \cdots & w\left(\tau K+i+K-1\right)^T \end{array}\right]^T, && (3.18)\\
\mathbf{z}_i(\tau) &\triangleq \left[\begin{array}{ccc} z\left(\tau K+i-(K-1)\right)^T & \cdots & z\left(\tau K+i\right)^T \end{array}\right]^T, && (3.19)\\
\mathbf{v}_i(\tau) &\triangleq \left[\begin{array}{cc} v_{\mu_K(i-(K-1))}\left(\tau K+i-(K-1)\right)^T & \cdots \\ & v_{\mu_K(i)}\left(\tau K+i\right)^T \end{array}\right]^T, && (3.20)\\
\mathbf{A} &\triangleq A^K, && (3.21)\\
\mathbf{B} &\triangleq \left[\begin{array}{cccc} A^{K-1}B & A^{K-2}B & \cdots & B \end{array}\right], && (3.22)\\
\mathbf{C}_i &\triangleq \left[\begin{array}{c} C_{\mu_K(i-(K-1))}A^{-(K-1)} \\ C_{\mu_K(i-(K-2))}A^{-(K-2)} \\ \vdots \\ C_{\mu_K(i)} \end{array}\right], && (3.23)\\
[\mathbf{D}_i]_{mn} &\triangleq \begin{cases} -C_{\mu_K(i-(K-m))}A^{m-n}B & \text{if } m < n, \\ 0 & \text{otherwise,} \end{cases} && (3.24)
\end{aligned}$$

where $[\cdot]_{mn}$ is the mn-th n_z-by-n_w subblock of the matrix $[\cdot]$. It is noted that for ease of notation $\mu_K(\tau K + i) = \mu_K(i)$ for all integers i and τ. The matrices in Eqs. 3.15 and 3.16 are time invariant with respect to τ when the system dynamics are time invariant and the measurements are periodic with period K. The process and measurement noise vectors $\mathbf{w}_i(\tau)$ and $\mathbf{v}_i(\tau)$ are zero mean and white with co-

variances of $\mathbf{Q} = \text{diag}(Q, \ldots, Q)$ and $\mathbf{R}_i = \text{diag}(R_{\mu_K(i-(K-1))}, \ldots, R_{\mu_K(i)})$, respectively. Thus, an IF can be run on the system represented by Eqs. 3.15 and 3.16 and will yield an identical estimate and information matrix as when running the IF on the system represented by Eqs. 3.1 and 3.2. In this case the information matrix prediction step is,

$$\mathbf{Y}_i(\tau+1 \mid \tau) = \left(\mathbf{A}\mathbf{Y}_i(\tau \mid \tau)^{-1}\mathbf{A}^T + \mathbf{B}\mathbf{Q}\mathbf{B}^T\right)^{-1} \tag{3.25}$$

where $\mathbf{Y}_i(k \mid l) = Y(kK+i \mid lK+i)$. This equation is the standard IF prediction equation analogous to Eq. 3.7. Applying the matrix inversion lemma yields

$$\begin{aligned}\mathbf{Y}_i(\tau+1 \mid \tau) = {} & \mathbf{A}^{-T}\mathbf{Y}_i(\tau \mid \tau)\mathbf{A}^{-1} - \\ & \mathbf{A}^{-T}\mathbf{Y}_i(\tau \mid \tau)\mathbf{A}^{-1}\mathbf{B}\left[\mathbf{Q}^{-1} + \mathbf{B}\mathbf{A}^{-T}\mathbf{Y}_i(\tau \mid \tau)\mathbf{A}^{-1}\mathbf{B}^T\right]^{-1}\mathbf{B}^T\mathbf{A}^{-T}\mathbf{Y}_i(\tau \mid \tau)\mathbf{A}^{-1}.\end{aligned} \tag{3.26}$$

The $\mathbf{D}_{\tau K}\mathbf{w}_i(\tau-1)$ term in Eq. 3.16 leads to a non-standard update step

$$\begin{aligned}\mathbf{Y}_i(\tau+1 \mid \tau+1) = {} & \mathbf{Y}_i(\tau+1 \mid \tau) + \left(\mathbf{C}_i^T + \mathbf{Y}_i(\tau+1 \mid \tau)\mathbf{S}_i\right) \cdot \\ & \left(\mathbf{R}_i + \mathbf{D}_i\mathbf{Q}\mathbf{D}_i^T - \mathbf{S}_i^T\mathbf{Y}_i(\tau+1 \mid \tau)\mathbf{S}_i\right)^{-1}\left(\mathbf{C}_i^T + \mathbf{Y}(\tau+1 \mid \tau)\mathbf{S}_i\right)^T\end{aligned} \tag{3.27}$$

where $\mathbf{S}_i \triangleq \mathbf{B}\mathbf{Q}\mathbf{D}_i^T$. The steady state predicted and updated information matrices for this LTI system shall be denoted by $\mathbf{Y}_i^{\text{p}}$ and $\mathbf{Y}_i^{\text{u}}$, respectively. It is noted that in steady state

$$\mathbf{Y}_i^{\text{u}} = Y^{\text{u}}(\tau K + i) \;\forall\; \tau = \{0, 1, \ldots\}. \tag{3.28}$$

Substituting this in Eq. 3.14 and letting $k_0 = 0$ yields the cost in terms of the steady state solution of Eqs. 3.26 and 3.27 for the periodic system in Eqs. 3.15–3.24

$$J = -\frac{1}{K}\,\text{trace}\sum_{i=0}^{K-1}\mathbf{Y}_i^{\text{u}}. \tag{3.29}$$

3.3.1 Cost Approximation

A relaxation is desired in order to simplify the problem from a combinatorial optimization over $\boldsymbol{\mu}_K$ to a convex one that can be solved using standard algorithms. Because there are many problems where $\mathbf{Q}$ is small or zero, such as the deep space problem considered here, we will consider an approximation of the cost J for small values of $\mathbf{Q}$ in the update equation only (Eq. 3.27), because only this equation contains a coupling which does not allow for a closed form solution. Note that assuming $\mathbf{Q} = 0$ in Eqs. 3.26 and 3.27 is not valid. In this case, combining Eqs. 3.26 and 3.27 in order to eliminate $\mathbf{Y}_i(\tau+1|\tau)$ and denoting the steady state solution by $\boldsymbol{\Upsilon}$ such that $\mathbf{Y}_i(\tau+1|\tau+1) = \mathbf{Y}_i(\tau|\tau) = \boldsymbol{\Upsilon}$ leads to the equation

$$\boldsymbol{\Upsilon} = \mathbf{A}^{-T}\boldsymbol{\Upsilon}\mathbf{A}^{-1} + \mathbf{C}_i^T\mathbf{R}_i\mathbf{C}_i. \tag{3.30}$$

And since $\mathbf{A}^{-T}$ is not stable, there exists no solution to this equation.

An alternative is to assume the process noise $\mathbf{Q}$ that appears in Eq. 3.27 is small under the assumption that $\mathbf{C}_i$ and $\mathbf{R}_i$ are the dominant terms. First, Eqs. 3.26 and 3.27 are rewritten in terms of two process noise terms, denoted by $\mathbf{Q}^{\mathrm{p}}$ and $\mathbf{Q}^{\mathrm{u}}$. In steady state, these are:

$$\begin{aligned}\mathbf{Y}^{\mathrm{p}}_{\mathrm{Q}i} &= -\mathbf{A}^{-T}\mathbf{Y}^{\mathrm{u}}_{\mathrm{Q}i}\mathbf{A}^{-1}\mathbf{B}\left[(\mathbf{Q}^{\mathrm{p}})^{-1} + \mathbf{B}\mathbf{A}^{-T}\mathbf{Y}^{\mathrm{u}}_{\mathrm{Q}i}\mathbf{A}^{-1}\mathbf{B}^T\right]^{-1}\mathbf{B}^T\mathbf{A}^{-T}\mathbf{Y}^{\mathrm{u}}_{\mathrm{Q}i}\mathbf{A}^{-1} + \\ &\quad \mathbf{A}^{-T}\mathbf{Y}^{\mathrm{u}}_{\mathrm{Q}i}\mathbf{A}^{-1}\end{aligned} \tag{3.31}$$

and

$$\begin{aligned}\mathbf{Y}^{\mathrm{u}}_{\mathrm{Q}i} &= \mathbf{Y}^{\mathrm{p}}_{\mathrm{Q}i} + \left(\mathbf{C}_i^T + \mathbf{Y}^{\mathrm{p}}_{\mathrm{Q}i}\mathbf{B}\mathbf{Q}^{\mathrm{u}}\mathbf{D}_i^T\right)\cdot \\ &\quad \left(\mathbf{R} + \mathbf{D}_i\mathbf{Q}^{\mathrm{u}}\mathbf{D}_i^T - \mathbf{D}_i\mathbf{Q}^{\mathrm{u}}\mathbf{B}^T\mathbf{Y}^{\mathrm{p}}_{\mathrm{Q}i}\mathbf{B}\mathbf{Q}^{\mathrm{u}}\mathbf{D}_i^T\right)^{-1}\cdot \\ &\quad \left(\mathbf{C}_i^T + \mathbf{Y}^{\mathrm{p}}_{\mathrm{Q}i}\mathbf{B}\mathbf{Q}^{\mathrm{u}}\mathbf{D}_i^T\right)^T,\end{aligned} \tag{3.32}$$

where $\mathbf{Y}^{\mathrm{p}}_{\mathrm{Q}i}$ and $\mathbf{Y}^{\mathrm{u}}_{\mathrm{Q}i}$ denote, respectively, the predicted and updated information matrices in steady state. The cost is now a function of the two process noise terms $\mathbf{Q}^{\mathrm{p}}$ and $\mathbf{Q}^{\mathrm{u}}$ and is denoted by J_{Q} such that,

$$J_{\mathrm{Q}}(\mathbf{Q}^{\mathrm{p}}, \mathbf{Q}^{\mathrm{u}}) = -\frac{1}{K} \text{ trace} \sum_{i=0}^{K-1} \mathbf{Y}^{\mathrm{u}}_{\mathrm{Q}i} \tag{3.33}$$

where $\mathbf{Y}^{\mathrm{u}}_{\mathrm{Q}i}$ satisfies Eqs. 3.31 and 3.32. In this case, $J_{\mathrm{Q}}(\mathbf{Q}, \mathbf{Q}) = J$. Equations 3.31–3.33 form the basis for the approximation $\mathbf{Q}^{\mathrm{u}} = 0$ in the measurement update. The zero-th order approximation of the cost is denoted by J_0 and is given by

$$\begin{aligned} J = J_{\mathrm{Q}}(\mathbf{Q}, \mathbf{Q}) &= J_{\mathrm{Q}}(\mathbf{Q}, 0) + O(\mathbf{Q}^{\mathrm{u}}) & (3.34) \\ &\approx J_{\mathrm{Q}}(\mathbf{Q}, 0) = J_0 & (3.35) \end{aligned}$$

The zero-th order term, J_0, can be found by setting $\mathbf{Q}^{\mathrm{u}} = 0$ in Eq. 3.32, $\mathbf{Q}^{\mathrm{p}} = \mathbf{Q}$ in Eq. 3.31, and eliminating $\mathbf{Y}^{\mathrm{p}}_{\mathrm{Q}i}$ by combining Eqs. 3.32 and 3.31. The resulting Riccati equation is:

$$\begin{aligned} \mathbf{Y}^{\mathrm{u}}_{0i} &= \mathbf{A}^{-T}\mathbf{Y}^{\mathrm{u}}_{0i}\mathbf{A}^{-1} + \mathbf{I}_i - \\ &\quad \mathbf{A}^{-T}\mathbf{Y}^{\mathrm{u}}_{0i}\mathbf{A}^{-1}\mathbf{B}\left(\mathbf{B}^T\mathbf{A}^{-T}\mathbf{Y}^{\mathrm{u}}_{0i}\mathbf{A}^{-1}\mathbf{B} + \tilde{\mathbf{Q}}^{-1}\right)^{-1}\mathbf{B}^T\mathbf{A}^{-T}\mathbf{Y}^{\mathrm{u}}_{0i}\mathbf{A}^{-1}, \end{aligned} \tag{3.36}$$

where $\mathbf{I}_i \triangleq \mathbf{C}_i^T\mathbf{R}_i^{-1}\mathbf{C}_i$ and at steady state it is assumed that $\mathbf{Y}^{\mathrm{u}}_{0i} \approx \mathbf{Y}^{\mathrm{u}}_{i}$. Eq. 3.36 can be easily solved for a given a measurement schedule $\boldsymbol{\mu}_K$. The resulting zero-th order cost is

$$J_0 = J(\mathbf{Q}, 0) = -\frac{1}{K}\text{trace} \sum_{i=0}^{K-1} \mathbf{Y}^{\mathrm{u}}_{0i}, \tag{3.37}$$

where the information matrices $\mathbf{Y}^{\mathrm{u}}_{0i}, i \in \{0, \ldots, K-1\}$ are evaluated by either solving Eq. 3.36 for some $i = \mathrm{i}$ and propagating $\mathbf{Y}^{\mathrm{u}}_{0\mathrm{i}}$ forward $K-1$ time steps using Eqs. 3.7 and 3.9, or by solving a total of K Riccati equations for $i = \{0, \ldots, K-1\}$.

Alternatively, the information matrix $\mathbf{Y}^{\mathrm{u}}_{0i}$ can be found by solving an LMI

problem[26, 8] corresponding to Eq. 3.36:

$$\min_{\mathbf{Y}_{0i}^{\mathrm{u}}} -\left[\text{trace } \left(\mathbf{Y}_{0i}^{\mathrm{u}}\right)\right], \quad \text{subject to } \mathbf{L}_i < 0 \tag{3.38}$$

where

$$\mathbf{L}_i \triangleq \begin{bmatrix} \mathbf{Y}_{0i}^{\mathrm{u}} - \mathbf{A}^{-T}\mathbf{Y}_{0i}^{\mathrm{u}}\mathbf{A}^{-1} - \mathbf{I}_i & \mathbf{A}^{-T}\mathbf{Y}_{0i}^{\mathrm{u}}\mathbf{A}^{-1}\mathbf{B} \\ - & -\mathbf{B}^T\mathbf{A}^{-T}\mathbf{Y}_{0i}^{\mathrm{u}}\mathbf{A}^{-1}\mathbf{B} - \mathbf{Q}^{-1} \end{bmatrix} \tag{3.39}$$

and where the $-$ in the mn-th position denotes the transpose of the element in the nm-th position. Instead of solving K LMI problems for each $\mathbf{Y}_{0i}^{\mathrm{u}}$ in order to find the cost J_0, the mean information $1/K\left(\sum_{i=0}^{K-1}\mathbf{Y}_{0i}^{\mathrm{u}}\right)$ and thus the zero-th order cost J_0 can be found by adding the costs and constraints for each LMI for $i = \{0, \cdots, K-1\}$ and solving

$$\min_{\bar{\mathbf{Y}}_0} -\left[\text{trace}\left(\bar{\mathbf{Y}}_0\left(\Lambda^{\mathrm{I}}\right)\right)\right], \quad \text{subject to } \bar{\mathbf{L}}\left(\Lambda^{\mathrm{I}}\right) < 0 \tag{3.40}$$

where

$$\bar{\mathbf{Y}}_0\left(\Lambda^{\mathrm{I}}\right) \triangleq \frac{1}{K}\sum_{i=0}^{K-1}\mathbf{Y}_{0i}^{\mathrm{u}} \tag{3.41}$$

$$\bar{\mathbf{L}}\left(\Lambda^{\mathrm{I}}\right) \triangleq \frac{1}{K}\sum_{i=0}^{K-1}\mathbf{L}_i \tag{3.42}$$

$$= \begin{bmatrix} \bar{\mathbf{Y}}_0 - \mathbf{A}^{-T}\bar{\mathbf{Y}}_0\mathbf{A}^{-1} - \bar{\mathbf{I}}\left(\Lambda^{\mathrm{I}}\right) & \mathbf{A}^{-T}\bar{\mathbf{Y}}_0\mathbf{A}^{-1}\mathbf{B} \\ - & -\mathbf{B}^T\mathbf{A}^{-T}\bar{\mathbf{Y}}_0\mathbf{A}^{-1}\mathbf{B} - \mathbf{Q}^{-1} \end{bmatrix} \tag{3.43}$$

$$\bar{\mathbf{I}}\left(\Lambda^{\mathrm{I}}\right) \triangleq \frac{1}{K}\sum_{i=0}^{K-1}\mathbf{I}_i = \sum_{j\in M}\lambda_j^{\mathrm{I}}\hat{\mathbf{I}}_j \tag{3.44}$$

$$\hat{\mathbf{I}}_j \triangleq \sum_{i=0}^{K-1}(A^{-i})^T C_j^T R_j^{-1} C_j A^{-i} \tag{3.45}$$

Note that the argument of $\bar{\mathbf{Y}}_0\left(\Lambda^{\mathrm{I}}\right)$ has been suppressed in the right hand side of Eq. 3.43 for clarity. In Eq. 3.44, λ_j^{I} is interpreted as the number of measurements made to spacecraft j over a single period, normalized by the period K. The vector

of λ_j^{I} is denoted by Λ^{I} such that $\Lambda^{\mathrm{I}} \triangleq \left[\cdots \ \lambda_j^{\mathrm{I}} \ \cdots\right]_{j\in M}^T$. By definition, $\lambda_j^{\mathrm{I}} K$ is an integer such that $\lambda_j^{\mathrm{I}} K > 0$ and $\sum_{j\in M} \lambda_j^{\mathrm{I}} K = K$. These constraints are summarized as follows

$$\begin{aligned} \mathrm{C1}_{\Lambda^{\mathrm{I}}}: &\quad \lambda_j^{\mathrm{I}} > 0 \\ \mathrm{C2}_{\Lambda^{\mathrm{I}}}: &\quad \sum_{j\in M} \lambda_j^{\mathrm{I}} = 1 \\ \mathrm{C3}_{\Lambda^{\mathrm{I}}}: &\quad K\lambda_j^{\mathrm{I}} \in \{1, 2, \ldots\} \end{aligned}$$

The derivation of Eqs. 3.40– 3.45 represents the key step in the process which converts the sensor scheduling problem from a combinatorial optimization problem over $\boldsymbol{\mu}_K$ to an integer-constrained LMI problem over λ_j^{I}. Each λ_j^{I} can be interpreted as a duty cycle value, e.g. if measurements are being made to two spacecraft, denoted by 1 and 2, and if $\lambda_1^{\mathrm{I}} = 0.1$ and $\lambda_2^{\mathrm{I}} = 0.9$ then 10% of the duty is spent measuring range and bearing to spacecraft 1 and 90% is spent on spacecraft 2.

Note that the ordering of the measurements does not factor into the solution of this LMI problem. This is a consequence of the assumption that the process noise terms $\mathbf{S}_i$ and $\mathbf{D}_i\mathbf{Q}\mathbf{D}_i^T$ terms in Eq. 3.27 are negligible.

If the integer constraint $\mathrm{C3}_{\Lambda^{\mathrm{I}}}$ is relaxed and the duty cycles are included as optimization variables, the scheduling problem can be posed as the following

$$\Lambda^* = \arg\min_{\bar{\mathbf{Y}}_0,\Lambda} -\left[\mathrm{trace}\left(\bar{\mathbf{Y}}_0\left(\Lambda\right)\right)\right], \ \text{ subject to } \bar{\mathbf{L}}\left(\Lambda\right) < 0, \ \mathrm{C1}_\Lambda, \ \sum_{j\in M} \lambda_j < 1 \quad (3.46)$$

where each element of $\Lambda \triangleq \left[\cdots \ \lambda_j \ \cdots\right]_{j\in M}^T$, is allowed to very continuously between 0 and 1. Note that the last constraint $\sum_{j\in M} \lambda_j < 1$ in the LMI problem is similar to $\mathrm{C2}_\Lambda$. Later in the chapter, it will be shown that the optimal solution to this LMI lies along the constraint $\mathrm{C2}_\Lambda$ by showing the gradient of the cost is always negative in the space enclosed by $\mathrm{C1}_\Lambda$ and $\mathrm{C2}_\Lambda$. Once the LMI problem is solved,

the unconstrained solution Λ^* can then be rounded up or down to satisfy the integer constraint $\mathrm{C3}_{\Lambda^{\mathrm{I}}}$, such that

$$\Lambda^{\mathrm{I}*} = \frac{1}{K}\mathrm{round}(K\Lambda^*) \tag{3.47}$$

or Λ^* can be used as an initial guess in the sensor scheduling algorithm described in Chapter 2. Note, however, that arbitrarily rounding each element of Λ^* as in Eq. 3.47 may violate one or both of the constraints $\mathrm{C1}_{\Lambda^{\mathrm{I}*}}$ and $\mathrm{C2}_{\Lambda^{\mathrm{I}*}}$. Later in the chapter, several methods are developed to find the optimal $\Lambda^{\mathrm{I}*}$ which satisfies $\mathrm{C1}_{\Lambda^{\mathrm{I}*}}$–$\mathrm{C3}_{\Lambda^{\mathrm{I}*}}$ given the unconstrained solution Λ^* found via Eq. 3.46. The accuracy of the approximation is explored in the example that follows.

3.3.2 Examples

Several examples are presented in order to analyze the accuracy of the LMI solution. Each example consists of a system of spacecraft in 2D deep space. The spacecraft are governed by double-integrator LTI dynamics and driven by low intensity process noise. Considering an estimation subsystem which is running on spacecraft N, the state consists of the position and velocity of spacecraft 1 through $N-1$ relative to a local frame centered at spacecraft N, referred to as the sensing spacecraft. The dynamics of the relative position and velocity of spacecraft j with

respect to spacecraft N is given by,

$$\begin{bmatrix} p_X^{j,N}(k+1) \\ p_Y^{j,N}(k+1) \\ v_X^{j,N}(k+1) \\ v_Y^{j,N}(k+1) \end{bmatrix} = \begin{bmatrix} I_2 & \Delta T \cdot I_2 \\ 0 & I_2 \end{bmatrix} \begin{bmatrix} p_X^{j,N}(k) \\ p_Y^{j,N}(k) \\ v_X^{j,N}(k) \\ v_Y^{j,N}(k) \end{bmatrix} + \frac{1}{m} \begin{bmatrix} \frac{\Delta T^2}{2} \cdot I_2 \\ \Delta T \cdot I_2 \end{bmatrix} \left(\begin{bmatrix} w_X^j(k) \\ w_Y^j(k) \end{bmatrix} - \begin{bmatrix} w_X^N(k) \\ w_Y^N(k) \end{bmatrix} \right). \quad (3.48)$$

where p represents the relative position states and v represents the relative velocity states. The state of the system at spacecraft N is,

$$x(k) \triangleq \left[p_X^{1,N}(k)\ p_Y^{1,N}(k)\ v_X^{1,N}(k)\ v_Y^{1,N}(k) \cdots \right. \\ \left. p_X^{N-1,N}(k)\ p_Y^{N-1,N}(k)\ v_X^{N-1,N}(k)\ v_Y^{N-1,N}(k) \right]^T, \quad (3.49)$$

and the dynamics matrices (cf. Eq. 3.1) are,

$$A = I_{N-1} \otimes \begin{bmatrix} I_2 & \Delta T \cdot I_2 \\ 0 & I_2 \end{bmatrix} \quad (3.50)$$

$$B = \begin{bmatrix} & & -1 \\ & I_{N-1} & -1 \\ & & -1 \end{bmatrix} \otimes \begin{bmatrix} \frac{\Delta T^2}{2} \cdot I_2 \\ \Delta T \cdot I_2 \end{bmatrix} \frac{1}{m} \quad (3.51)$$

where I_{N-1} is the $N-1$-by-$N-1$ identity matrix and $\otimes$ represents the Kronecker product.

The measurements at spacecraft N are based on a relative range/bearing sensor (RBS) that can take a measurement to only one spacecraft at a time. Thus, the measurement equation is,

$$z(k) = h_{\mu(k)}[x(k)] + v_{\mu(k)}(k), \quad (3.52)$$

where the index set $\mu(k) \in \{1, \ldots, N-1\}$ and the nonlinear measurement function h is (neglecting the k time indices),

$$h_\mu[x] = \begin{bmatrix} R_\mu \\ \phi_\mu \end{bmatrix} = \begin{bmatrix} \sqrt{\left[p_X^{\mu,N}\right]^2 + \left[p_Y^{\mu,N}\right]^2} \\ \tan^{-1}\frac{p_Y^{\mu,N}}{p_X^{\mu,N}} \end{bmatrix}. \tag{3.53}$$

The system is clearly not observable when measuring the range and bearing of a single spacecraft exclusively. Therefore, sensor scheduling must be employed to switch measurements between each spacecraft.

Three separate formations are considered. In the first formation, three spacecraft are nominally spaced 50 m apart, forming the vertices of a virtual equilateral triangle. Spacecraft 1 is located 50 m from spacecraft 3, at a bearing of $-\pi/6$ rad and spacecraft 2 is located 50 m from spacecraft 3, at a bearing of $\pi/6$ rad. The bearings are referenced from the X axis. These states denote the system operating point, defined as x_S, where the subscript denotes a symmetrical formation. The second formation is an asymmetrical case, which is the same as the first, except the range and bearing to spacecraft 1 is (200 m, $\pi/2$ rad). The system operating point in this case is denoted by x_A where the subscript denotes the asymmetrical case. The third formation consists of five spacecraft. The nominal positions of each spacecraft have been chosen at random and the system operating point is denoted by x_F. These formation parameters are summarized in Table 3.1. The system sampling time is $\Delta T = 4$ s and the mass of each spacecraft is 100 kg. The noise covariances are, $Q = qI_{2N}$ and, following the nominal performance of the Autonomous Formation Flying sensor[2], $R_\mu = [\text{diag}(2 \text{ cm}, 1 \text{ arcsec})]^2$. Linearizing the sensor output equation $h_\mu[x(k)]$ about the operating point $x_{(\cdot)}$, yields the nominal measurement matrices used in the optimization,

$$C_\mu = \left.\frac{\partial h_\mu(x)}{\partial x}\right|_{x_{(\cdot)}}, \tag{3.54}$$

Table 3.1: Nominal range and bearing to each spacecraft relative to the sensing spacecraft for each of the three example formations.

$x_{(\cdot)}$	N	$h_1[x_{(\cdot)}]$	$h_2[x_{(\cdot)}]$	$h_3[x_{(\cdot)}]$	$h_4[x_{(\cdot)}]$
x_S	3	50 m, $-\pi/6$ rad	50 m, $\pi/6$ rad	-	-
x_A	3	200 m, $-\pi/6$ rad	50 m, $\pi/6$ rad	-	-
x_F	5	25.1 m, 2.60 rad	112 m, 2.56 rad	41.2 m, 1.82 rad	35.4 m, -1.21 rad

where the subscript $(\cdot)$ is either S, A or F.

In this section, the truth cost is compared to the zero-th order cost for varying period K and process noise q. The truth cost is found by solving a covariance Riccati equation for a given measurement sequence as outlined in the Appendix. In the $N = 3$ cases, the truth optimal measurement sequence is found by enumerating all possible sequences and evaluating the cost J. This can be done for relatively low K; for example, $K = 15$ yields a total of approximately $2^{15} = 32768$ possible measurement sequences. However, in the case where $N = 5$, the number of sequences becomes prohibitively large for even small values of K. In this case, and in the $N = 3$ case for $K > 15$, the truth optimal sequence is found by enumerating all possible Λ and, for each Λ, evaluating the truth cost at several sequences, typically four to six. These sequences include: a "slow" switching sequence, where $\boldsymbol{\mu}_K = \{1, 1, \ldots, 2, 2, \ldots, 3, 3, \ldots\}$; a "fast" sequence which is found via the greedy algorithm described in Chapter 2; and several randomly generated sequences. It will be shown that solutions derived from the zero-th order approximation are optimal for low values of K and q. In this chapter, it is assumed that the nominal value of q in deep space is $(10\mu N)^2$.

Figures 3.1 and 3.2 illustrate the validity of the zero-th order approximation for small process noise q over several values of the period K. For the

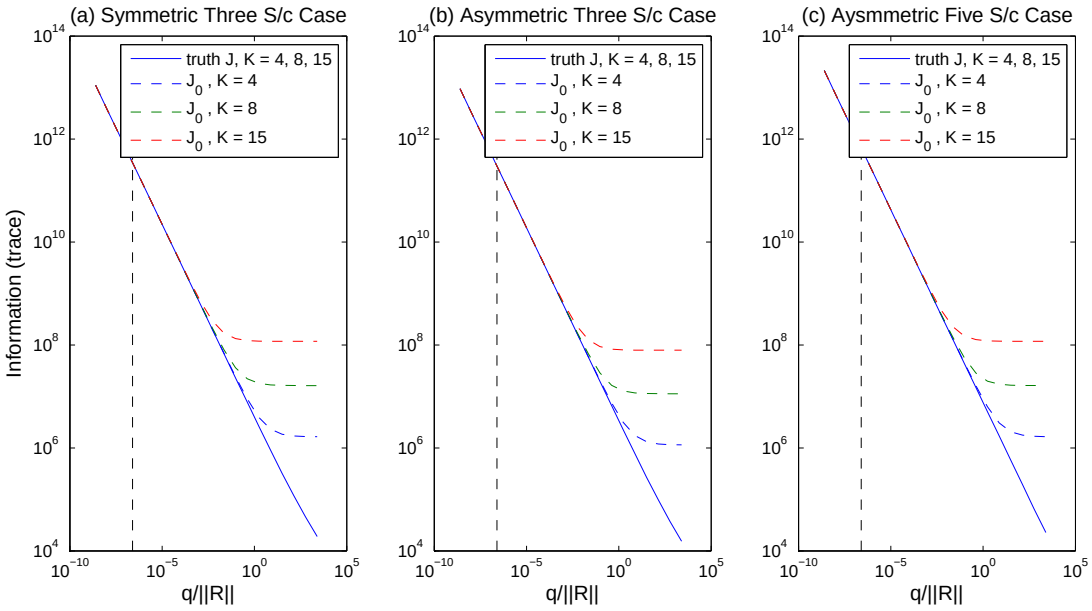

Figure 3.1: Comparison of the approximate cost $-J_0 = \text{trace}\left(\hat{\mathbf{Y}}_0\right)$ and the truth cost $-J = (1/K)\left[\text{trace}\left(\sum_{i=0}^{K-1}\mathbf{Y}_i^{\text{u}}\right)\right]$ for $K = 4$, 8 and 15 for the three formations. The vertical dotted line denotes the nominal Q and R matrices for deep space missions.

cases where $N = 3$, the costs are evaluated for the measurement sequence $\boldsymbol{\mu}_K = \{1, 2, 1, 2, \ldots\}$. For the $N = 5$ case, the sequence $\boldsymbol{\mu}_K = \{1, 2, 3, 4, 1, \ldots\}$ is used. Figure 3.1 shows the zero-th order information, $\bar{\mathbf{Y}}_0$ and the truth information $(1/K)\left[\text{trace}\left(\sum_{i=0}^{K-1}\mathbf{Y}_i^{\text{u}}\right)\right]$ as a function of the process noise q. Figure 3.2 shows the error for the zero-th order costs $|(J_0 - J)/J| \ll 1$. The results show that the approximation degrades with increasing K and q.

Figure 3.2 shows that for $K = 15$, the approximation in each case breaks down at approximately $q/\|R\| = 10^{-2}$. For process/sensor noise ratios below this value, the ordering of the measurements is a small factor in the cost and the cost is dominated by the duty cycles Λ. Conversely, for $q/\|R\| > 10^{-2}$ the ordering of the measurements increasingly affects the cost. Figure 3.3 illustrates this point for the

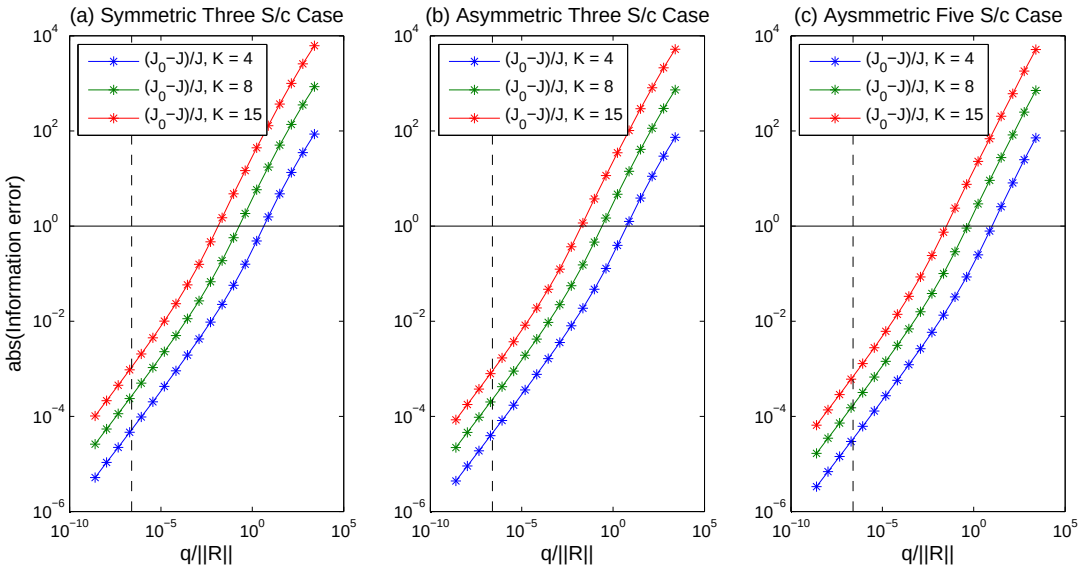

Figure 3.2: Error in the approximate cost J_0 relative to the truth cost $|(J_0 - J)/J|$ for $K = 4$, 8 and 15 for the three formations. The vertical dotted line denotes the nominal Q and R matrices for deep space missions. The approximation is considered to be valid for error values $|(J_0 - J)/J| \ll 1$, denoted by the horizontal line.

symmetric formation. This figure plots the truth information vs. Λ for all possible measurement sequences $\boldsymbol{\mu}_K$ for four values of $q/\|R\|$. For each value of $q/\|R\|$, the information resulting from all possible periodic sequences is determined and is plotted as a series of points. As an example, for $q/\|R\| = 0.001$ (Figure 3.3(a)), the sequence $\boldsymbol{\mu}_{15} = \{1, 2, 2, \ldots\}$ yields $\lambda_1 = 1/15$ and $-J = 5.2$. This results in the point (1/15,5.2). The sequence $\boldsymbol{\mu}_{15} = \{2, 1, 2, 2, \ldots\}$ also yields the point (1/15,5.2) since the periodicity of the sequence results in the same mean information. The sequence $\boldsymbol{\mu}_{15} = \{2, 1, 1, \ldots\}$ results in the point (14/15,5.2), as does the sequence $\boldsymbol{\mu}_{15} = \{1, 2, 1, 1, \ldots\}$.

For $q/\|R\| < 10^{-2}$ as in 3.3(a) ($q/\|R\| = 0.001$) and 3.3(b) ($q/\|R\| = 0.005$) plotting the mean information $(1/K)\left[\text{trace}\sum_{i=0}^{K-1}\mathbf{Y}_i^{\text{u}}\right]$ for every possible sequence $\boldsymbol{\mu}_K$ shows the information (and cost J) is approximately constant for a given

Λ. This is not the case for higher process noise as in 3.3(c), $q/\|R\| = 0.02$, and 3.3(d), $q/\|R\| = 0.1$ where, for a given Λ, different measurement schedules result in varying costs (as shown by the spread of points, or costs, for different sequences with the same Λ). Similar results are found for the other two example formations, as can be seen in Figure 3.4 for the asymmetrical three spacecraft formation and Figure 3.5 for the five spacecraft case.

The sensitivity of the optimal Λ^* in each example to variations in q is explored to find the optimal measurement sequence for several values of K. Figure 3.6 plots Λ as found by the exhaustive search algorithm using the truth cost J. The figure shows that for the symmetric three spacecraft formation, Λ^* remains constant even for high process noise. However, for the asymmetric $N = 3$ and $N = 5$ formations as shown in Figures 3.7 and 3.8, for very large q the duty cycles converge to a solution where $\lambda_{i_0} = 1$ for some i_0 and $\lambda_i = 0$ for all other $i \neq i_0$. This is because as q gets very large, the optimization at each time step can be considered to be one with no prior information, i.e. $Y(k \mid k-1) \approx 0$. And so, the choice on whether to take one measurement over the other results in taking the one with the greatest measurement information matrix $I(k)$ (i.e. the spacecraft that is closest; in the case of the asymmetric $N = 3$ formation, spacecraft 2). At the next time step, the high process noise eliminates this information, and the sensor scheduling problem repeats, again resulting in a measurement of spacecraft 2.

Figures 3.9 and 3.10 illustrate the sensitivity of the zero-th order solution with the period length K for each of the three cases. Plotted are the truth solutions and the solutions to the zero-th order approximation versus the period length K for the nominal values of q and R. Results for the $N = 3$ formations are shown in Figure 3.9, while Figure 3.10 shows the results for the $N = 5$ case. In each case, the

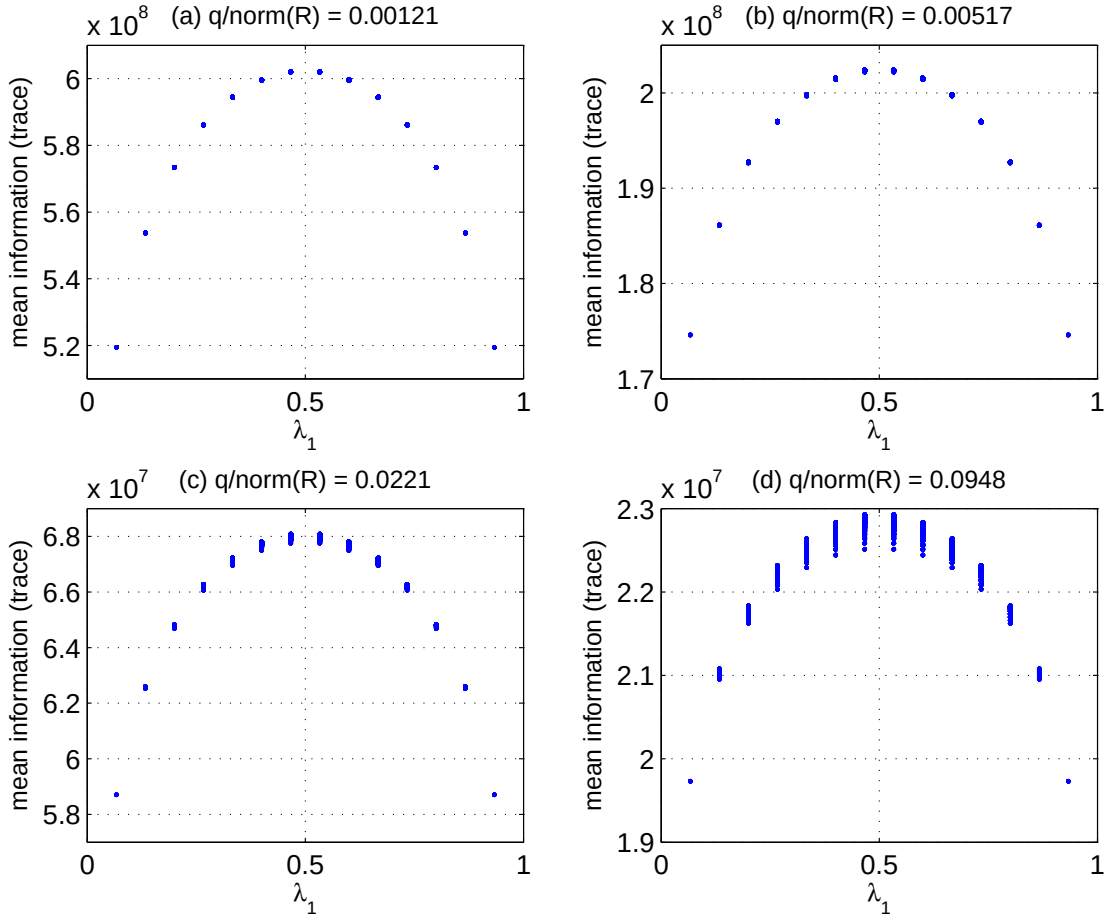

Figure 3.3: Truth mean information $-J = (1/K)\left[\text{trace}\sum_{i=0}^{K-1}\mathbf{Y}_i^{\text{u}}\right]$ in the symmetrical three spacecraft formation for all possible $\boldsymbol{\mu}_K$ where $K = 15$, yielding a total of approximately 2^{15} possible measurement sequences. Each point represents the duty cycle Λ and resulting information for a single measurement sequence. Note that the symmetry of the three spacecraft example yields equivalent cost for $\Lambda = [a\ b]^T$ and $\Lambda = [b\ a]^T$.

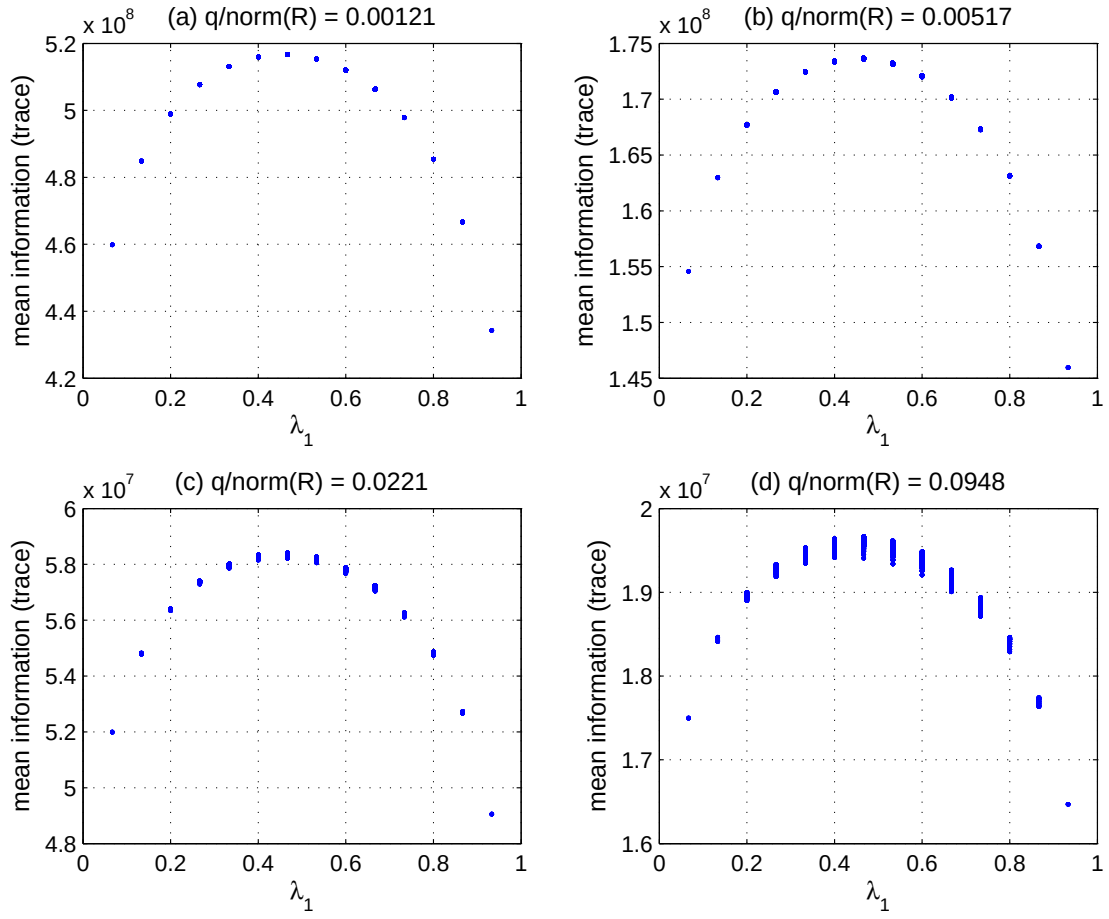

Figure 3.4: Truth mean information $-J = (1/K)\left[\text{trace}\sum_{i=0}^{K-1}\mathbf{Y}_i^{\text{u}}\right]$ for the asymmetric three spacecraft case where $K = 15$ for several values of process noise process noise and all possible $\boldsymbol{\mu}_K$.

truth solution approaches a constant, and in the symmetric case, the zero-th order LMI solution never deviates from this constant. However, in the asymmetric cases, the zero-th order LMI solution diverges from the optimal solution with increasing K. This is likely due to the increasing error in the zero-th order cost. Interestingly, the constant that the truth solutions approach is the solution to the zero-th order LMI problem with $K = 1$. In almost every case, the truth solution lies within an envelope with a width of $1/K$ centered around the optimal LMI solution for

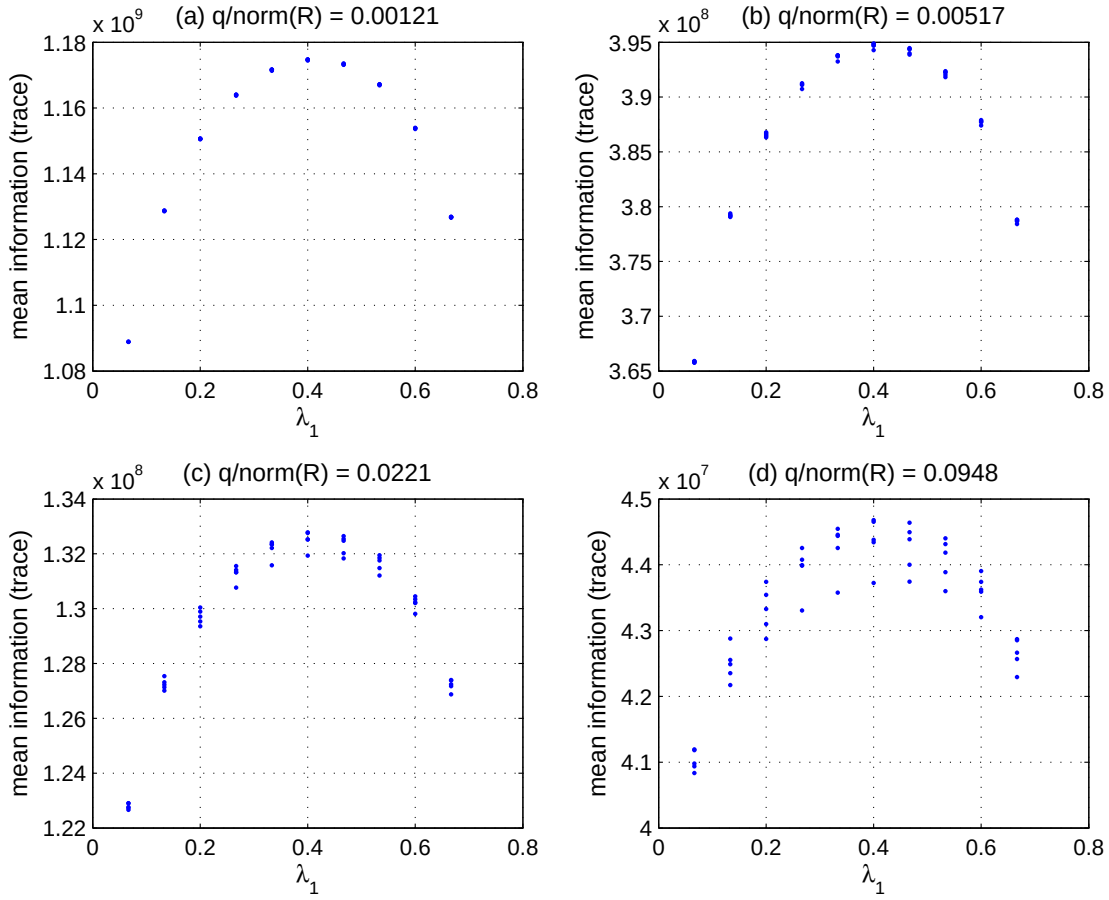

Figure 3.5: Truth mean information $-J = (1/K)\left[\text{trace}\sum_{i=0}^{K-1}\mathbf{Y}_i^{\text{u}}\right]$ in the five spacecraft case where $K = 15$ for increasing process noise and all possible $\boldsymbol{\mu}_K$ where $\lambda_3 = \lambda_4 = 2/15$.

$K = 1$, as shown by the dashed lines. The cases where the optimal solutions lie slightly outside the envelope are due to the constraint $\sum_i \lambda_i = 1$. For instance, in Figure 3.10, the truth solution for the lowest $K = 5$ lies outside the envelope for $i = 1$, however the solution $\lambda_1 = 0.2$, which is within the envelope, is inadmissible because $\Lambda = [0.2, 0.2, 0.2, 0.2]$ violates the constraint. The results suggest that for large K, the optimal solution may be found by solving for the case where $K = 1$. At the very least, the system designer should check the two solutions–the solutions

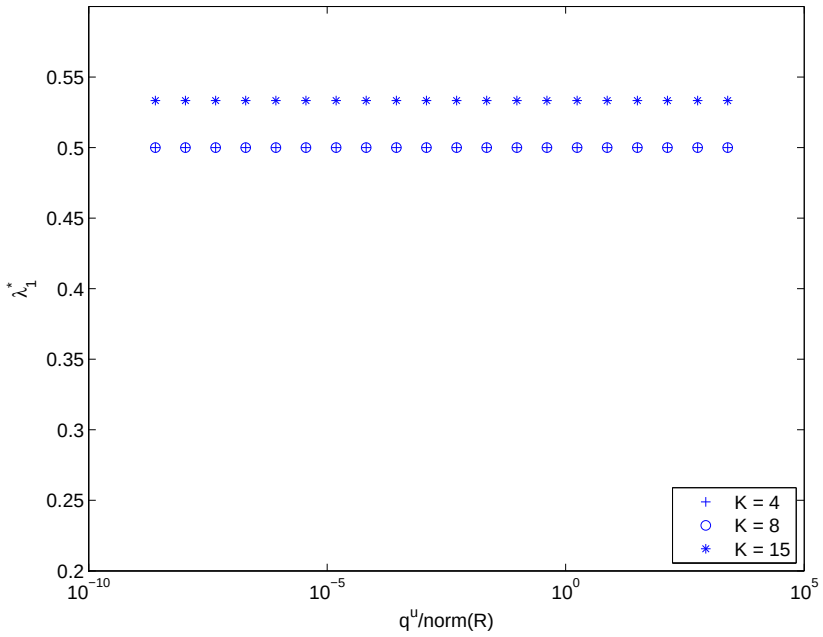

Figure 3.6: Plot of optimal λ_1^* found by an exhaustive search over all possible $\boldsymbol{\mu}_K$ for the symmetrical three spacecraft formation. Increasing process noise does not affect the optimal measurement duty cycles.

resulting from $K = 1$ and the desired period K–against the truth cost and take the one which yields the highest information.

3.3.3 Integer Optimization Techniques

Since the LMI based optimization in Eq. 3.46 finds a continuous optimal schedule Λ^* which does not satisfy the problem's integer constraint $\mathrm{C3}_{\Lambda^{\mathrm{I}}}$, and since arbitrarily rounding the unconstrained solution according to Eq. 3.47 may violate one of both of the constraints $\mathrm{C1}_{\Lambda^{\mathrm{I}}}$ and $\mathrm{C2}_{\Lambda^{\mathrm{I}}}$, alternative methods are developed based on integer least squares optimization techniques. The objective, therefore, is to find the optimal integer-constrained solution $\Lambda^{\mathrm{I}*}$ which satisfies constraints $\mathrm{C1}_{\Lambda^{\mathrm{I}}}$, $\mathrm{C2}_{\Lambda^{\mathrm{I}}}$

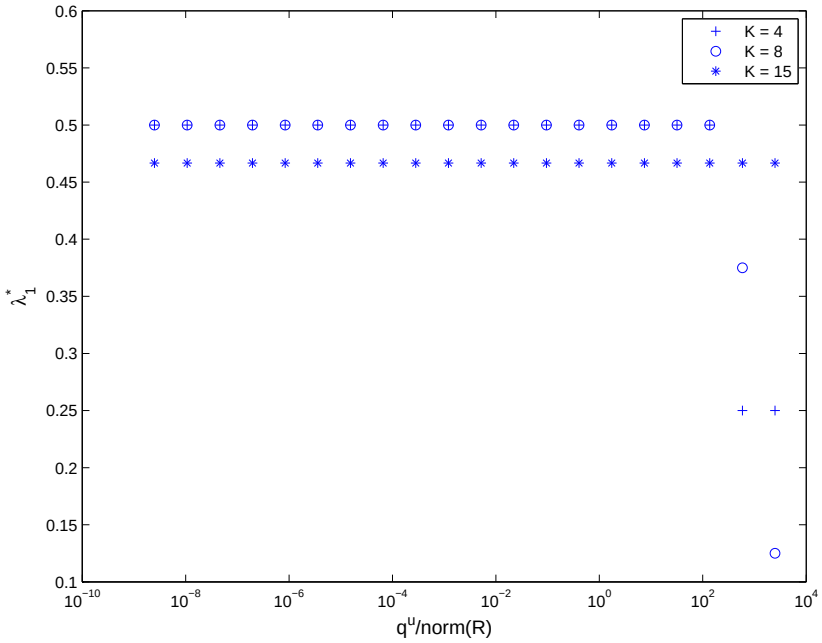

Figure 3.7: Plot of optimal λ_1^* found by an exhaustive search over all possible $\boldsymbol{\mu}_K$ for the asymmetrical three spacecraft formation. The optimal measurement duty cycles are constant for small $q/\|R\|$ but diverge to $\lambda_2 \approx 1$ for large $q/\|R\|$.

and $C3_{\Lambda^I}$ based on an initial solution Λ^* found by the LMI problem in Eq. 3.46. Ref. [25] presents a set of algorithms for solving integer constrained quadratic least squares problems for estimates of GPS integer parameters. A similar implementation is used here in order to minimize the zero-th order approximate cost J_0 for the integer solution. Although the relaxed scheduling problem described herein is not a linear least squares problem, it is approximated as such using the gradient and Hessian of the cost function in the neighborhood of a candidate solution, in this case, the unconstrained solution Λ^*.

To begin, the zero-th order cost J_0 is expanded to second order about the

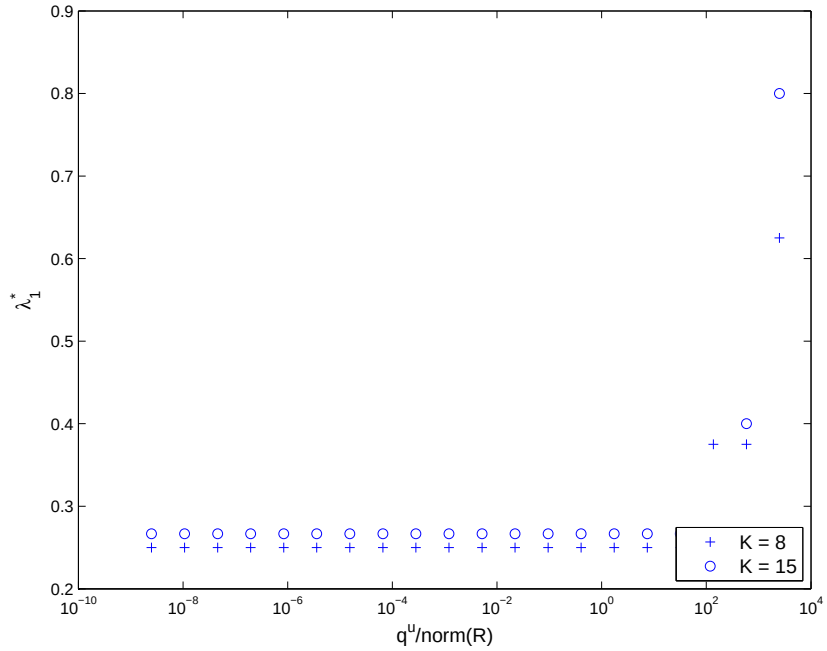

Figure 3.8: Plot of optimal λ_1^* found by an exhaustive search over all possible $\boldsymbol{\mu}_K$ for the asymmetrical five spacecraft formation. The optimal measurement duty cycles are constant for small $q/\left\|R\right\|$ but diverge to $\lambda_1 \approx 1$ for large $q/\left\|R\right\|$.

continuous solution Λ^* as,

$$J_0(\Lambda^{\mathrm{I}}) = J_0(\Lambda^*) + \left.\frac{\partial J_0}{\partial \Lambda}\right|_{\Lambda^*}^T \left(\Lambda^{\mathrm{I}} - \Lambda^*\right) + \frac{1}{2}\left(\Lambda^{\mathrm{I}} - \Lambda^*\right)^T \left.\frac{\partial^2 J_0}{\partial \Lambda^2}\right|_{\Lambda^*} \left(\Lambda^{\mathrm{I}} - \Lambda^*\right) + O(\bar{\Lambda}^3) \tag{3.55}$$

where $\partial J_0/\partial\bar{\Lambda}$ and $\partial^2 J_0/\partial\bar{\Lambda}^2$ are the gradient and Hessian, respectively, defined as

$$\left[\frac{\partial J_0}{\partial \Lambda}\right]_j = \frac{\partial J_0}{\partial \lambda j} = -\mathrm{trace}\ \frac{\partial \bar{\mathbf{Y}}_0}{\partial \lambda_j} \tag{3.56}$$

and

$$\left[\frac{\partial^2 J_0}{\partial \Lambda^2}\right]_{j_1 j_2} = \frac{\partial^2 J_0}{\partial \lambda_{j_1} \partial \lambda_{j_2}} = -\mathrm{trace}\ \frac{\partial^2 \bar{\mathbf{Y}}_0}{\partial \lambda_{j_1} \partial \lambda_{j_2}}. \tag{3.57}$$

The gradient and Hessian are found by noting that, given a value of the unconstrained duty cycle Λ, the solution to the LMI in Eq. 3.40 for the zero-th order mean information matrix $\bar{\mathbf{Y}}_0(\Lambda)$ is equivalent to the solution to the Riccati

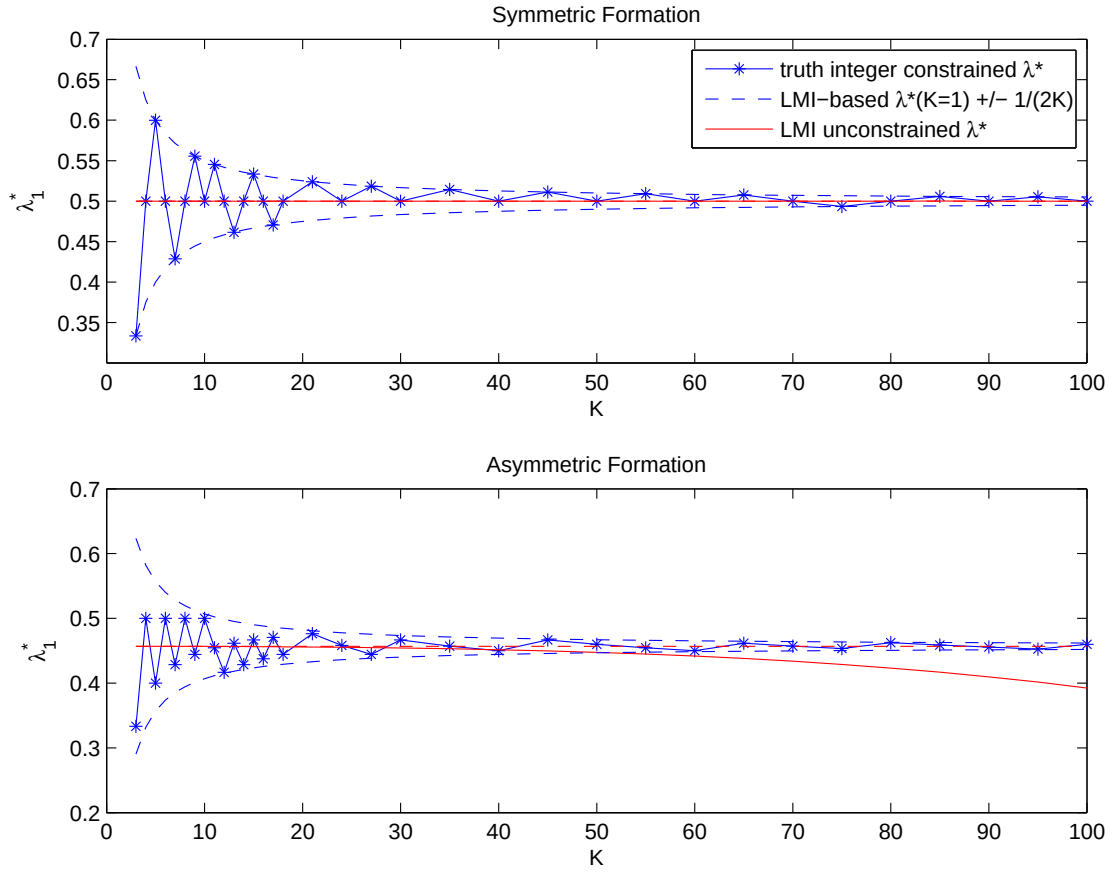

Figure 3.9: Truth solution and LMI-based zero-th order solution for Λ^* for the symmetric and asymmetric three spacecraft cases. The LMI-based solution drifts from the truth optimal value with increasing K in the asymmetric case.

equation[26, 8]

$$\begin{aligned}\bar{\mathbf{Y}}_0 &= \mathbf{A}^{-T}\bar{\mathbf{Y}}_0\mathbf{A}^{-1} + \sum_{j\in M}\lambda_j\hat{\mathbf{I}}_j - \\ &\quad \mathbf{A}^{-T}\bar{\mathbf{Y}}_0\mathbf{A}^{-1}\mathbf{B}\left(\mathbf{B}^T\mathbf{A}^{-T}\bar{\mathbf{Y}}_0\mathbf{A}^{-1}\mathbf{B} - \mathbf{Q}^{-1}\right)^{-1}\mathbf{B}^T\mathbf{A}^{-T}\bar{\mathbf{Y}}_0\mathbf{A}^{-1} \quad (3.58)\end{aligned}$$

where the argument of $\bar{\mathbf{Y}}_0(\Lambda)$ is suppressed for clarity. The gradient in Eq. 3.56 is now found by differentiating 3.58 and collecting terms to yield a Lyapunov

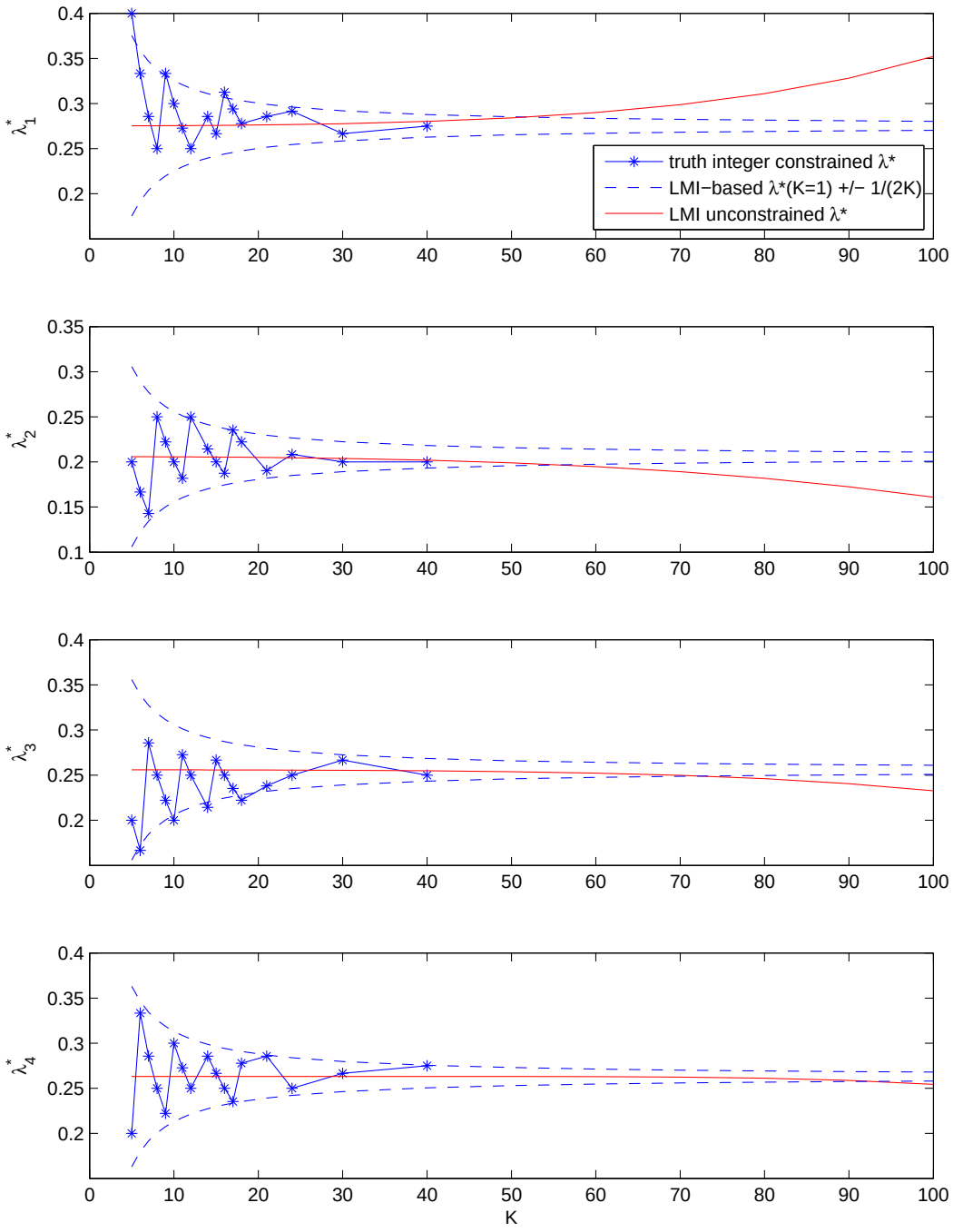

Figure 3.10: Truth solution and LMI-based zero-th order solutions for Λ^* for the five spacecraft example. As in the three spacecraft asymmetric example, the LMI-based solution drifts from the truth optimal value with increasing K.

equation,

$$\frac{\partial \bar{\mathbf{Y}}_0}{\partial \lambda_j} = \Phi \frac{\partial \bar{\mathbf{Y}}_0}{\partial \lambda_j} \Phi^T + \hat{\mathbf{I}}_j \tag{3.59}$$

where

$$\Phi = \mathbf{A}^{-T} - \mathbf{A}^{-T}\bar{\mathbf{Y}}_0\mathbf{A}^{-1}\mathbf{B}\left(\mathbf{B}^T\mathbf{A}^{-T}\bar{\mathbf{Y}}_0\mathbf{A}^{-1}\mathbf{B} + \mathbf{Q}^{-1}\right)^{-1}\mathbf{B}^T\mathbf{A}^{-T}. \tag{3.60}$$

A compact expression for Φ is found by post-multiplying this expression by $\bar{\mathbf{Y}}_0\mathbf{A}^{-1}$ and adding $\hat{\mathbf{I}}$ resulting in

$$\begin{aligned} \Phi\bar{\mathbf{Y}}_0\mathbf{A}^{-1} + \hat{\mathbf{I}} &= \mathbf{A}^{-T}\bar{\mathbf{Y}}_0\mathbf{A}^{-1} + \hat{\mathbf{I}} - \\ &\quad \mathbf{A}^{-T}\bar{\mathbf{Y}}_0\mathbf{A}^{-1}\mathbf{B}\left(\mathbf{B}^T\mathbf{A}^{-T}\bar{\mathbf{Y}}_0\mathbf{A}^{-1}\mathbf{B} - \mathbf{Q}^{-1}\right)^{-1}\mathbf{B}^T\mathbf{A}^{-T}\bar{\mathbf{Y}}_0\mathbf{A}^{-1} \\ &= \bar{\mathbf{Y}}_0 \end{aligned} \tag{3.61}$$

which yields

$$\Phi = (\bar{\mathbf{Y}}_0 - \hat{\mathbf{I}})\mathbf{A}\bar{\mathbf{Y}}_0^{-1}. \tag{3.62}$$

Note that since $\bar{\mathbf{I}}_j$ is nonzero and positive semidefinite, $\partial\bar{\mathbf{Y}}_0/\partial\lambda_j^{\mathrm{I}}$ is also nonzero and positive semidefinite. Therefore $[\partial J_0/\partial\Lambda]_j < 0$. This justifies replacing the equality constraint $\sum_{j\in M}\lambda_j = 1$ with the inequality constraint $\sum_{j\in M}\lambda_j < 1$ in the LMI problem of Eq. 3.46 because the minimum cost always approaches the equality constraint.

The Hessian in Eq. 3.57 can be found by differentiating Eq. 3.59 to yield the Lyapunov equation

$$\frac{\partial^2\bar{\mathbf{Y}}_0}{\partial\lambda_{j_1}\partial\lambda_{j_2}} = \Phi\frac{\partial^2\bar{\mathbf{Y}}_0}{\partial\lambda_{j_1}\partial\lambda_{j_2}}\Phi^T + \frac{\partial\Phi}{\partial\lambda_{j_2}}\frac{\partial\bar{\mathbf{Y}}_0}{\partial\lambda_{j_1}}\Phi^T + \Phi\frac{\partial\bar{\mathbf{Y}}_0}{\partial\lambda_{j_1}}\frac{\partial\Phi}{\partial\lambda_{j_2}}^T, \tag{3.63}$$

where $\partial\Phi/\partial\lambda_{j_2}$ if found by differentiating Eq. 3.62

$$\frac{\partial\Phi}{\partial\lambda_{j_2}} = \frac{\partial\bar{\mathbf{Y}}_0}{\partial\lambda_{j_2}}\mathbf{A}\bar{\mathbf{Y}}_0^{-1} - \left(\bar{\mathbf{Y}}_0 - \hat{\mathbf{I}}\right)\mathbf{A}\bar{\mathbf{Y}}_0^{-1}\frac{\partial\bar{\mathbf{Y}}_0}{\partial\lambda_{j_2}}\bar{\mathbf{Y}}_0^{-1}. \tag{3.64}$$

and where $\partial\bar{\mathbf{Y}}_0/\partial\lambda_{j_1}$ and $\partial\bar{\mathbf{Y}}_0/\partial\lambda_{j_2}$ are found via Eq. 3.59 with $j = j_1$ and $j = j_2$ respectively.

The constant term $J_0(\Lambda^*)$ in Eq. 3.55 can be eliminated from the optimization because it is not a function of the unknown constrained duty cycle Λ^{I}. And, in order to simplify the quadratic problem formulation, the first order term in Eq. 3.55 is eliminated using the first order necessary condition that the gradient of the cost J_0 with respect to Λ is zero at Λ^*. However, this condition is satisfied only along the constraint $\sum_{j\in M}\lambda_j^{\mathrm{I}} = 1$. This is achieved by using the constraint to eliminate one of the elements of Λ. Thus, let

$$\lambda_l^{\mathrm{I}} = 1 - \sum_{j\in M\setminus l}\lambda_j^{\mathrm{I}} \tag{3.65}$$

for some $l \in M$. For simplicity, $l = N$ is chosen, however, the methods described herein are easily generalized to remove an arbitrary element of Λ^{I}. Denoting the reduced $N-1$ element vector as $\Lambda_{\mathrm{R}}^{\mathrm{I}} = \begin{bmatrix}\lambda_1^{\mathrm{I}} & \cdots & \lambda_{N-1}^{\mathrm{I}}\end{bmatrix}^T$ leads to the equation

$$\Lambda^{\mathrm{I}} = e_N + G\Lambda_{\mathrm{R}}^{\mathrm{I}} \tag{3.66}$$

where

$$e_N = \begin{bmatrix} 0 \\ \vdots \\ 0 \\ 1 \end{bmatrix}, G = \begin{bmatrix} & I_{N-1} & \\ & & \\ -1 & \cdots & -1 \end{bmatrix}. \tag{3.67}$$

Reduced vectors Λ_{R} and Λ_{R}^* are similarly defined as satisfying

$$\Lambda = e_N + G\Lambda_{\mathrm{R}} \tag{3.68}$$

$$\Lambda^* = e_N + G\Lambda_{\mathrm{R}}^*. \tag{3.69}$$

Subtracting Eq. 3.69 from Eq. 3.66 leads to the equation

$$\Lambda^{\mathrm{I}} - \Lambda^* = G\left(\Lambda_{\mathrm{R}}^{\mathrm{I}} - \Lambda_{\mathrm{R}}^*\right). \tag{3.70}$$

Substituting this in Eq. 3.55 yields the cost J_0 as a function of $\Lambda_{\mathrm{R}}^{\mathrm{I}}$

$$\begin{aligned} J_0(\Lambda_{\mathrm{R}}^{\mathrm{I}}) = J_0(\Lambda^*) + \tfrac{\partial J_0}{\partial \Lambda}\big|_{\Lambda^*}^T G\left(\Lambda_{\mathrm{R}}^{\mathrm{I}} - \Lambda_{\mathrm{R}}^*\right) + \\ \tfrac{1}{2}\left(\Lambda_{\mathrm{R}}^{\mathrm{I}} - \Lambda_{\mathrm{R}}^*\right)^T G^T \left.\tfrac{\partial^2 J_0}{\partial \Lambda^2}\right|_{\Lambda^*} G\left(\Lambda_{\mathrm{R}}^{\mathrm{I}} - \Lambda_{\mathrm{R}}^*\right) + O\left(\left(\Lambda^{\mathrm{I}}\right)^3\right). \end{aligned} \tag{3.71}$$

The constant term $J_0(\Lambda_{\mathrm{R}}^*)$ in Eq. 3.71 is not a function of the unknown $\Lambda_{\mathrm{R}}^{\mathrm{I}}$ and is eliminated, and the first order term is eliminated due to the first order necessary condition that the gradient $\partial J_0/\partial\Lambda|_{\Lambda^*}^T G = 0$ along the constraint $\mathrm{C2}_{\Lambda^{\mathrm{I}}}$. Neglecting the higher order terms, the quadratic cost is

$$J_{\Lambda^{\mathrm{I}}}(\Lambda_{\mathrm{R}}^{\mathrm{I}}) = J_0(\Lambda_{\mathrm{R}}^{\mathrm{I}}) - J_0(\Lambda^*) \approx \frac{1}{2}\left(\Lambda_{\mathrm{R}}^{\mathrm{I}} - \Lambda_{\mathrm{R}}^*\right)^T G^T \left.\frac{\partial^2 J_0}{\partial\Lambda^2}\right|_{\Lambda^*} G\left(\Lambda_{\mathrm{R}}^{\mathrm{I}} - \Lambda_{\mathrm{R}}^*\right) \quad (3.72)$$

The Hessian $G^T\left(\partial^2 J_0/\partial\Lambda^2|_{\Lambda^*}\right)G$ is now used to search for the optimal integer constrained solution. Note that the derivation of Eq. 3.72 could have been derived by introducing Eq. 3.65 in the LMI problem in Eq. 3.46 before the Taylor expansion in Eq. 3.55. In this case, the resulting cost in a Taylor expansion of this reduced LMI problem would similarly yield Eq. 3.71.

Note that the calculation of the cost, gradient and Hessian can be used to implement the optimization for Λ^* in a Newton-type minimization algorithm. This can potentially yield much faster solution times than an LMI solver used for the optimization in Eq. 3.38.

A typical small-scale problem is shown in Figure 3.11. In this problem, the number of remote spacecraft $N = 3$ and the period length $K = 10$. In the upper left, the inverted triangle denotes the optimal solution Λ^* which lies on the constraint $\mathrm{C2}_{\Lambda^{\mathrm{I}*}}$, denoted by the shaded triangular plane. Also shown is a level curve of the cost function $J_0(\Lambda)$ projected on to the constraint plane, as well as the planes of each of the three λ_1–λ_3 axes. Each of the three projections are shown in detail in the remaining three figures. Also shown on each are the ellipsoidal level sets given by the Hessian in Equation 3.72, illustrating the accuracy of the second order approximation, and the admissible and inadmissible points for the integer constrained solution, as defined by constraints $\mathrm{C1}_{\Lambda^{\mathrm{I}}}$–$\mathrm{C3}_{\Lambda^{\mathrm{I}}}$.

Using the gradient and Hessian, three solution methods are presented, in in-

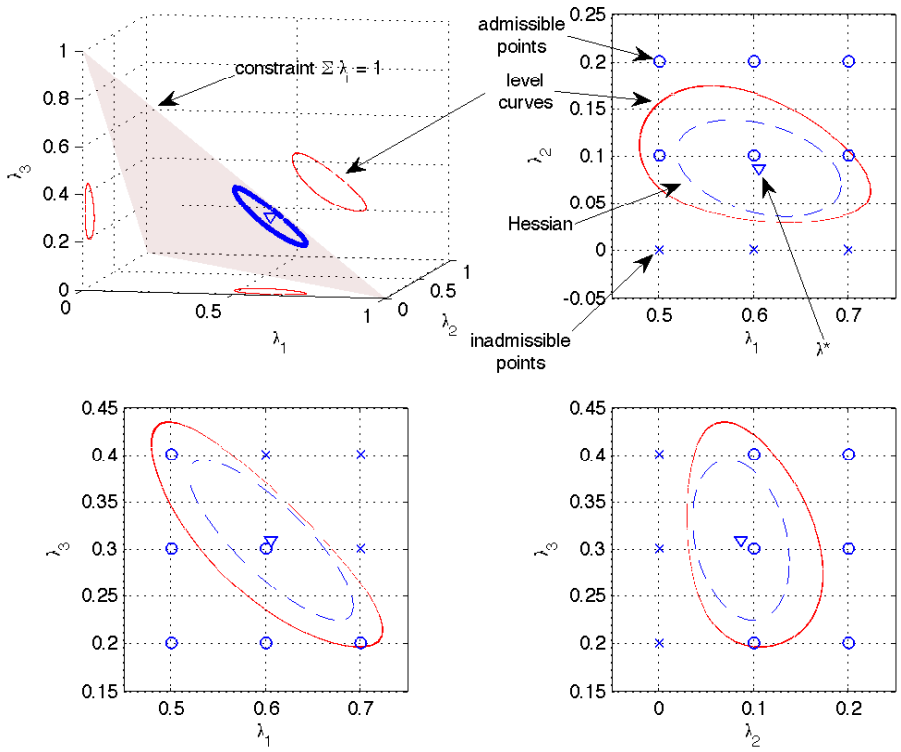

Figure 3.11: Comparison of the Hessian and the level sets of J_0. Also shown are the admissible and inadmissible points of the integer solution due the constraints on Λ.

creasing order of complexity, to find the optimal integer -constrained Λ^{I*} which satisfies the constraints $C1_{\Lambda^{I*}}$–$C3_{\Lambda^{I*}}$, given the unconstrained solution Λ^*. The methods are based on the principle of iterating from the unconstrained solution Λ^* to find a constrained solution which yields the smallest increase in cost. The three methods are:

- Batch Rounding (BR): rounding Λ^*_R to the nearest integer,
- Successive Rounding (SR): successive rounding of individual elements of Λ^* coupled with solving reduced order problems in a manner analogous to the

back substitution method of Ref. [25], and

- Integer Transformed Batch Rounding (ITBR): applying an integer-preserving transformation[32] to Λ and rounding in the transformed space similar to (1).

Batch Rounding (BR)

In this method, $\Lambda_{\mathrm{R}}^{\mathrm{I}} = \frac{1}{K}\mathrm{round}(K\Lambda_{\mathrm{R}}^{*})$. Since the rounding operation may violate the constraint $\mathrm{C1}_{\Lambda^{\mathrm{I}}}$, the Hessian in Eq. 3.57 is used to find the direction in which to increment or decrement the element of Λ^{I} which results in the smallest change in cost J_0 in Eq. 3.71. The algorithm is as follows:

1. $\Lambda^{\mathrm{I-BR}*} = e_N + \frac{1}{K}G\mathrm{round}(K\Lambda_{\mathrm{R}}^{*})$
2. $S^{\mathrm{I-BR}} = \{j \mid \lambda_j^{\mathrm{I-BR}} = 0\},\ S_{\perp}^{\mathrm{I-BR}} = M \setminus S^{\mathrm{I-BR}},\ \lambda_j^{\mathrm{I-BR}*} = 1/K\ \forall\ j \in S^{\mathrm{I-BR}},$
3. for $\kappa = 1, \ldots, \left|S^{\mathrm{I-BR}}\right|, j_\kappa = \arg\min_{j \in S_{\perp}^{\mathrm{I-BR}}} e_j^T \left(\partial^2 J_0/\partial\Lambda^2|_{\Lambda^*}\right) e_j,\ S_{\perp}^{\mathrm{I-BR}} = S_{\perp}^{\mathrm{I-BR}} \setminus j_\kappa,\ \lambda_{j_\kappa}^{\mathrm{I-BR}*} = \lambda_{j_\kappa}^{\mathrm{I-BR}*} - 1/K$

where $\left|S^{\mathrm{I-BR}}\right|$ denotes the cardinality of the set $S^{\mathrm{I-BR}}$ and $\setminus$ denotes set subtraction. Step 1 performs the initial rounding operation in the reduced space which ensures that constraint $\mathrm{C2}_{\Lambda^{\mathrm{I-BR}*}}$ is satisfied. Step 2 initializes the set $S^{\mathrm{I-BR}}$ to the indices of the elements of $\Lambda^{\mathrm{I-BR}*}$ which are zero, and $S_{\perp}^{\mathrm{I-BR}}$ to those which are nonzero, and sets the zero elements of $\Lambda^{\mathrm{I-BR}*}$ to the minimum value of $1/K$. Step 3 is the main loop, which finds the smallest change in cost via the Hessian, and decrements those values of $\Lambda^{\mathrm{I-BR}*}$ by $1/K$ to preserve the constraint $\mathrm{C2}_{\Lambda^{\mathrm{I-BR}*}}$.

Successive Rounding (SR)

In this method, the gradient and the Hessian in Eqs. 3.56 and 3.57, respectively, are used to guide the direction of the rounding of a single element of $\Lambda_{\mathrm{R}}^{\mathrm{I}}$. This element is then fixed, and the LMI problem 3.46 is solved for the remaining $N-1$ elements of $\Lambda_{\mathrm{R}}^{\mathrm{I}}$. The gradient and Hessian are recalculated, and a new rounding direction is chosen. This process repeats until all the elements of $\Lambda_{\mathrm{R}}^{\mathrm{I}}$ have been found. The algorithm proceeds as follows:

1. $S^{\mathrm{I-SR}} = \{1, \ldots, N-1\},\ \Lambda_{\mathrm{R}}^{\mathrm{I-SR}} = \Lambda_{\mathrm{R}}^{*},\ g = \left(\partial J_0/\partial\Lambda|_{\Lambda^*}\right) G,\ H = G^T \left(\partial^2 J_0/\partial\Lambda^2|_{\Lambda^*}\right) G$
2. $J^* = \infty$, for $j \in S^{\mathrm{I-SR}},\ \Lambda^+ = \Lambda^- = \Lambda_{\mathrm{R}}^{\mathrm{I-SR}},\ \lambda_j^+ = \frac{1}{K}\left\lceil K\lambda_{\mathrm{R}j}^{\mathrm{I-SR}}\right\rceil,\ \lambda_j^- = \frac{1}{K}\left\lfloor K\lambda_{\mathrm{R}j}^{\mathrm{I-SR}}\right\rfloor$

$$J^+ = g^T(\Lambda^+ - \Lambda_{\mathrm{R}}^{\mathrm{I-SR}}) + \frac{1}{2}(\Lambda^+ - \Lambda_{\mathrm{R}}^{\mathrm{I-SR}})^T H(\Lambda^+ - \Lambda_{\mathrm{R}}^{\mathrm{I-SR}})$$
$$J^- = g^T(\Lambda^- - \Lambda_{\mathrm{R}}^{\mathrm{I-SR}}) + \frac{1}{2}(\Lambda^- - \Lambda_{\mathrm{R}}^{\mathrm{I-SR}})^T H(\Lambda^- - \Lambda_{\mathrm{R}}^{\mathrm{I-SR}})$$
$$\text{if } J^+ < J^*,\ J^* = J^+,\ \Lambda_{\mathrm{R}}^{\mathrm{I-SR}*} = \Lambda^+,\ j^* = j$$
$$\text{if } J^- < J^*,\ J^* = J^-,\ \Lambda_{\mathrm{R}}^{\mathrm{I-SR}*} = \Lambda^-,\ j^* = j$$

3. $\Lambda_{\mathrm{R}}^{\mathrm{I-SR}} = \Lambda_{\mathrm{R}}^{\mathrm{I-SR}*},\ S^{\mathrm{I-SR}} = S^{\mathrm{I-SR}} \setminus j^*$, solve LMI problem 3.46 with constant $\lambda_j^{\mathrm{I-SR}}\ \forall\ j \notin S^{\mathrm{I-SR}},\ g = \left(\partial J_0/\partial\Lambda|_{\Lambda_{\mathrm{R}}^{\mathrm{I-SR}}}\right) G,\ H = G^T\left(\partial^2 J_0/\partial\Lambda^2|_{\Lambda_{\mathrm{R}}^{\mathrm{I-SR}}}\right) G$
4. if $S^{\mathrm{I-SR}} \neq \emptyset$, go to line 2; otherwise, $\Lambda^{\mathrm{I-SR}*} = e_N + G\Lambda_{\mathrm{R}}^{\mathrm{I-SR}}$
5. if $\lambda_N^{\mathrm{I-SR}*} = 0,\ \lambda_N^{\mathrm{I-SR}*} = 1/K,\ j = \arg\min_{j\in\{1,\ldots,N-1\}} e_j^T \left(\partial^2 J_0/\partial\Lambda^2|_{\Lambda^{\mathrm{I-SR}*}}\right) e_j$, $\lambda_j^{\mathrm{I-SR}*} = \lambda_j^{\mathrm{I-SR}*} - 1/K$

Line 1 performs the initialization of $S^{\mathrm{I-SR}}$, which contains the indices of measurements to be optimized; this set will be empty upon completion of the algorithm.

Also, the gradient, g, and Hessian, H, are initialized. Lines 2, 3 and 4 constitute the main loop. Line 2 rounds each free element of $\Lambda_{\mathrm{R}}^{\mathrm{I-SR}}$ up and down via the floor and ceiling operations $\lfloor\cdot\rfloor$ and $\lceil\cdot\rceil$, and selects the duty cycle change which results in the lowest cost perturbation. In Line 3, the index of the rounded measurement j^* is removed from the set $S^{\mathrm{I-SR}}$. The LMI problem is resolved for the elements of Λ which have not been rounded while holding constant those elements which have already been rounded. The gradient and Hessian are then reevaluated at the new solution. In Line 4, if $S^{\mathrm{I-SR}}$ is not empty, the algorithm loops back to line 2. Line 5 ensures that constraint $\mathrm{C1}_{\Lambda^{\mathrm{I-SR}*}}$ is met via a calculation similar to a single step in the BR algorithm.

Integer Transformed Batch Rounding (ITBR)

This method is similar to BR, but before Λ_{R}^* is rounded, a full rank integer-preserving transformation, denoted by Z, is applied such that $\Gamma_{\mathrm{R}}^* = Z\Lambda_{\mathrm{R}}^*$ and $\Gamma_{\mathrm{R}}^{\mathrm{I}*} = Z\Lambda_{\mathrm{R}}^{\mathrm{I}*}$. The transformation Z is defined such that the entries of Z and Z^{-1} are integers in order to preserve $\Gamma_{\mathrm{R}}^{\mathrm{I}}$ being an integer. Ref. [32] presents an algorithm to find Z, which, when applied to the Hessian of a least squares cost function, attempts to diagonalize the resulting transformed Hessian. The transformation Z is found via an LDL decomposition[16] of the form

$$G^T \left.\frac{\partial^2 J_0}{\partial \Lambda^2}\right|_{\Lambda^*} G = LDL^T \tag{3.73}$$

where D is diagonal, and L is lower triangular with ones along the diagonal such that $L_{ii} = 1$. The individual elements of L are rounded to yield

$$Z = \mathrm{round}(L^T). \tag{3.74}$$

Note that because Z is lower upper triangular and unimodular (i.e. integer-preserving), then Z^{-1} is also upper triangular and unimodular. The transformation

is applied to Eq. 3.72 to yield

$$J_\Lambda(\Gamma_{\mathrm{R}}^{\mathrm{I}}) = \frac{1}{2}\left(\Gamma_{\mathrm{R}}^{\mathrm{I}} - \Gamma_{\mathrm{R}}^{*}\right)^T Z^{-T} G^T \left.\frac{\partial^2 J_0}{\partial \Lambda^2}\right|_{\Lambda^*} G Z^{-1}\left(\Gamma_{\mathrm{R}}^{\mathrm{I}} - \Gamma_{\mathrm{R}}^{*}\right) \tag{3.75}$$

If the resulting matrix $Z^{-T}G^T\,\partial^2 J_0/\partial\Lambda^2|_{\Lambda^*}\,GZ^{-1}$ is exactly diagonal, and the rounded solution in Eq. 3.79 satisfies the constraints $\mathrm{C1}_{\Lambda^{\mathrm{I}}}$–$\mathrm{C3}_{\Lambda^{\mathrm{I}}}$, then the rounded solution is the optimal integer solution (to third order). However, the integer constraint on Z does not guarantee diagonalization of the Hessian.

Thus, given the unconstrained solution Λ^*, the integer solution is obtained via

$$\begin{aligned}
\Gamma_{\mathrm{R}}^{\mathrm{I-ITBR}*} &= \frac{1}{K}\mathrm{round}\left(K\Gamma_{\mathrm{R}}^{*}\right) && (3.76)\\
&= \frac{1}{K}\mathrm{round}\left(KZ^{-1}\Lambda_{\mathrm{R}}^{*}\right). && (3.77)
\end{aligned}$$

The final solution is

$$\begin{aligned}
\Lambda_{\mathrm{R}}^{\mathrm{I-ITBR}*} &= Z\Gamma_{\mathrm{R}}^{\mathrm{I-ITBR}*} && (3.78)\\
&= \frac{1}{K}Z\left[\mathrm{round}\left(KZ^{-1}\Lambda_{\mathrm{R}}^{*}\right)\right]. && (3.79)
\end{aligned}$$

Note that the choice of Λ_{R}, i.e. the choice of which element to remove from Λ in order to eliminate the constraint $\mathrm{C2}_\Lambda$, can affect the result of the SR and ITBR algorithms. A solution to this is to run either algorithm for the N possible choices of Λ_{R}. Since running a single SR algorithm requires solving N individual LMI problems, running the algorithm N times is considered to be prohibitively expensive. However, the LDL decomposition in the ITBR algorithm can be performed quickly and so the algorithm can be run multiple times.

Table 3.2: Formation parameters for testing the integer optimization algorithms.

N	3	3	3	3	3	3	3	3	3	4	5	6
K	4	6	8	10	14	18	22	26	30	16	20	24

Integer Rounding Algorithm Performance

Each of the three algorithms were run on several formations consisting of between three and six remote spacecraft. The parameters for each test are outlined in Table 3.2. For each case, the optimization was performed for three formations and two different cost functions: (1) the cost defined in Eq. 3.40, referred to as the system information, and (2) a modified version of Eq. 3.40, based on the center state information, as it is defined in Chapter 2 to be

$$\min_{\mathbf{Y}_{0\mathrm{C}}} \left[- \text{ trace } \left\{ \Theta^T \bar{\mathbf{Y}}_0 \Theta \right\} \right], \quad \text{subject to } \bar{\mathbf{L}} < 0 \tag{3.80}$$

where $\Theta = [I \ \cdots \ I]^T$, yielding a total of $12 \times 2 \times 2 = 48$ cases. In every case but one, at least one of the three algorithms finds the correct solution. The BR algorithm finds the correct solution in 41 of the 48 cases, the SR algorithm finds the correct solution in 36 of the cases, and the ITBR algorithm finds the correct solution in 47 of the 48 cases. The relatively poor performance of the SR algorithm is likely due to the choice of Λ_{R} when solving the problem. Since the ITBR algorithm uses all N possible Λ_{R}, it finds the optimal solution much more frequently.

Note that each algorithm is open to modification. For example, in step 2 of the SR algorithm the perturbations to the cost, J^+ and J^- can be evaluated exactly using the Riccati equation in Eq. 3.58. In Ref. [32], the integer transformation Z is found by rounding the elements of L^{-T} instead of L^T. However, based on the performance, the algorithms described here are considered to be complete.

3.4 Conclusions

Solutions to the sensor scheduling problem have been presented based on LMI analysis and an assumption that the process noise in deep space is relatively low. The relaxation of the scheduling problem described allows for a fast convex optimization of the individual measurement duty cycles of each sensor. Once the optimal duty cycles are determined, they are used as an initial guess in established integer least squares algorithms which account for the finite measurement sequence period. Results show that the affects of the approximation are negligible.

Key insights gained into the scheduling problem are:

- The scheduling problem is convex for low process noise if the integer constraint on the measurement rates Λ is relaxed, i.e. Λ is continuous.
- The zero-th order cost is independent of the ordering of the measurements.
- As the period K becomes large, the measurement rates as found by performing an exhaustive search using the truth schedule approaches a constant Λ_{const}, as denoted by the envelopes in Figures 3.9 and 3.10. Also, as K becomes large, the error in the zero-th order cost $J - J_0$ grows. In some cases, this will affect the optimal $\bar{\Lambda}$ found using the cost J_0.
- This Λ_{const} is equivalent to the optimal Λ^* found by the unconstrained solution to the zero-th order cost when $K = 1$. Note that the zero-th order cost $J_0 = J$ when $K = 1$. This is because the information update in Eq. 3.32 does not contain the $\tilde{\mathbf{Q}}$ cross-terms for $K = 1$.
- The increase in error between the continuous solution Λ^* and the truth integer constrained solution $\Lambda^{\text{I}*}$, with increasing K, as shown in Figures 3.9 and 3.10,

is due to the increase in the error between the zero-th order cost J_0 and the truth J as K increases.

CHAPTER 4

COMMUNICATION-ENABLED DISTRIBUTED STATE FUSION

4.1 Introduction

In this Chapter, a sequential state fusion algorithm is developed. Related work includes Ref. [14] in which the authors present the least squares fusion method for N Kalman filters in a batch method by combining all estimates at once. The method described in this chapter fuses each estimate iteratively and can account for time delays in the communication subsystem in between iterations. Another benefit of fusing sequentially is that the intermediate results are valid state estimates and can be used for command and control while the algorithm proceeds. Ref. [11] uses a similar method for fusing so that two existing Kalman filters need not be altered. Among the different methods presented in that paper, the author describes the method of reinitializing the two filters with the least squares solution in what is essentially a feedback loop. However, this was done for only two filters. In the algorithm developed in this Chapter, the result of the state fusion, performed on one spacecraft at a time, is used to reinitialize the local estimator, which operates on the locally generated RBS measurements.

The covariance intersection algorithm [20] has been explored as a method for state fusion when cross-correlations are unknown. However, it has been shown that such a filter can actually converge to a state where new information is discarded [1]. The authors of Ref. [1] propose a tuning method to avoid this, however this method does not lend itself easily to automation. The least squares method proposed in this Chapter uses cross correlation matrices which are calculated online via the suboptimal steady state extended Kalman filter gains. For the formation keeping

problem, steady state filter gains for the local measurements can be found and these are assumed to be known at each spacecraft. If the initial covariances and cross covariance matrices are known, then they can be propagated forward in time assuming the

In our previous work, Ref. [21] describes a circular communication/estimation system which is based on the information filter[24]. By making the assumption of low process noise in deep space missions, an approximation is arrived at that enables the separate local measurements to be encapsulated in a single information vector and associated information (i.e. inverse covariance) matrix having dimensions equivalent to the number of states in the system. This measurement vector and matrix is transmitted from one spacecraft to another and is augmented by each spacecraft with locally stored measurements. The measurement vector and matrix is also updated at each time step with the dynamics model, accounting for time delays in the communication subsystem. However, the approximation leads to an optimistic estimate at each spacecraft with a covariance that is smaller than the optimal covariance as given by the standard Kalman filter. The work presented herein is shown to yield a conservative estimate at each spacecraft with covariance that is always larger than the Kalman filter covariance. In addition, although it uses the same circular communication architecture, it does not require the transmission of a large information matrix. Only local estimates, each with a dimension equivalent to the number of states in the formation system, are communicated throughout the formation.

This Chapter is outlined as follows: Section 4.2 outlines the communication-constrained estimation problem and assumptions such as dynamics, the sensor model, and elements of the formation keeping controller. The distributed fusion

filter is described in Section 4.3. Section 4.4 details the performance of the filter as compared to a standard Kalman filter which operates on the raw measurements, as well as the performance of the system in terms of fuel usage and RMS position error.

4.2 Problem Statement and Assumptions

The central assumption in this Chapter is that each spacecraft must use only a single fixed transmit and receive communication link. This is considered to be the minimal communication requirement in that each spacecraft is an information source via the local RBS sensor, and therefore must transmit this information in some form to the fleet. Similarly, each spacecraft in the fleet must also posses some means of receiving information from the fleet. Therefore, for a fleet of N spacecraft, a total of N unidirectional communication links are required. In contrast, the channel filter method [17] uses a spanning tree network which requires $N-1$ bidirectional communication links. In addition, almost every node in the network requires two bidirectional communication links. The problem lies in forming accurate state estimates while transmitting local state estimates only, as opposed to transmitting raw measurements or estimates and associated covariances. The remainder of this Section describes the governing dynamics, and the components of the sensing, communication and control subsystems.

4.2.1 Spacecraft Dynamics

Each spacecraft is governed by second order dynamics, thus for N spacecraft, the discrete-time dynamics of the i-th spacecraft, $\forall\ i \in \{1, ..., N\}$, are as follows,

$$x_i(k+1) = Ax_i(k) + B_i u_i(k) + B_i w_i(k), \tag{4.1}$$

$$x_i(k) = \begin{bmatrix} x_i^{(1)}(k) \\ \dot{x}_i^{(1)}(k) \\ x_i^{(2)}(k) \\ \dot{x}_i^{(2)}(k) \end{bmatrix},\ u_i(k) = \begin{bmatrix} u_i^{(1)}(k) \\ u_i^{(2)}(k) \end{bmatrix},\ w_i(k) = \begin{bmatrix} w_i^{(1)}(k) \\ w_i^{(2)}(k) \end{bmatrix}, \tag{4.2}$$

$$A = \begin{bmatrix} 1 & \Delta T & 0 & 0 \\ 0 & 1 & 0 & 0 \\ 0 & 0 & 1 & \Delta T \\ 0 & 0 & 0 & 1 \end{bmatrix},\ B_i = \frac{1}{M_i} \begin{bmatrix} \Delta T^2/2 & 0 \\ \Delta T & 0 \\ 0 & \Delta T^2/2 \\ 0 & \Delta T \end{bmatrix}, \tag{4.3}$$

where x_i is the state of spacecraft i in an inertial frame, u_i is the control input, w_i is zero mean white process noise with covariance Q_i, M_i is the mass of the i-th spacecraft and ΔT is the sampling time. Two dimensional systems are presented here for simplicity but the approach is fully generalized to three dimensions.

Given the linear dynamics and the lack of an inertial position sensor, the i-th spacecraft maintains estimates of $N-1$ relative states. The relative dynamics are found by subtracting Eq. 4.1 from itself and replacing i with j,

$$x_{j,i}(k+1) = Ax_{ji}(k) + B_j u_j(k) - B_i u_i(k) + B_j w_j(k) - B_i w_i(k), \tag{4.4}$$

$$x_{j,i}(k) \triangleq x_j(k) - x_i(k)\ \forall\ j \neq i. \tag{4.5}$$

Note that this does not require the mass of each spacecraft to be identical. The key is that the state transition matrices are identical for each spacecraft across the

fleet eliminating the need for inertial states, and thus, measurements in an inertial frame.

Equations 4.4 and 4.5 can be rewritten to yield a full set of dynamics of the formation relative to spacecraft i:

$$\mathbf{x}_i(k+1) = \mathbf{A}\mathbf{x}_i(k) + \mathbf{B}_i\mathbf{u}(k) + \mathbf{B}_i\mathbf{w}(k) \tag{4.6}$$

$$\mathbf{x}_i(k) = \begin{bmatrix} \vdots \\ x_{j,i}(k) \\ \vdots \end{bmatrix}_{j\in\{1,\ldots,N\}\setminus i}, \tag{4.7}$$

$$\{\mathbf{u},\mathbf{w}\}(k) \triangleq \begin{bmatrix} \{u,w\}_1(k) \\ \vdots \\ \{u,w\}_N(k) \end{bmatrix}, \tag{4.8}$$

$$\mathbf{A} \triangleq \begin{bmatrix} A & & \\ & \ddots & \\ & & A \end{bmatrix}, \tag{4.9}$$

$$\mathbf{B}_i \triangleq \begin{bmatrix} B_1 & & & -B_i & & & \\ & \ddots & & \vdots & & & \\ & & B_{i-1} & -B_i & & & \\ & & & -B_i & B_{i+1} & & \\ & & & \vdots & & \ddots & \\ & & & -B_i & & & B_N \end{bmatrix}. \tag{4.10}$$

where the column of $-B_i$ matrices is in the i-th (block) column of $\mathbf{B}_i$. The definition of the formation relative state $\mathbf{x}_i(k)$ in Equation 4.7 is read as a vector consisting of the $N-1$ relative states defined in Eq. 4.5 such that $\mathbf{x}_i \in \mathbb{R}^{4(N-1)}$. It follows from the definitions that $\mathbf{w}$ is zero mean and its covariance is $E\left[\mathbf{w}(j)\mathbf{w}(k)^T\right] =$

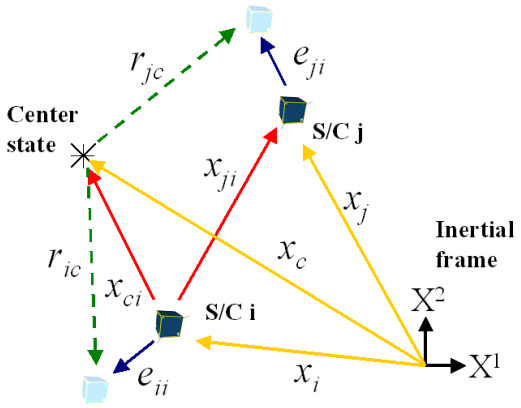

Figure 4.1: Virtual center state x_{ci} relative to spacecraft i, denoted by *. Also shown are reference states $r_{\cdot c}$, error states $e_{\cdot i}$ and relative state x_{ji}.

$\mathbf{Q}\delta_{jk}$ where,

$$\mathbf{Q} = \begin{bmatrix} Q_1 & & \\ & \ddots & \\ & & Q_N \end{bmatrix}. \tag{4.11}$$

The relative state vectors are shown conceptually in Figure 4.1.

Transformation matrices from the frame of one spacecraft to another are useful when communicating local state estimates. First, a transformation matrix from the inertial state to the relative state of the i-th spacecraft is found. Denoting the system state in the inertial frame by $\mathbf{x}(k)$ such that $\mathbf{x}(k) = \left[x_1(k)^T \cdots x_N(k)^T\right]^T$, a matrix, T_i, is found such that $\mathbf{x}_i(k) = T_i\mathbf{x}(k)$. Such a matrix is defined similar

to the definition of $\mathbf{B}_i$ and as such, it takes the form

$$T_i = \begin{bmatrix} I & & & -I & & & \\ & \ddots & & \vdots & & & \\ & & I & -I & & & \\ & & & -I & I & & \\ & & & \vdots & & \ddots & \\ & & & -I & & & I \end{bmatrix} \tag{4.12}$$

where the column of $-I$ matrices is in the i-th (block) column of T_i. Note that the range of each T_i spans the same subspace of $\mathbb{R}^{4N}$. This is shown by noting that the null space of each T_i is the same and is given by $[I \ \cdots \ I]^T$. Therefore, a matrix, $T_{i,j}$, can be found such that $\mathbf{x}_i(k) = T_{i,j}\mathbf{x}_j(k)$. This transformation is given by

$$T_{i,j} = T_i T_j^\dagger \tag{4.13}$$

where $T_j^\dagger$ denotes the Moore-Penrose pseudoinverse of T_j defined as $T_j^\dagger = T_j^T \left(T_j T_j^T\right)^{-1}$.

4.2.2 Virtual Center Reference States

For formation control, a reference state for each vehicle in the formation must be defined. Following the development in Chapter 2, a *virtual center state*, x_c, is defined relative to the desired formation geometry in the inertial reference frame; a local frame centered at x_c is then defined such that the difference between the inertial frame and the virtual center frame is only a translation. A local reference frame at each spacecraft i is similarly defined and the location of the virtual center in the i-th local frame is denoted by $x_{\mathrm{c}i} = x_\mathrm{c} - x_i$, similar in notation to Eq. 4.5. Over relatively short time horizons, the formation is allowed to drift in the inertial

frame. Therefore, it is sufficient to specify the reference states in the virtual center frame, denoted by $r_{ci} \in \mathbb{R}^4 \; \forall \; i \in \{1, ..., N\}$.

4.2.3 RBS Measurements

The measurements provided by the RBS at each spacecraft $i \in \{1, \ldots, N\}$ are relative range and bearing to a remote spacecraft m_i, each corrupted with white Gaussian noise. Thus, at each time step k, a measurement is made to a single spacecraft,

$$
\begin{aligned}
z_i(k) &= \mathbf{h}_i\left(\mathbf{x}_i(k)\right) + v_i(k) && (4.14)\\
&= h(x_{m_i,i}(k)) + v_i(k), && (4.15)\\
h(x_{m_i,i}(k)) &= \begin{bmatrix} R_{m_i,i}(k) \\ \phi_{m_i,i}(k) \end{bmatrix} = \begin{bmatrix} \sqrt{(x^{(1)}_{m_i,i}(k))^2 + (x^{(2)}_{m_i,i}(k))^2} \\ \tan^{-1} \frac{x^{(2)}_{m_i,i}(k)}{x^{(1)}_{m_i,i}(k)} \end{bmatrix}. && (4.16)
\end{aligned}
$$

where v_i is zero mean, white Gaussian noise with covariance R_i. The state of spacecraft m_i relative to spacecraft i is denoted by $x_{m_i,i}$, as per Eq. 4.5 with $j = m_i$. Because the spacecraft is assumed equipped with an inertial attitude sensor, the relative range/bearing measurements are assumed to be made in the inertial frame without loss of generality; the statistical errors present in the attitude sensor are assumed to be built into the RBS noise covariance R_i. The sensor is also assumed to be able to provide measurements at all ranges under consideration.

The set $\{m_1, \ldots, m_N\}$ describes the sensing topology of the formation. Note that care must be taken with the selection of the $\{m_1, \ldots, m_N\}$ in order to ensure that the system is observable with the measurements $\{z_1(k), \ldots, z_N(k)\}$.

4.2.4 Local Steady State Extended Kalman Filter

For the formation keeping problem, the measurement $\mathbf{h}_i(\cdot)$ is linearized about the reference formation and the steady state EKF gains are found for each spacecraft for the observable part of the formation state. Assuming that at spacecraft i a relative range/bearing measurement to spacecraft m_i is made, the observable part of the system is governed by the reduced system Equations 4.4 and 4.15 with $j = m_i$. The steady state gain is given by

$$K_i = P_i C_i \left(C_i P_i C_i^T + R_i \right)^{-1} \tag{4.17}$$

such that P_i satisfies the Riccati equation

$$P_i = A P_i A^T + \left[\mathbf{B}_i\right]_{m_i} \mathbf{Q} \left[\mathbf{B}_i\right]_{m_i}^T - A P_i C_i^T \left[C_i P_i C_i^T + R_i \right]^{-1} C_i P_i A^T \tag{4.18}$$

and where $\left[\mathbf{B}_i\right]_{m_i}$ is the m_i-th block row of $\mathbf{B}_i$ corresponding to the effect the process noise $\mathbf{w}(k)$ has on the observable state $x_{m_i,i}(k)$. The linearized measurement matrix C_i is given by

$$C_i = \left. \frac{\partial h}{\partial x} \right|_{r_{cm_i} - r_{ci}} . \tag{4.19}$$

The gain K_i corresponding to the observable state can be integrated into a filter that operates on the full relative state $\mathbf{x}_i(k)$. The equation for the full state estimate is given by

$$\hat{\mathbf{x}}_i(k+1) = \mathbf{A}\hat{\mathbf{x}}_i(k) + \mathbf{B}_i\mathbf{u}(k) + \mathbf{K}_i \left[z_{m_i,i}(k+1) - \mathbf{h}\left(\mathbf{A}\hat{\mathbf{x}}_i(k) + \mathbf{B}_i\mathbf{u}(k) \right) \right] \tag{4.20}$$

where

$$\mathbf{K}_i = \begin{bmatrix} 0 \\ \vdots \\ 0 \\ K_i \\ 0 \\ \vdots \\ 0 \end{bmatrix} \tag{4.21}$$

such that the m_i-th row of $\mathbf{K}_i$ contains K_i and is zeros elsewhere, thereby updating the observable state corresponding to $x_{m_i i}$ in Eq. 4.20. Similarly, a full linearized measurement matrix, denoted by $\mathbf{C}_i$ is defined such that

$$\mathbf{C}_i = \begin{bmatrix} 0 & \cdots & 0 & C_i & 0 & \cdots & 0 \end{bmatrix} \tag{4.22}$$

$$= \begin{bmatrix} 0 & \cdots & 0 & \frac{\partial h}{\partial x}\big|_{r_{m_i c} - r_{ic}} & 0 & \cdots & 0 \end{bmatrix} \tag{4.23}$$

such that the m_i-th column of $\mathbf{C}_i$ contains C_i and is zeros elsewhere, corresponding to the relative state to the observed spacecraft m_i. Note that, in the absence of additional measurements or communication, the filter in Eq. 4.20 will diverge due to the lack of observability of the unmeasured spacecraft.

4.2.5 Time Optimal Controller

An optimal controller (minimum time) based on thrust limited ($u_i^{(\{1,2\})} \in \{-U_{max}, 0, U_{max}\}$) propulsion is used in the same vein as that developed in Ref. [9]. Because the satellite can be represented with second order free space dynamics in each axis (decoupled), a feed forward, formation keeping controller based on minimum time optimal control is developed. The controller is activated if the satellite

drifts away from its reference position by more than an error ellipse, which is written as

$$\left[\begin{array}{c} e_{ii}(k) \end{array}\right]^T \left[\begin{array}{c} \text{diag}\{e_{max}^{(1)}, \dot{e}_{max}^{(1)}, e_{max}^{(2)}, \dot{e}_{max}^{(2)}\} \end{array}\right] \left[\begin{array}{c} e_{ii}(k) \end{array}\right] > 1 \tag{4.24}$$

where $e_{max}^{(\cdot)}, \dot{e}_{max}^{(\cdot)}$ are tuning parameters and $e_{ii}(k) = x_{ci}(k) + r_{ic}(k)$. If this occurs, a minimum time controller is calculated in each axis. For second order dynamics, the minimum time controller is a bang-bang controller with a single switch time. Thus, the control is given by

$$u_i^{(\cdot)}(k) = \begin{cases} -\text{sgn}(e^{(\cdot)} + \dot{e}^{(\cdot)}|\dot{e}^{(\cdot)}|/2)U_{max}, & 0 < k - k_o < T_{mt1,i}^{(\cdot)}/T \\ \text{sgn}(e^{(\cdot)} + \dot{e}^{(\cdot)}|\dot{e}^{(\cdot)}|/2)U_{max}, & T_{mt1,i}^{(\cdot)}/T < k - k_o < T_{mtF,i}^{(\cdot)}/T \end{cases} \tag{4.25}$$

where k_o is the time at the start of the maneuver. The switch time and final control time are written as

$$T_{mt1,i}^{(\cdot)} = \frac{-\dot{e}_{ii}^{(\cdot)}(k) \pm \sqrt{1/2(\dot{e}_{ii}^{(\cdot)}(k))^2 - e_{ii}^{(\cdot)}(k)\bar{U}_{max}}}{\bar{U}_{max}} \tag{4.26}$$

$$T_{mtF,i}^{(\cdot)} = \frac{-\dot{e}_{ii}^{(\cdot)}(k) \pm \sqrt{2(\dot{e}_{ii}^{(\cdot)}(k))^2 - 4e_{ii}^{(\cdot)}(k)\bar{U}_{max}}}{\bar{U}_{max}} \tag{4.27}$$

where $\bar{U}_{max} = U_{max}/m$. It is noted that other control methodologies, such as bounds on relative velocity, minimum fuel, etc. could be used, however this controller is sufficient to evaluate the proposed estimation architecture.

4.3 Iterated Fusion Filter

The proposed distributed iterated fusion filter (IFF) is based on each spacecraft $i = \{1, \cdots, N\}$ maintaining an estimate of the relative formation state $\mathbf{x}_i(k)$, which is denoted by $\hat{\mathbf{x}}_i(k)$. These estimates are updated on each spacecraft from time $k-1$

to time k with the data being generated by the local RBS $z_i(k)$ and the steady state extended Kalman filter gain according to Eq. 4.20. At certain times the individual estimates $\hat{\mathbf{x}}_i(k)$ are fused in an sequential manner using a communication architecture and the one-way transmission of the full system state estimate at one spacecraft to a single neighboring spacecraft. The process is analogous to *sequential* least squares estimation. Existing methods are focused on batch implementations of the state fusion operation (analogous to *batch* least square estimation) where all local estimates are transmitted to a single centralized node, the fusion is performed and the result is broadcast to the network. Such an approach places a high burden on the central node in terms of the computation and communication resources required.

The circular communication architecture is described in Section 4.3.1. The algorithm consists of two distinct steps. The global covariance update step occurs when the local Kalman filters are updated using the local measurements on the transition from time step k to time step $k+1$ and is outlined in Section 4.3.2. The fusion update step described in Section 4.3.3 occurs when an estimate is transmitted from one spacecraft to another. Square root implementations of each step are described in Section 4.3.4.

4.3.1 Circular Communication Architecture

In the proposed communication architecture, information, in the form of locally stored formation state estimates is transmitted from one spacecraft to another in a circular manner. Consider a simple formation, composed of two spacecraft denoted by $i \in \{1, 2\}$. At some initial time k_0, spacecraft 1 transmits its local estimate $\hat{\mathbf{x}}_1(k_0)$ to spacecraft 2. Due to time delays in the channel, this estimate is received

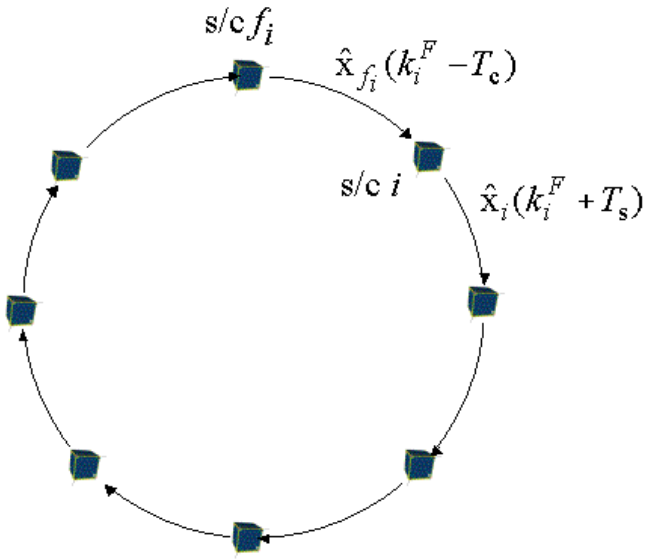

Figure 4.2: Illustration of the circular communication architecture and iterated state fusion. At time k_i^{F} spacecraft i receives the time delayed state estimate $\hat{\mathbf{x}}_{f_i}(k_i^{\mathrm{F}} - T_{\mathrm{c}})$ from spacecraft f_i, which is fused with the local estimate $\hat{\mathbf{x}}_{f_i}(k_i^{\mathrm{F}})$. At time $k_i^{\mathrm{F}} + T_{\mathrm{s}}$ spacecraft i sends the estimate $\hat{\mathbf{x}}_i(k_i^{\mathrm{F}} + T_{\mathrm{s}})$ to the next spacecraft in the circuit, i.e. spacecraft j such that $f_j = i$.

by spacecraft 2 at time $k_0 + T_{\mathrm{c}}$ where T_{c} denotes the communication delay time. Spacecraft 2 fuses its estimate $\hat{\mathbf{x}}_2(k_0 + T_{\mathrm{c}})$ with the received $\hat{\mathbf{x}}_1(k_0)$ and updates $\hat{\mathbf{x}}_2(k_0 + T_{\mathrm{c}})$ accordingly. There is an internal delay at each spacecraft, denoted by T_{s}, between the fusion and transmission times, during which each spacecraft updates its local estimate using the local RBS measurements. Therefore, at time $k_0 + T_{\mathrm{c}} + T_{\mathrm{s}}$, spacecraft 2 transmits its estimate $\hat{\mathbf{x}}_2(k_0 + T_{\mathrm{c}} + T_{\mathrm{s}})$ to spacecraft 1. Spacecraft 1 receives this estimate at time $k_0 + 2T_{\mathrm{c}} + T_{\mathrm{s}}$ and fuses $\hat{\mathbf{x}}_2(k_0 + T_{\mathrm{c}} + T_{\mathrm{s}})$ with its local estimate $\hat{\mathbf{x}}_1(k_0 + 2T_{\mathrm{c}} + T_{\mathrm{s}})$. After T_{s} time steps, spacecraft 1 transmits $\hat{\mathbf{x}}_3(k_0 + 2T_{\mathrm{c}} + 2T_{\mathrm{s}})$ to spacecraft 2, completing the cycle. This process is illustrated in Figure 4.2 for N spacecraft. The spacecraft from which spacecraft i receives

the formation estimate is denoted by f_i, which is analogous to m_i, defined in Section 4.2.3.

The time delay between successive fusion steps at any given spacecraft is equal to the round trip communication delay in the circular network and is denoted by T_{RT} such that

$$T_{\mathrm{RT}} = N\left(T_{\mathrm{s}} + T_{\mathrm{c}}\right) \tag{4.28}$$

The times at which a fusion occurs at spacecraft i is denoted by k_i^{F}. In the above example, $k_1^{\mathrm{F}} = \{k_0 - T_{\mathrm{s}} + T_{\mathrm{RT}}, k_0 - T_{\mathrm{s}} + 2T_{\mathrm{RT}}, \ldots\}$. Similarly, for spacecraft 2, $k_2^{\mathrm{F}} = \{k_0 - T_{\mathrm{s}} + T_{\mathrm{RT}}/2, k_0 - T_{\mathrm{s}} + 3T_{\mathrm{RT}}/2, \ldots\}$.

This approach is advantageous because it requires only a single transmit and receive communication link at each spacecraft. Moreover, transmitting the state is preferred over a method where individual measurements are transmitted throughout the formation and implementing a standard Kalman filter using the measurements delayed by the communication channel. This is due to the effects of the round trip time T_{RT}. If the communication proceeds from spacecraft $1 \rightarrow 2 \rightarrow \cdots \rightarrow N \rightarrow 1 \rightarrow \cdots$, at time step k_N^{F}, and EKF at spacecraft N would be required to incorporate all of the measurements generated in the formation, subject to the time delays described above. These measurements are $\{z_1(k_N^{\mathrm{F}} - 2T_{\mathrm{RT}}), \ldots, z_1(k_N^{\mathrm{F}} - T_{\mathrm{RT}}), z_2(k_N^{\mathrm{F}} - 2T_{\mathrm{RT}} + T_{\mathrm{c}} + T_{\mathrm{s}}), \ldots, z_2(k_N^{\mathrm{F}} - T_{\mathrm{RT}} + T_{\mathrm{c}} + T_{\mathrm{s}}), \ldots\}$, the number of which is $O(N^2(T_{\mathrm{c}} + T_{\mathrm{s}}))$. Section 4.4.2 compares the performance of such a filter with the IFF.

4.3.2 Global Covariance Measurement Update

In the absence of any communication, the local estimates are updated using the local RBS measurements only. At the transition from time step k to time stop $k+1$ the covariance matrices are stored at each spacecraft and are updated using the steady state Kalman filter gains. Consider the filter error dynamics at spacecraft i, found by subtracting Eq. 4.20 from Eq. 4.6 and linearizing in order to eliminate $\mathbf{h}(\cdot)$:

$$\mathbf{e}_i(k+1) = (\mathbf{A} - \mathbf{K}_i\mathbf{C}_i\mathbf{A})\mathbf{e}_i(k) + (\mathbf{B} - \mathbf{K}_i\mathbf{C}_i\mathbf{B})\mathbf{w}(k) - \mathbf{K}_i v_i(k+1), \tag{4.29}$$

where $\mathbf{e}_i(k) = \mathbf{x}_i(k) - \hat{\mathbf{x}}_i(k)$. In block form, the collected KF error dynamics are written as

$$\mathbf{e}_{\mathrm{G}}(k+1) = \mathbf{A}_{\mathrm{G}}\mathbf{e}_{\mathrm{G}}(k) + \mathbf{B}_{\mathrm{G}}\mathbf{w}(k) - \mathbf{K}_{\mathrm{G}}\mathbf{v}(k) \tag{4.30}$$

where,

$$\mathbf{e}_{\mathrm{G}}(k) = \begin{bmatrix} \mathbf{e}_1(k) \\ \vdots \\ \mathbf{e}_N(k) \end{bmatrix}, \mathbf{v}(k) = \begin{bmatrix} v_1(k) \\ \vdots \\ v_N(k) \end{bmatrix}, \tag{4.31}$$

and,

$$\mathbf{A}_{\mathrm{G}} = \begin{bmatrix} \mathbf{A} - \mathbf{K}_1\mathbf{C}_1\mathbf{A} & & \\ & \ddots & \\ & & \mathbf{A} - \mathbf{K}_N\mathbf{C}_N\mathbf{A} \end{bmatrix}, \tag{4.32}$$

$$\mathbf{B}_{\mathrm{G}} = \begin{bmatrix} \mathbf{B} - \mathbf{K}_1\mathbf{C}_1\mathbf{B} \\ \vdots \\ \mathbf{B} - \mathbf{K}_N\mathbf{C}_N\mathbf{B} \end{bmatrix}, \tag{4.33}$$

$$\mathbf{K}_{\mathrm{G}} = \begin{bmatrix} \mathbf{K}_1 & & \\ & \ddots & \\ & & \mathbf{K}_N \end{bmatrix}. \tag{4.34}$$

The global error covariance is denoted by $\mathbf{P}_{\mathrm{G}}(k) = E\left[\mathbf{e}_{\mathrm{G}}(k)\mathbf{e}_{\mathrm{G}}(k)^T\right]$ and is composed of the individual covariance and cross-covariance matrices such that $\left[\mathbf{P}_{\mathrm{G}}(k)\right]_{i,j} = \mathbf{P}_{i,j}$ where $[\cdot]_{i,j}$ denotes the ij-th sub-block of the matrix $\cdot$. If no communication (and therefore, no fusion) occurs and if $\mathbf{P}_{\mathrm{G}}$ is known at time step k, $\mathbf{P}_{\mathrm{G}}(k)$ can be propagated via the linear equation

$$\mathbf{P}_{\mathrm{G}}(k+1) = \mathbf{A}_{\mathrm{G}}\mathbf{P}_{\mathrm{G}}(k)\mathbf{A}_{\mathrm{G}}^T + \mathbf{B}_{\mathrm{G}}\mathbf{Q}\mathbf{B}_{\mathrm{G}}^T + \mathbf{K}_{\mathrm{G}}\mathbf{R}\mathbf{K}_{\mathrm{G}}^T \tag{4.35}$$

where $\mathbf{R} = \mathrm{diag}\left(R_1, \ldots, R_N\right)$. Note that, at each transition from time step k to time step $k+1$, each spacecraft updates its local estimate $\hat{\mathbf{x}}_i(k)$, and the global error covariance $\mathbf{P}_{\mathrm{G}}(k)$ using Eq. 4.35.

4.3.3 Fusion Update

When an estimate is transmitted from one spacecraft to the next, the receiving spacecraft performs a least squares fusion using the received estimate and its locally maintained estimate. These estimates are modeled as

$$\hat{\mathbf{x}}_i(k) = \mathbf{x}_i(k) + \mathbf{e}_i(k) \tag{4.36}$$

where $\mathbf{x}_i(k)$ is considered a constant, and $\mathbf{e}_i(k)$ is modeled as a zero-mean normally distributed random variable with covariance $E\left[\mathbf{e}_i(k)\mathbf{e}_i^T(k)\right] = \mathbf{P}_{i,i}(k)$. The cross covariance between any two of these errors is denoted by $\mathbf{P}_{i,m_i}(k)$ such that $\mathbf{P}_{i,m_i}(k) = E\left[\mathbf{e}_i(k)\mathbf{e}_{m_i}^T(k)\right]$. Note that Eq. 4.36 is an approximation because $\mathbf{x}_i(k)$ is not a constant. In Ref. [13] it is shown that this approximation leads to a state fusion algorithm that is suboptimal. However, the resulting fused estimates were shown to be conservative (i.e. having greater covariance) when compared to an EKF solution.

At time k_i^{F}, spacecraft i receives from spacecraft f_i the measurement $\hat{\mathbf{x}}_{f_i}(k_i^{\mathrm{F}} - T_{\mathrm{c}}$ where T_{c} is the time delay in the communication channel. Consider, first, the case where $T_{\mathrm{c}} = 0$. Because the estimates are jointly Gaussian and are modeled as in Eq. 4.36, fusing estimates from spacecraft i and f_i at time step k_i^{F} can be posed as a linear least squares problem. The log-likelihood function resulting from Eq. 4.36 is

$$\begin{aligned}
&\ln p\left(\mathbf{x}_i(k_i^{\mathrm{F}}) \mid \hat{\mathbf{x}}_i(k_i^{\mathrm{F}}), \hat{\mathbf{x}}_{f_i}(k_i^{\mathrm{F}})\right) \propto \\
&\quad -\left[\mathbf{T}_{f_i,i}\mathbf{x}_i(k_i^{\mathrm{F}}) - \hat{\mathbf{x}}_{i,f_i}^{\mathrm{F}}(k_i^{\mathrm{F}})\right]^T \mathbf{P}_{i,f_i}^{\mathrm{F}}(k_i^{\mathrm{F}})^{-1}\left[\mathbf{T}_{f_i,i}\mathbf{x}_i(k_i^{\mathrm{F}}) - \hat{\mathbf{x}}_{i,f_i}^{\mathrm{F}}(k_i^{\mathrm{F}})\right], \quad (4.37)
\end{aligned}$$

where

$$\mathbf{P}_{i,f_i}^{\mathrm{F}}(k_i^{\mathrm{F}}) = \begin{bmatrix} \mathbf{P}_{i,i}(k_i^{\mathrm{F}}) & \mathbf{P}_{i,f_i}(k_i^{\mathrm{F}}) \\ \mathbf{P}_{i,f_i}^T(k_i^{\mathrm{F}}) & \mathbf{P}_{f_i,f_i}(k_i^{\mathrm{F}}) \end{bmatrix}, \quad (4.38)$$

$$\mathbf{T}_{f_i,i} = \begin{bmatrix} I \\ T_{f_i,i} \end{bmatrix}, \quad \hat{\mathbf{x}}_i^{\mathrm{F}}(k_i^{\mathrm{F}}) = \begin{bmatrix} \hat{\mathbf{x}}_i(k_i^{\mathrm{F}}) \\ \hat{\mathbf{x}}_{f_i}(k_i^{\mathrm{F}}) \end{bmatrix} \quad (4.39)$$

Maximizing the likelihood function in Eq. 4.37 is therefore equivalent to solving the least squares problem

$$\hat{\mathbf{x}}_i(k_i^{\mathrm{F}}) \leftarrow \min_{\mathbf{x}_i(k_i^{\mathrm{F}})} \left[\mathbf{T}_{f_i,i}\mathbf{x}_i(k_i^{\mathrm{F}}) - \hat{\mathbf{x}}_{i,f_i}^{\mathrm{F}}(k_i^{\mathrm{F}})\right]^T \mathbf{P}_{i,f_i}^{\mathrm{F}}(k_i^{\mathrm{F}})^{-1}\left[\mathbf{T}_{f_i,i}\mathbf{x}_i(k_i^{\mathrm{F}}) - \hat{\mathbf{x}}_{i,f_i}^{\mathrm{F}}(k_i^{\mathrm{F}})\right], \quad (4.40)$$

where the $\leftarrow$ denotes the updating of $\hat{\mathbf{x}}_i(k_i^{\mathrm{F}})$ with the RHS of Eq. 4.40, which is a function of $\hat{\mathbf{x}}_i(k_i^{\mathrm{F}})$ and $\hat{\mathbf{x}}_{f_i}(k_i^{\mathrm{F}})$. The solution to Eq. 4.40 is

$$\begin{aligned}
\hat{\mathbf{x}}_i(k_i^{\mathrm{F}}) &\leftarrow \left(\mathbf{T}_{f_i,i}^T\mathbf{P}_{i,f_i}^{\mathrm{F}}(k_i^{\mathrm{F}})^{-1}\mathbf{T}_{f_i,i}\right)^{-1}\mathbf{T}_{f_i,i}^T\mathbf{P}_{i,f_i}^{\mathrm{F}}(k_i^{\mathrm{F}})^{-1}\hat{\mathbf{x}}_{ij}^{\mathrm{F}}(k_i^{\mathrm{F}}) \quad (4.41)\\
&= \begin{bmatrix} K_i^{\mathrm{F}} & K_{f_i}^{\mathrm{F}} \end{bmatrix}\begin{bmatrix} \hat{\mathbf{x}}_i(k_i^{\mathrm{F}}) \\ \hat{\mathbf{x}}_{f_i}(k_i^{\mathrm{F}}) \end{bmatrix}. \quad (4.42)
\end{aligned}$$

In batch form, the global covariance update, reflecting the state fusion update, is

$$\mathbf{P}_{\mathrm{G}}(k_i^{\mathrm{F}}) \leftarrow \mathbf{K}_i^{\mathrm{F}} \mathbf{P}_{\mathrm{G}}(k_i^{\mathrm{F}}) {\mathbf{K}_i^{\mathrm{F}}}^T, \quad \mathbf{K}_i^{\mathrm{F}} = \begin{bmatrix} I & & & & & & \\ & \ddots & & & & & \\ & & I & & & & \\ & & & K_i^{\mathrm{F}} & & K_{f_i}^{\mathrm{F}} & \\ & & & & I & & \\ & & & & & \ddots & \\ & & & & & & I \end{bmatrix} \tag{4.43}$$

such that $\left[\mathbf{K}_i^{\mathrm{F}}\right]_{i,i} = K_i^{\mathrm{F}}$ and $\left[\mathbf{K}_i^{\mathrm{F}}\right]_{i,f_i} = K_{f_i}^{\mathrm{F}}$. Note that $\mathbf{K}_i^{\mathrm{F}}$ is full rank.

Although the minimization in Eq. 4.40 is optimal in a maximum a posteriori sense, it was shown in Ref. [13] that it is not optimal in a minimum mean square error sense. This is because of the lack of a priori information in Eq. 4.37. It can be argued that the lack of a priori information leads to a conservative estimate of $\mathbf{x}_i(k_i^{\mathrm{F}})$. The results in Ref. [13] confirm this in several numerical results.

As with the global covariance measurement update, when a fusion occurs at a spacecraft in the formation, only that spacecraft performs the state fusion in Eq. 4.42. However, each spacecraft performs the update in Eq. 4.43 and updates $\mathbf{P}_{\mathrm{G}}(k_i^{\mathrm{F}})$ accordingly.

Known time delays in the communication subsystem are accounted for by storing and recalling past estimates and global covariance matrices. Therefore, when, at time step k_i^{F}, spacecraft i receives from spacecraft f_i the estimate $\hat{\mathbf{x}}_{f_i}(k_i^{\mathrm{F}} - T_c)$, spacecraft i recalls from memory the estimate $\hat{\mathbf{x}}_i(k_i^{\mathrm{F}} - T_c)$ along with the associated global covariance matrix $\mathbf{P}_{\mathrm{G}}(k_i^{\mathrm{F}} - T_c)$. It performs the fusion to yield $\hat{\mathbf{x}}_i(k_i^{\mathrm{F}} - T_c)$ and runs the filter forward, using the locally stored measurements, to time step k_i^{F}.

4.3.4 Square Root Implementation

The global covariance and fusion update steps can be implemented in a square root fashion[6] to improve numerical accuracy and filter stability. Denoting the square root of the system covariance matrix, $\mathbf{P}_{\mathrm{G}}(k)$, as $\mathbf{S}_{\mathrm{G}}(k)$ such that

$$\mathbf{P}_{\mathrm{G}}(k) = \mathbf{S}_{\mathrm{G}}(k)^T \mathbf{S}_{\mathrm{G}}(k) \tag{4.44}$$

allows Eq. 4.35 to be written as

$$\mathbf{S}_{\mathrm{G}}(k+1)^T \mathbf{S}_{\mathrm{G}}(k+1) = \mathbf{A}_{\mathrm{G}} \mathbf{S}_{\mathrm{G}}(k)^T \mathbf{S}_{\mathrm{G}}(k) \mathbf{A}_{\mathrm{G}}^T + \mathbf{N}. \tag{4.45}$$

where $\mathbf{N} = \mathbf{B}_{\mathrm{G}} \mathbf{Q} \mathbf{B}_{\mathrm{G}}^T + \mathbf{K}_{\mathrm{G}} \mathbf{R} \mathbf{K}_{\mathrm{G}}^T$. Taking the square root of the right side leads to

$$\mathbf{S}_{\mathrm{G}}(k+1)^T \mathbf{S}_{\mathrm{G}}(k+1) = \begin{bmatrix} \mathbf{A}_{\mathrm{G}} \mathbf{S}_{\mathrm{G}}(k)^T & \mathbf{S}_N^T \end{bmatrix} \begin{bmatrix} \mathbf{S}_{\mathrm{G}}(k) \mathbf{A}_{\mathrm{G}}^T \\ \mathbf{S}_N \end{bmatrix} \tag{4.46}$$

where $\mathbf{S}_N$ denotes the square roots of the noise covariance matrix $\mathbf{N}$ such that $\mathbf{N} = \mathbf{S}_N^T \mathbf{S}_N$. The QR decomposition of $\begin{bmatrix} \mathbf{A}_{\mathrm{G}} \mathbf{S}_{\mathrm{G}}(k)^T & \mathbf{S}_N^T \end{bmatrix}^T$ yields the desired $\mathbf{S}_P(k+1)$ as

$$\begin{bmatrix} \mathbf{S}_{\mathrm{G}}(k+1) \\ 0 \end{bmatrix} = \mathbf{Z}_{\mathrm{G}}^T \begin{bmatrix} \mathbf{S}_{\mathrm{G}}(k) \mathbf{A}_{\mathrm{G}}^T \\ \mathbf{S}_N \end{bmatrix} \tag{4.47}$$

where $\mathbf{Z}_{\mathrm{G}}$ is unitary. Similarly, the square root noise $\mathbf{S}_N$ is found by a QR decomposition by noting that, by definition

$$\mathbf{N} = \mathbf{S}_N^T \mathbf{S}_N = \begin{bmatrix} \mathbf{B}_{\mathrm{G}} \mathbf{S}_Q^T & \mathbf{K}_{\mathrm{G}} \mathbf{S}_R^T \end{bmatrix} \begin{bmatrix} \mathbf{S}_Q \mathbf{B}_{\mathrm{G}}^T \\ \mathbf{S}_R \mathbf{K}_{\mathrm{G}}^T \end{bmatrix}. \tag{4.48}$$

where $\mathbf{S}_Q$ and $\mathbf{S}_R$ are the square roots of the process and measurement noise covariance matrices $\mathbf{Q}$ and $\mathbf{R}$, respectively, such that $\mathbf{Q} = \mathbf{S}_Q^T \mathbf{S}_Q$ and $\mathbf{R} = \mathbf{S}_R^T \mathbf{S}_R$. The QR decomposition of $\begin{bmatrix} \mathbf{B}_{\mathrm{G}} \mathbf{S}_Q^T & \mathbf{K}_{\mathrm{G}} \mathbf{S}_R^T \end{bmatrix}^T$ yields

$$\begin{bmatrix} \mathbf{S}_N \\ 0 \end{bmatrix} = \mathbf{Z}_N^T \begin{bmatrix} \mathbf{S}_Q \mathbf{B}_{\mathrm{G}}^T \\ \mathbf{S}_R \mathbf{K}_{\mathrm{G}}^T \end{bmatrix} \tag{4.49}$$

where $\mathbf{Z}_N$ is unitary. Note that the computation in Eq. 4.49 can be performed off line and stored in memory.

The square root version of the fusion update step in Eqs. 4.42 and 4.43 proceeds by first finding the square root of the matrix $\mathbf{P}^{\mathrm{F}}_{i,f_i}(k)$, denoted by $\mathbf{S}_{i,f_i}(k)$, given $\mathbf{S}_{\mathrm{G}}(k)$. Note that by definition

$$\begin{aligned} \mathbf{P}^{\mathrm{F}}_{i,f_i}(k) &= \mathbf{S}_{i,f_i}(k)^T \mathbf{S}_{i,f_i}(k) \\ &= A^T_{i,f_i} \mathbf{P}_{\mathrm{G}}(k) A_{i,f_i} \\ &= A^T_{i,f_i} \mathbf{S}_{\mathrm{G}}(k)^T \mathbf{S}_{\mathrm{G}}(k) A_{i,f_i} \end{aligned} \tag{4.50}$$

where

$$A_{i,f_i} = \begin{bmatrix} & & \\ I & & \\ & & \\ & I & \\ & & \end{bmatrix} \tag{4.51}$$

such that $[A_{i,f_i}]_{i,1} = I$ and $[A_{i,f_i}]_{f_i,2} = I$ and zeros elsewhere. The QR decomposition of $\mathbf{P}_{\mathrm{G}}(k) A_{i,f_i}$ yields the square root of $\mathbf{P}_{i,f_i}(k)$ as

$$\begin{bmatrix} \mathbf{S}_{i,f_i}(k+1) \\ 0 \end{bmatrix} = \mathbf{Z}^T_{i,f_i} \mathbf{P}_{\mathrm{G}}(k) A_{i,f_i} \tag{4.52}$$

where $\mathbf{Z}_{i,f_i}$ is unitary.

The least squares cost in Eq. 4.40 is rewritten in square root form as

$$\begin{aligned} J_{\mathrm{F}} &= \left[\mathbf{T}_{f_i,i}\mathbf{x}_i(k) - \hat{\mathbf{x}}^{\mathrm{F}}_{i,f_i}(k)\right]^T \left(\mathbf{S}_{i,f_i}(k)^T\mathbf{S}_{i,f_i}(k)\right)^{-1} \cdot \\ &\quad \left[\mathbf{T}_{f_i,i}\mathbf{x}_i(k) - \hat{\mathbf{x}}^{\mathrm{F}}_{i,f_i}(k)\right] \qquad (4.53) \\ &= \left[\mathbf{T}_{f_i,i}\mathbf{x}_i(k) - \hat{\mathbf{x}}^{\mathrm{F}}_{i,f_i}(k)\right]^T \mathbf{S}_{i,f_i}(k)^{-1}\mathbf{S}_{i,f_i}(k)^{-T} \cdot \\ &\quad \left[\mathbf{T}_{f_i,i}\mathbf{x}_i(k) - \hat{\mathbf{x}}^{\mathrm{F}}_{i,f_i}(k)\right] \qquad (4.54) \\ &= \mathbf{e}_{\mathrm{F}}(k)^T\mathbf{e}_{\mathrm{F}}(k) \qquad (4.55) \end{aligned}$$

where

$$\begin{aligned} \mathbf{e}_{\mathrm{F}}(k) &= \mathbf{S}_{i,f_i}(k)^{-T}\left[\mathbf{T}_{f_i,i}\mathbf{x}_i(k) - \hat{\mathbf{x}}^{\mathrm{F}}_{i,f_i}(k)\right] \qquad (4.56) \\ &= \mathbf{S}_{i,f_i}(k)^{-T}\mathbf{T}_{f_i,i}\mathbf{x}_i(k) - \mathbf{S}_{i,f_i}(k)^{-T}\hat{\mathbf{x}}^{\mathrm{F}}_{i,f_i}(k). \qquad (4.57) \end{aligned}$$

Performing a QR decomposition on $\mathbf{S}_{i,f_i}(k)^{-T}\mathbf{T}_{f_i,i}$ yields

$$\begin{bmatrix} \mathbf{S}_{\mathrm{F}}(k) \\ 0 \end{bmatrix} = \mathbf{Z}_{\mathrm{F}}^T\mathbf{S}_{i,f_i}(k)^{-T}\mathbf{T}_{f_i,i}. \qquad (4.58)$$

where $\mathbf{Z}_{\mathrm{F}}$ is unitary. Premultiplying Eq. 4.57 by $\mathbf{Z}_{\mathrm{F}}^T$ yields

$$\mathbf{Z}_{\mathrm{F}}^T\mathbf{e}_{\mathrm{F}}(k) = \begin{bmatrix} \mathbf{S}_{\mathrm{F}}(k) \\ 0 \end{bmatrix}\mathbf{x}_i(k) - \mathbf{Z}_{\mathrm{F}}^T\mathbf{S}_{i,f_i}(k)^{-T}\hat{\mathbf{x}}^{\mathrm{F}}_{i,f_i}(k) = \begin{bmatrix} \mathbf{e}_J(k) \\ \mathbf{e}_{\mathrm{R}}(k) \end{bmatrix}, \qquad (4.59)$$

where $\mathbf{e}_{\mathrm{R}}(k)^T\mathbf{e}_{\mathrm{R}}(k)$ is the residual cost and is not a function of $\mathbf{x}_j^+(k)$. Because $\mathbf{S}_{\mathrm{F}}(k)$ is invertible, the error $\mathbf{e}_J(k)$ can be chosen to be zero by the appropriate choice of $\mathbf{x}_i(k)$, thus minimizing the cost J_{F}. In order to isolate $\mathbf{e}_J(k)$, Eq. 4.59 is premultiplied by $A_I = \begin{bmatrix} I & 0 \end{bmatrix}$ and is set equal to zero resulting in

$$\begin{aligned} 0 &= A_I\begin{bmatrix} \mathbf{S}_{\mathrm{F}}(k) \\ 0 \end{bmatrix}\mathbf{x}_i(k) - A_I\mathbf{Z}_{\mathrm{F}}^T\mathbf{S}_{i,f_i}(k)^{-T}\hat{\mathbf{x}}^F_{ij}(k) \qquad (4.60) \\ &= \mathbf{S}_{\mathrm{F}}(k)\mathbf{x}_i(k) - A_I\mathbf{Z}_{\mathrm{F}}^T\mathbf{S}_{i,f_i}(k)^{-T}\hat{\mathbf{x}}^F_{ij}(k). \qquad (4.61) \end{aligned}$$

Solving for $\mathbf{x}_i(k)$ and updating $\hat{\mathbf{x}}_i(k)$ with the result yields

$$\hat{\mathbf{x}}_i(k) \leftarrow \mathbf{S}_{\mathrm{F}}(k)^{-1} A_I \mathbf{Z}_{\mathrm{F}}^T \mathbf{S}_{i,f_i}(k)^{-T} \hat{\mathbf{x}}_{i,f_i}^{\mathrm{F}}(k) \tag{4.62}$$

$$= \begin{bmatrix} \mathbf{K}_i^{\mathrm{F}} & \mathbf{K}_j^{\mathrm{F}} \end{bmatrix} \begin{bmatrix} \hat{\mathbf{x}}_i(k) \\ \hat{\mathbf{x}}_{f_i}(k) \end{bmatrix} \tag{4.63}$$

Finally, the fused global square root covariance is updated by recalling Eq. 4.43

$$\mathbf{S}_{\mathrm{G}}(k)^T \mathbf{S}_{\mathrm{G}}(k) \leftarrow \mathbf{K}_i^{\mathrm{F}} \mathbf{S}_{\mathrm{G}}(k)^T \mathbf{S}_{\mathrm{G}}(k) \mathbf{K}_i^{\mathrm{F}^T} \tag{4.64}$$

resulting in

$$\mathbf{S}_{\mathrm{G}}(k) \leftarrow \mathbf{S}_{\mathrm{G}}(k) \mathbf{K}_i^{\mathrm{F}^T}. \tag{4.65}$$

As previously noted, prior to the fusion update in Eq. 4.65, both $\mathbf{S}_{\mathrm{G}}(k)$ and $\mathbf{K}_i^{\mathrm{F}}$ are square and full rank and so no other processing needs to be performed on the updated $\mathbf{S}_{\mathrm{G}}(k)$. In other words, although $\mathbf{S}_{\mathrm{G}}(k)$ may not be upper triangular, it is a valid square root matrix.

Numerical performance of the combined communication/estimation system is presented in the following section. The filter is shown to be consistent[3] and give performance in steady state that is close to optimal when compared to a Kalman filter operating, at each spacecraft on the raw measurements, subject to the delays as described in Section 4.3.1.

4.3.5 Thrust Compensation

Note that the time update of Eq. 4.20 requires that control maneuvers $\mathbf{u}(k)$ be known instantaneously at each spacecraft. Given time delays in the communication subsystem described herein, this would require additional sensing or communication resources in order to achieve this knowledge. If these additional resources are

not available, the thrust inputs are neglected by augmenting the process noise to include the effects of the thrust input. Because the thrust is clearly not Gaussian noise, this is only an approximation. However, simulations in Section 4.4 show that the proper choice of $\mathbf{Q}$ yields system performance that is comparable to a system which includes instantaneous knowledge of $\mathbf{u}(k)$.

4.4 Numerical Results

In this section, formations of three and eight spacecraft are simulated to verify the performance of the filter. Consistency testing results are detailed in Section 4.4.1. Results of a numerical comparison of the IF filter to the optimal Kalman filter in steady state are presented in Section 4.4.2. The full system is simulated for a period of forty-eight hours and results are presented in Section 4.4.3.

4.4.1 Consistency Testing

Monte Carlo testing on the estimation system presented herein has shown that the filter is consistent in steady state, i.e. that the errors are zero mean and that the numerically calculated covariance (across trials) is statistically equivalent to the covariance output of the IFF[3]. This has been determined for formations consisting of between three and eight spacecraft and for various values of T_c and T_s. The consistency test consists of a chi-square test on the null hypothesis: that the filter error is zero mean, and has mean square magnitude stastically equivalent to the filter covariance matrix $\mathbf{P}_{\mathrm{G}}$. Recalling the definition of the filter error

$$\mathbf{e}_i(k) = \mathbf{x}_i(k) - \hat{\mathbf{x}}_i(k), \tag{4.66}$$

the normalized squared estimate error is

$$\epsilon_i(k) = \mathbf{e}_i(k)^T \mathbf{P}_{i,i}(k)^{-1} \mathbf{e}_i(k). \tag{4.67}$$

where $\mathbf{P}_{i,i}(k) = [\mathbf{P}_{\mathrm{G}}(k)]_{i,i}$. Under the null hypothesis, $\epsilon_i(k)$ is chi-square distrituted with $n_x(N-1)$ degrees of freedom. The Monte Carlo test consists of running the filter a number of times, using identical initial conditions, but different sequences of process and measurement noise. A total of N_{T} trials a run, each generating, for some fixed k_{T}, the normalized squared estimate error $\epsilon_i^m(k_{\mathrm{T}})$ for $m = \{1, \ldots, N_{\mathrm{T}}\}$. The sum of these errors is

$$\bar{\epsilon}_i(k_{\mathrm{T}}) = \frac{1}{N_{\mathrm{T}}} \sum_{m=1}^{N_{\mathrm{T}}} \epsilon_i^m(k_{\mathrm{T}}) \tag{4.68}$$

and thus, $N_{\mathrm{T}}\bar{\epsilon}_i(k_{\mathrm{T}})$ chi-squared with $n_x(N-1)N_{\mathrm{T}}$ degrees of freedom. The filter is considered to be consistent if $\bar{\epsilon}_i(k_{\mathrm{T}}) \in [\epsilon_{max}, \epsilon_{min}]$. The interval $[\epsilon_{max}, \epsilon_{min}]$ is defined by the error probability α such that

$$P\left\{\bar{\epsilon}_i(k_{\mathrm{T}}) \in [\epsilon_{max}, \epsilon_{min}]\right\} = 1 - \alpha. \tag{4.69}$$

For the consistency tests performed, $\alpha = 0.05$, $N_{\mathrm{T}} = 20$, $N = 8$, and, in 2D, $n_x = 4$. This results in $[\epsilon_{max}, \epsilon_{min}] = [24.8, 31.4]$.

4.4.2 Comparison to Optimal Kalman Filter

Figure 4.3 illustrates the difference between the IFF and optimal EKF. In this simulation, $N = 8$ and $f_i = m_i = i - 1$ for $i = \{2, \ldots, 8\}$ and $f_1 = m_1 = 8$ yielding a circular communication and sensing topology. The nominal formation is shown in Figure 2.11 and the simulation parameters described in Section 2.6 are used for the simulations herein. The position and velocity errors are shown with 3σ bounds for the error in the estimate of the states x_{61}^1 and $\dot{x}_{61}^1$. The fusion process does not

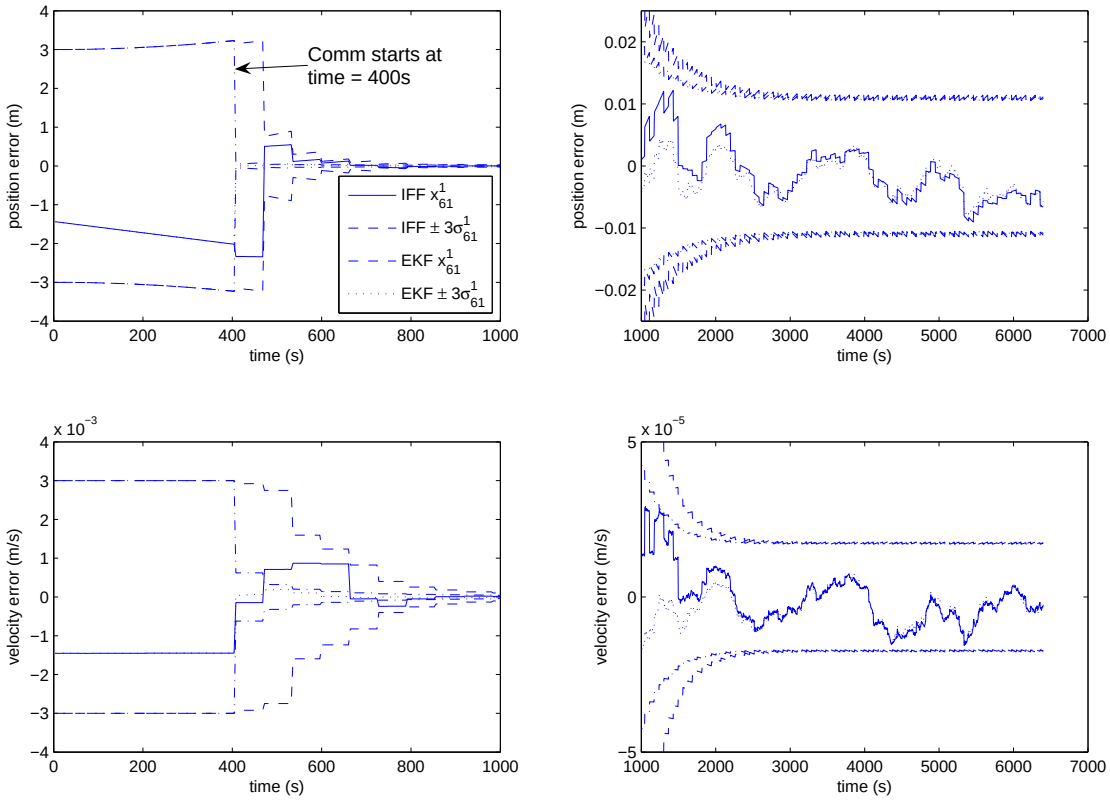

Figure 4.3: Iterated fusion filter performance for an $N = 8$ formation.

begin until 400 s into the simulation, resulting in increasing error in the estimates. At 400 s, the EKF estimate rapidly converges, because it uses the optimal gains on all the measurements it receives. Since it uses static local gains and the suboptimal fusion ste, the IFF filter takes longer to converge. However, at steady state, the filters perform almost identically.

The covariance resulting from the optimal extended Kalman filter (EKF), subject to the same communication delays as the IFF, at the i-th spacecraft is denoted by $\mathbf{P}_i^{KF}(k)$. The performance metric by which the two filters are compared is the mean (over time) of the trace of the covariance matrix when the filters are in steady state. Since both the IFF and EKF are consistent, according to the definition of

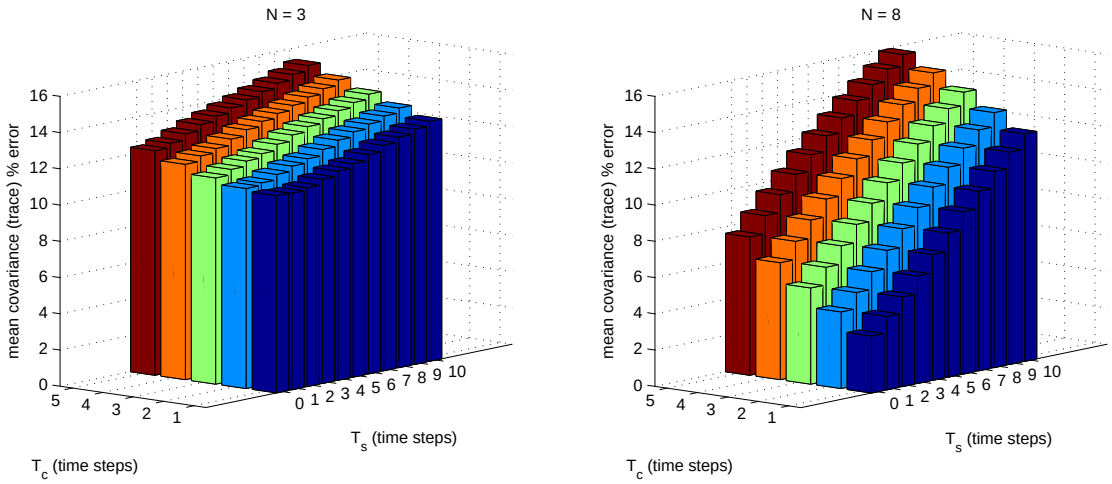

Figure 4.4: Relative error $\mathbf{E}_N(T_c, T_s)$ between the mean steady state Iterated Fusion filter (IFF) and optimal EKF covariances (trace) for $N = 3$ and $N = 8$.

consistency in Section 4.4.1, this metric can be used for evaluating the performance in lieu of a computationally intensive Monte Carlo simulation where the mean square error is calculated numerically. If the mean of the IF filter is always larger then the mean of the steady state optimal filter, the normalized error

$$\mathbf{E}_N(T_c, T_s) = \frac{\text{trace } \left[\sum_{k=k_0}^{k_f} \mathbf{P}_{i,i}(k)\right] - \text{trace } \left[\sum_{k=k_0}^{k_f} \mathbf{P}_i^{KF}(k)\right]}{\text{trace } \left[\sum_{k=k_0}^{k_f} \mathbf{P}_i^{KF}(k)\right]} \tag{4.70}$$

is always positive and denotes how well the IFF performs. If this error is close to zero, then the filter is performing well. Simulations were performed for various values of the time delays T_c and T_s. Note that k_0 must be chosen to be large enough so that the filter is in steady state, and the integration time $k_f - k_0$ must be chosen to be large enough to capture the variations in the filter due to the cyclic communication. For N spacecraft, the round trip time of the filter is $N\,(T_s + T_c)$ and so $k_f - k_0$ is at least several times this value.

The simulations verify that in steady state, not only is the error ratio greater

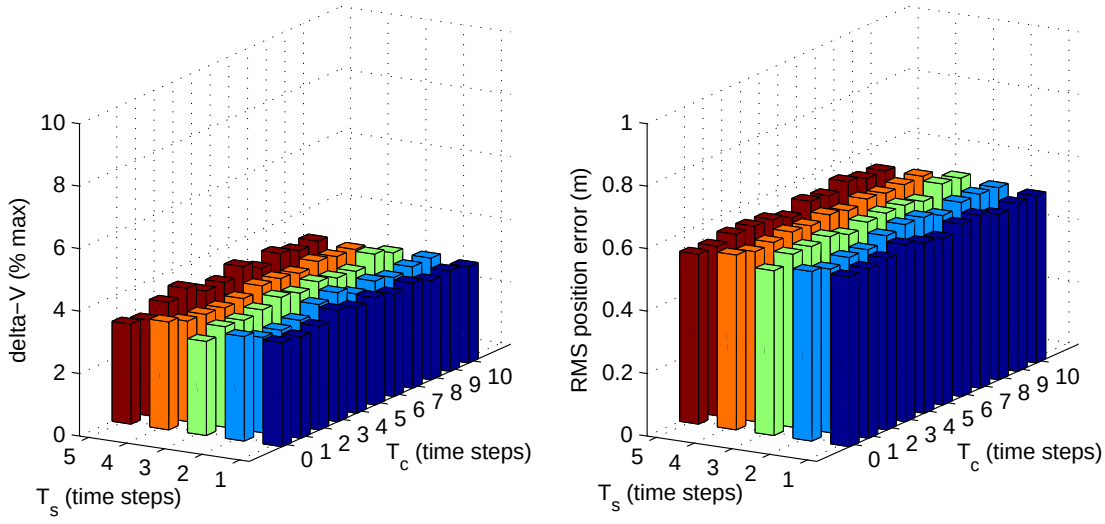

Figure 4.5: Mean delta-V and RMS position error for a formation with $N = 8$ over various values of T_c and T_s.

than zero, but that for all j, $[\mathbf{P}_{i,i}(k)]_{j,j} > \left[\mathbf{P}_i^{KF}(k)\right]_{j,j}$ for all values of T_s and T_c. The results are consistent with the trend found in Ref. [13], i.e. that the IFF provides conservative estimates. Interestingly, the filter covariance error decreases for larger N.

4.4.3 System Performance

Performance of the system in terms of fuel usage and RMS position error is determined via Monte Carlo simulation. The simulation consists of an eight spacecraft formation running continuously for forty-eight hours for two cases: (1) the case there thrust inputs are known instantaneously at each spacecraft, and (2) where the filter process noise is augmented to accommodate for the lack of this information. For the case where the thrust inputs are known, Figure 4.5 shows the system performance as a function of the communication delay T_c and the internal

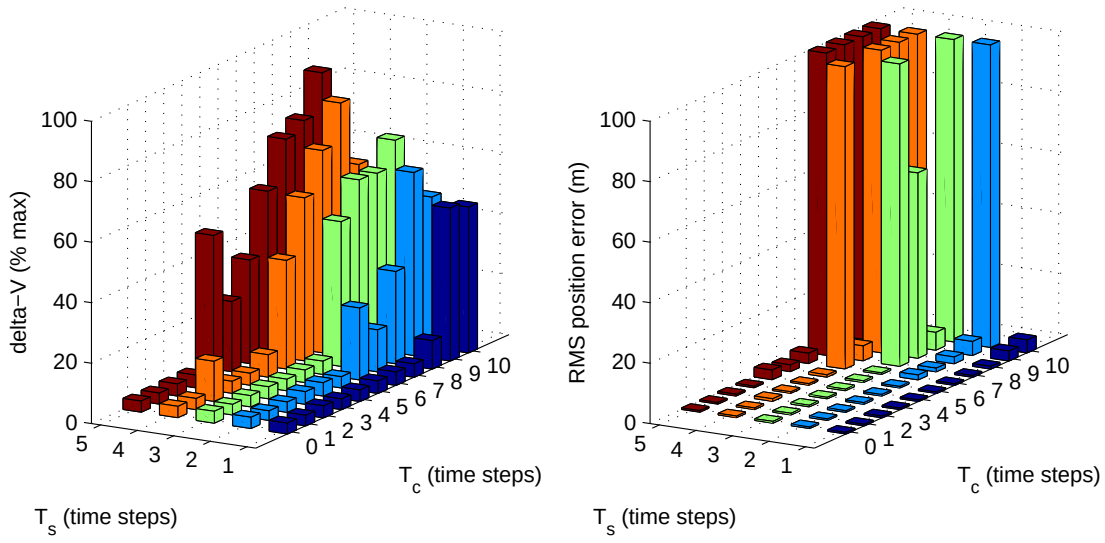

Figure 4.6: Mean delta-V and RMS position error for a formation with $N = 8$ over various values of T_c and T_s for a formation where the thrust is unknown to the local estimators.

delay T_s. Each point in the figure represents the performance of a forty-eight hour simulation run. For all values of T_c and T_s the system exhibits good performance of about 3.5 % thruster on-time and 0.55 m in position error.

For the case where the thrust inputs are not known at any spacecraft, the system equations are augmented to include an additional noise term $\mathbf{w}_u(k)$ such that

$$\mathbf{x}_i(k+1) = \mathbf{A}\mathbf{x}_i(k) + \mathbf{B}_i\mathbf{w}_u(k) + \mathbf{B}_i\mathbf{w}(k) \tag{4.71}$$

where the covariance of $\mathbf{w}_u(k)$ is $\mathbf{Q}_u = \mathbf{q}_u I$. The value of $\mathbf{q}_u$ is chosen to be U_{max}^2, i.e. the covariance resulting from the thrusters being on all the time. The system exhibits good performance for small values of T_c and T_s. Figure 4.6 shows the system performance and Figure 4.7 is a contour map for the position error. Interestingly, the contours are nearly coincident with the lines given by the function $T_c + T_s = c$ where c is a constant. This suggests that performance is a function

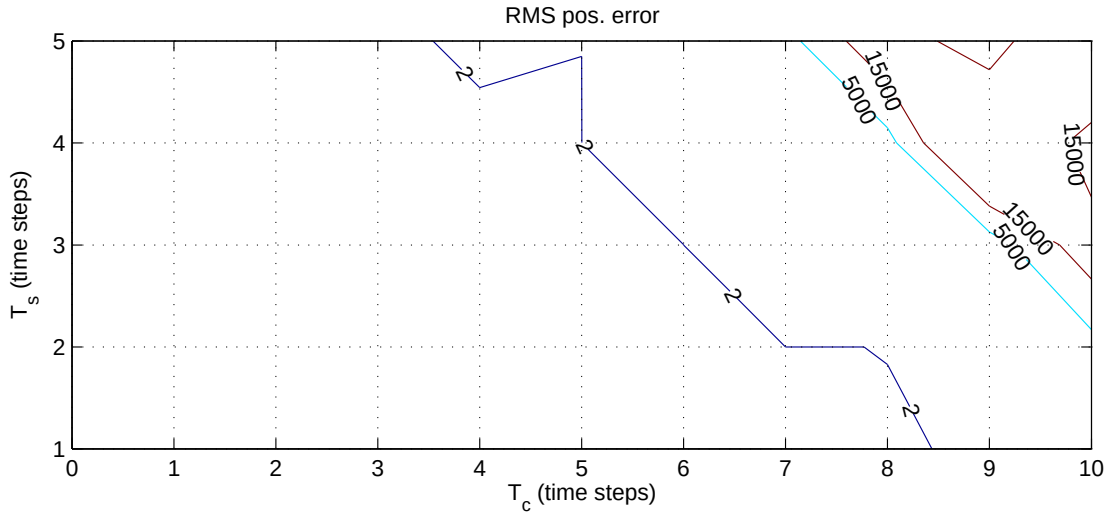

Figure 4.7: Contour map of the formation position error in Figure 4.6 (right).

of the overall delay $T_c + T_s$. The contour map shows that the system performance rapidly degrades for delays above $T_c + T_s = 9$. Note that for large overall delay $T_c + T_s$, the system becomes unstable resulting in performance values that are too large to plot in Figure 4.6.

CHAPTER 5

CONCLUSIONS

The major contributions contained in this dissertation are as follows: in Chapter 2, the information weighted virtual center algorithm is shown to add robustness to the system by dampening the effects of noisy state estimates. It is also shown to significantly decrease the controller reaction time to a collision, while providing near-optimal performance in terms of the two key formation performance metrics identified herein: RMS position error and fuel usage.

Chapters 2 and 3 contain similar algorithms for finding the optimal periodic measurement sequence. The steepest descent search in Chapter 2 uses the full cost model when evaluating candidate solutions, assuming convexity of the cost function, which is not guaranteed. In Chapter 3 it is shown that even when convexity is guaranteed, the integer constraint may cause a gradient solver to converge to a suboptimal solution. In contrast, the approximation of the cost function in Chapter 3 leads to a convex optimization problem when the integer constraint is relaxed. Imposing the integer constraint uses established integer least squares methods by approximating the cost function using the Hessian, guaranteeing optimality (in the cases where the Hessian can be fully diagonalized with a unimodular transformation) to third order.

The GNC architecture developed in Chapter 2 does not assume the presence of a communication subsystem for state fusion. It assumed that the RBS sensor could be switched at a fairly high rate (comparable to the measurement rate) assuring formation observability at each spacecraft. The architecture proposed in Chapter 4 uses the minimal amount of communication hardware in terms of the number of required unidirectional Tx and Rx channels for fusing state estimates maintained

at each spacecraft. The estimation system is shown to yield statistically consistent estimates while being conservative when compared to a computationally intensive, high communication extended Kalman filter. Simulations show that an eight spacecraft formation performs well in the presence of single hop communication delays of up to 30 seconds.

BIBLIOGRAPHY

[1] P. O. Arambel, C. Rago, and R. K. Mehra. Covariance intersection algorithm for distributed spacecraft state estimation. In *Proceedings of the American Control Conference*, pages 4398–4403, Wahington, DC, June 2001. IEEE.

[2] M. Aung, G. H. Purcell, J. Y. Tien, L. E. Young, L. R. Amari, J. Srnvasan, M. A. Ciminera, and Y. J. Chong. Autonomous formation-flying sensor for the starlight mission. IPN Progress report 42-152, JPL, February 2003.

[3] Y. Bar-Shalom, X. Rong Li, and T. Kirubarajan. *Estimation with Applications to Tracking and Navigation*. John Wiley & Sons, Inc., 2001.

[4] C.A. Beichman, D.R. Coulter, C.A. Lindensmith, and P.R. Lawson. Summary report on architecture studies for the terrestrial planet finder. JPL Publication 02-011, JPL, June 2002.

[5] Dimitri P. Bertsekas. *Dynamic Programming and Optimal Control*. Athena Scientific, 2001.

[6] G. J. Bierman. *Factorization Methods for Discrete Sequential Estimation*. Academic Press, Inc., 1977.

[7] S. Bittanti, P. Colaneri, and G. De Nicolao. The periodic riccati equation. In S. Bittanti, A.J. Laub, and J.C. Willems, editors, *The Riccati Equation*, pages 127–162. Springer-Verlag, New York, 1991.

[8] S. Boyd, L. El Ghaoui, E. Feron, and V. Balakrishnan. *Linear Matrix Inequalities in System and Control Theory*. SIAM, 1994.

[9] M. Campbell. Planning algorithm for multiple satellite clusters. *Journal of Guidance, Control, and Dynamics*, 26(5):770–780, 2003.

[10] J. R. Carpenter. Decentralized control of satellite formations. *Internation Journal of Robust and Nonlinear Control*, 12(2):141–161, February 2002.

[11] J. R. Carpenter and R. H. Bishop. Navigation filter estimate fusion for enhanced spacecraft rendezvous. *Journal of Guidance, Control, and Dynamics*, 20(12):338–345, March 1997.

[12] K.G. Carpenter et al. The stellar imager (si) mission concept. In *Proceedings of SPIE*, volume 4854, pages 293–302. SPIE, February 2003.

[13] K. C. Chang, R. K. Saha, and Y. Bar-Shalom. On optimal track-to-track fusion. *IEEE Transations on Aerospace and Electronic Systems*, 33(4):1271–1276, October 1997.

[14] H. Chen, Kirubarajan T, and Y. Bar-Shalom. Performance limits of track-to-track fusion versus centralized estimation: Theory and application. *IEEE Transactions on Aerospace and Electronic Systems*, 39(2):386–400, 2003.

[15] E. Feron and C. Olivier. Targets, sensors and infinite-horizon tracking optimality. In *29th IEEE Conference on Decision and Control, Proceedings of the*, volume 4, pages 2291–2292, Wahington, DC, December 1990. IEEE.

[16] G. H. Golub and C. F. Van Loan. *Matrix Computations*. JHU Press, 1996.

[17] S. Grime and H. F. Durrant-Whyte. Data fusion in decentralized sensor fusion networks. *Control Engineering Practice*, 2(5):849–863, 1994.

[18] V. Gupta, T. Chung, B. Hassibi, and R. M. Murray. On a stochastic sensor selection algorithm with applications in sensor scheduling and sensor coverage. *Automatica*, 42(2):251–260, February 2006.

[19] F. Y. Hadaegh, D. P. Scharf, and S. R. Ploen. Initialization of distributed spacecraft for precision formation flying. In *Proceedings of the IEEE Conference on Control Applications*, volume 1. IEEE, June 2003.

[20] S. J. Julier and J. K. Uhlmann. A non-divergent estimation algorithm in the presence of unknown correlations. In *Proceedings of the American Control Conference*, volume 4, pages 2369–2373, Wahington, DC, June 1997. IEEE.

[21] T. H. McLoughlin and M. Campbell. Robust information fusion for spacecraft formations. In *Proceedings of the AIAA Guidance, Navigation, and Control Conference*, Wahington, DC, August 2006. AIAA.

[22] L. Meier, J. Peschon, and R. B. Dressler. Optimal control of measurement systems. *IEEE Transations on Automatic Control*, AC-12(5):528–536, October 1967.

[23] I. Miller and M. Campbell. Validation of simplified formation models at l2. In *Proceedings of the IEEEAmerican Control Conference*. IEEE, June 2005.

[24] A. G. O. Mutambara. *Decentralized Estimation and Control for Multisensor Systems*. CRC Press, 1998.

[25] M. L. Psiaki and S. Mohiuddin. Global positioning system integer ambiguity resolution using factorized least-squares techniques. *Journal of Guidance, Control, and Dynamics*, 30(2):346–356, February 2007.

[26] A. C. M. Ran and R. Vreugdenhil. Existence and comparison theorems for algebraic riccati equations for continuous- and discrete-time systems. *Linear Algebra Appl.*, 99:63–83, 1988.

[27] A. V. Savkin, R. J. Evans, and E. Skafidas. The problem of optimal robust sensor scheduling. In *Proceedings of the IEEE Conference on Decision and Control*, volume 4, pages 3791–3796. IEEE, December 2000.

[28] D. P. Scharf, F. Y. Hadaegh, and B. H. Kang. On the validity of the double integrator approximation in deep space formation flying. In *Int. Symp. Formation Flying Missions & Technologies*, Toulouse, France, 2002.

[29] D. P. Scharf, F. Y. Hadaegh, and S. R. Ploen. A survey of spacecraft formation flying guidance and control (part ii): Control. In *American Control Conference, Proceedings of the IEEE*, volume 4, pages 2976–2985. IEEE, 2004.

[30] M. Tillerson, L. Breger, and J. P. How. Distributed coordination and control of formation flying spacecraft. In *Proceedings of the IEEE American Control Conference*. IEEE, June 2003.

[31] D.L. Windt, S.M. Kahn, and G.E. Sommargen. Diffraction-limited astronomical x-ray imaging and x-ray interferometry using normal-incidence multilayer optics. In *Proceedings of SPIE*, volume 4851, pages 441–450. SPIE, March 2003.

[32] P. Xu. Random simulation and gps decorrelation. *Journal of Geodesy*, 75(7–8):408–423, September 2001.